HIGH PRECISION COULOMETRY AS A TECHNIQUE FOR EVALUATING THE PERFORMANCE AND LIFETIME OF LI-ION BATTERIES

by

John Christopher Burns

Submitted in partial fulfillment of the requirements
for the degree of Master of Science

at

Dalhousie University
Halifax, Nova Scotia
August 2011

DALHOUSIE UNIVERSITY

DEPARTMENT OF PHYSICS AND ATMOSPHERIC SCIENCE

The undersigned hereby certify that they have read and recommend to the Faculty of Graduate Studies for acceptance a thesis entitled "HIGH PRECISION COULOMETRY AS A TECHNIQUE FOR EVALUATING THE PERFORMANCE AND LIFETIME OF LI-ION BATTERIES" by John Christopher Burns in partial fulfillment of the requirements for the degree of Master of Science.

Dated: August 12, 2011

Supervisor: _____

Readers: _____

_____

DALHOUSIE UNIVERSITY

DATE: August 12, 2011

AUTHOR: John Christopher Burns

TITLE: HIGH PRECISION COULOMETRY AS A TECHNIQUE FOR EVALUATING THE PERFORMANCE AND LIFETIME OF LI-ION BATTERIES

DEPARTMENT OR SCHOOL: Department of Physics and Atmospheric Science

DEGREE: M.Sc. CONVOCATION: October YEAR: 2011

_____

Signature of Author

To my parents

Table of Contents

List of Tables

List of Figures

Abstract

The aim of this thesis is to develop a better understanding about the degradation mechanisms occurring within lithium-ion cells which eventually lead to their failure. An introduction to the components and operation of Li-ion cells is followed by proposed degradation mechanisms which limit the lifetime of cells. These mechanisms and how they can be identified from electrochemical testing are discussed.

Electrolyte additives can be used to improve the safety of Li-ion cells or decrease the rate of cell degradation. Different types of additives and testing methods are discussed followed by an introduction to high precision coulometry which can be used to detect the impact of additives on cycling performance. The High Precision Charger that was constructed for this project is described and shown to meet the desired precision.

The use of additives and different materials to extend lifetime of cells is shown to be detectable through the use of high precision coulometry. High precision coulometry proves to be a more efficient way of estimating the lifetime of cells under realistic conditions in a reasonably short amount of time.

List of Abbreviations and Symbols Used

V	Cell voltage
μ	Chemical potential in joules per atom
e	Electron charge, 1.602×10^{-19} C
LTO	Lithium titantate, $Li_{1+x}(Li_{1/3}Ti_{5/3})O_2$
NMC	$Li_x(Ni_{1/3}Mn_{1/3}Co_{1/3})O_2$
LiBOB	Lithium bis(oxalato)borate
HQ115	lithium (bis) trifluoromethanesulfonimide
EC	Ethylene carbonate
DEC	Diethyl carbonate
EMC	Ethyl methyl carbonate
PC	Propylene carbonate
DMC	Dimethyl carbonate
Q	Cell capacity (further described by subscript)
I	Current (further described by subscript)
t	Measured time for half cycle
CE	Coulombic efficiency
SEI	Solid Electrolyte Interphase
q	Capacity due to parasitic reaction (further described by subscript)
E	Active lithium in the electrolyte after a single cycle
S	Lithium lost to the solid electrolyte interphase growth in the first cycle
Δ	Endpoint slippages (specified by subscript)
M	Metal atom from the positive electrode
X	Solvent molecule
HPC	High Precision Charger
ΔI	Error in delivered current
ΔV	Error in voltage measurement
Δt	Time between voltage measurements
ΔT	Error in cell temperature

RTD	Resistance temperature detectors
ARC	Accelerating rate calorimetry
DSC	Differential scanning calorimetry
EIS	Electrochemical impedance spectroscopy
XPS	X-ray photoelectron spectroscopy
NCA	$Li_x(Ni_{0.8}Co_{0.15}Al_{0.05})O_2$
VEC	Vinyl ethylene carbonate
TCEP	Tri(β-chloromethyl) phosphate
TTP	Triphenylphosphate
ATFEC	Allyl tris(2,2,2trifluoroethyl) carbonate
FEC	Fluoroethylene carbonate
VC	Vinylene carbonate
TMOBX	Trimethoxyboroxine
TPFPB	Tris(pentafluorophenyl) borane
LiDFOB	Lithium difluoro(oxalate)borate
HFiP	Tris(hexafluoro-iso-propyl)phosphate
MCMB	Mesocarbon microbeads
CIE	Coulombic inefficiency
CIE/hour	Coulombic inefficiency divided by time per cycle in hours
D_0	Discharge capacity before storage
D_1	Discharge capacity immediately after storage
D_2	Discharge capacity after a full charge post storage

Acknowledgements

I would like to thank my Jeff Dahn for giving me the chance to work in this group. His advice and the opportunity to learn from his experience has been invaluable. The High Precision Charger would not be where it is today if not for all the help from Aaron Smith, Simon Trussler and all of the summer students who assisted in the initial workload to get the system up and running. Finally I'd like to thank all members of the lab for making working in this lab enjoyable and Mark McArthur for going through the MSc. program and all his help along the way.

Chapter 1 Introduction

Lithium-ion batteries are commonly used in laptops, cell phones and other portable electronics. The use of Li-ion batteries is currently expanding to electrified vehicles and in the future could include grid energy storage. These new and future applications of Li-ion batteries are much more demanding (in both cycle life and cell performance) than portable electronics.

A Li-ion battery is composed of multiple Li-ion cells. These cells convert chemical potential energy to electrical energy through oxidation and reduction reactions. Li-ion cells are two electrode electrochemical cells consisting of a positive and negative electrode coated on current collectors connected to an external circuit. The cell voltage is given by the difference between the chemical potential (μ) of lithium atoms in the chosen positive and negative electrodes in joules per lithium at in the host material divided by the charge of an electron in coulombs,

$$V_{cell} = \frac{\mu_{negative} - \mu_{positive}}{e} . \qquad 1.1$$

The cell is filled with a lithium salt containing electrolyte through which lithium ions can be transported between the electrodes while associated electrons flow through the current collectors and external circuit. The Li-ion cell was first commercialized by Sony in 1991. These cells are used to store energy over long periods of time which requires both good cycle and calendar life. Also, more energy can be stored in cells that use materials with higher capacities or that lead to higher cell voltage.

The aim of this thesis is to develop a better understanding of Li-ion cells. If the operation and failure mechanisms of cells are better understood, it can lead to better methods of testing cell performance. The goal of this work is to develop a technique to measure cell performance over a relatively short amount of time (several hundred hours) which can indicate the long term cycle life of the cell. In this way, the impact of changes on the cell design can be tested without needing to cycle the cell until it fails which can

take many years. In order to understand the factors impacting the lifetime of Li-ion cells, the components (electrodes and electrolyte) and possible degradation mechanisms must be considered.

Chapter 2 introduces Li-ion cells and their components. The discussion includes different materials used as both positive and negative electrodes as well as different salts and solvents used for electrolyte. The chapter ends by discussing basic electrochemical testing and properties of lithium-ion cells.

Chapter 3 discusses possible degradation mechanisms that can occur in a Li-ion cell. These parasitic reactions convert active lithium (lithium which is available to be inserted into or removed from either the positive or negative electrode) to inactive lithium (lithium which has reacted to form a product where the lithium can no longer be inserted into an electrode) in the cell. This decrease in the supply of active lithium in the cell leads to capacity loss and the cell eventually becoming unusable.

Chapter 4 introduces high precision coulometry as a new approach for testing Li-ion cells. The requirements for these precision measurements will be explained and data will be presented to illustrate the importance of the technique. The instrument constructed by the author and his colleague, Aaron Smith, will be described in detail and its performance demonstrated.

Chapter 5 will review literature about electrolyte additives. There are countless experiments which have been conducted to show the impact of different additives on the performance and safety of cells with different types of electrode materials. Important experiments will be highlighted and discussed.

Chapter 6 will present work done on measuring the lifetime of cells with different combinations of electrolyte additives and electrode materials. This experiment confirms the power of high precision coulometry as well as shows the impact of different electrodes and electrolyte additives on cell performance.

Chapter 7 will summarize and conclude the thesis. It will also discuss possible future experiments and methods of testing that can be done in the field to further the work from this thesis.

Chapter 2 Lithium-ion Batteries

2.1 Electrode Materials

Considerations for electrode materials include the cost, cycle life, operating potential, and charge storage per unit mass and volume (gravimetric and volumetric specific capacity). The operating potential of an electrode material is determined by the chemical potential of the lithium atoms in the material. Therefore, based on Equation 1.1, it is desirable to have a positive electrode material where lithium is inserted at a high potential versus Li/Li^+ (low chemical potential of lithium when intercalated) and a negative electrode material with a low potential versus Li/Li^+ (high chemical potential of lithium when intercalated) resulting in a higher cell voltage and thus more energy storage for the same capacity. On the other hand, a material with higher specific capacity at the same operating voltage will also result in more energy storage in a cell.

Active materials for Li-ion batteries are often intercalation compounds since the structure of the host generally does not change greatly while lithium is intercalated and de-intercalated from the electrode during charge and discharge (cycling). However, some Li-ion batteries use materials that alloy with lithium at low potentials as negative electrodes. These alloy materials are normally silicon, tin or aluminum-based due to their high specific capacity; 3579 mAh/g for $Li_{15}Si_4$ [1,2], 994 mAh/g for $Li_{22}Sn_5$ [3,4], 993 mAh/g for LiAl and 2234 mAh/g for Al_4Li_9 [5]. Despite the low cost, low operating potential and high specific capacity of some alloy materials, they are plagued with volume expansion issues during the alloying process of up to 280% for silicon [6], which generally leads to poor cycle life. For this reason, alloy materials only make up a small percentage of negative electrodes in use today. The Sony Nexelion cell is currently the only cell being manufactured with a Sn-Co-C alloy negative electrode [7].

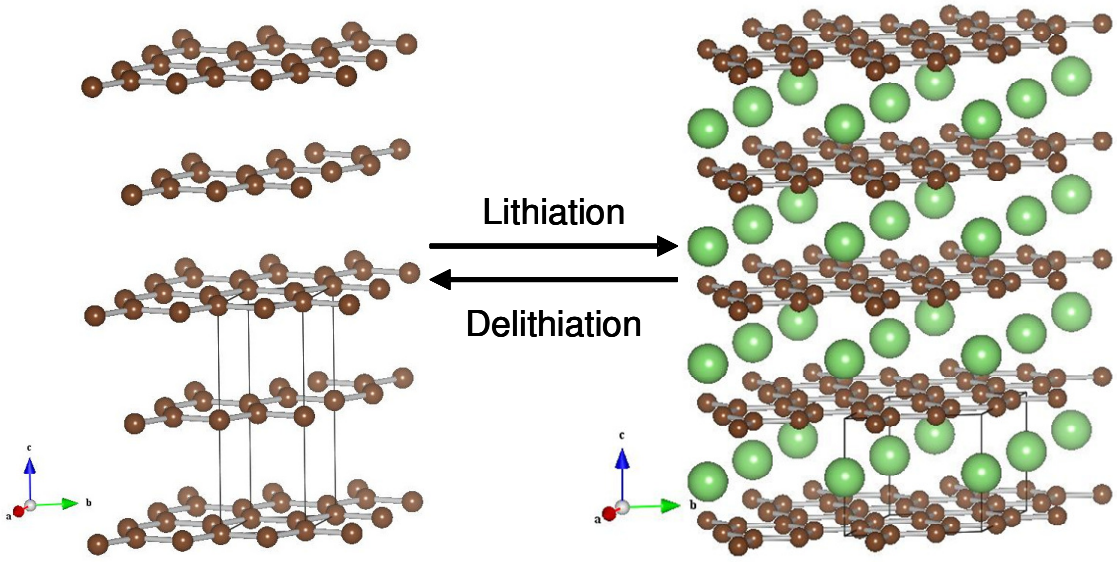

Figure 2.1 The structure of graphite in a fully lithiated and delithiated state. Carbon atoms are brown and lithium is shown in green.

The most common negative electrode material is graphite which has a theoretical specific capacity of 372 mAh/g [8]. Figure 2.1 illustrates the intercalation and de-intercalation of lithium ions between the sheets of graphite during cycling of a graphite electrode. This process is highly reversible and occurs at an average potential of 0.1 V versus Li/Li^+ and only results in about 10% volume expansion [9]. Graphite electrodes can intercalate and de-intercalate lithium for thousands of cycles. Another negative electrode intercalation material used is lithium titanate, $Li_4Ti_5O_{12}$ (LTO), which has a spinel structure where lithium is intercalated in a three dimensional network of tunnels rather than between sheets of atoms. Figure 2.2 shows the structure of LTO during cycling. While LTO has better cycle life capabilities than graphite, it is not often used commercially because it is expensive to produce, has a lower theoretical capacity than graphite (175 mAh/g) and an average potential about 1.4 V higher than that of graphite [10,11]. This leads to a more expensive cell with lower capacity, lower cell voltage and therefore less energy storage.

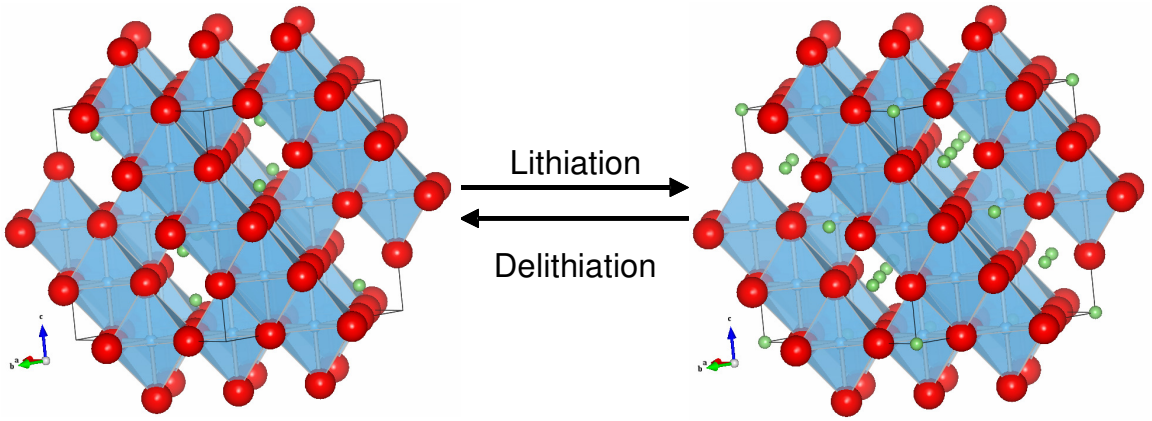

Figure 2.2 The structure of lithium tianate in a fully lithiated and partially delithiated state. The structure is in space group Fd-3m where lithium atoms (green) occupy the 8a sites in the delithiated state and 16c sites when the material is fully lithiated. Oxygen atoms (red) occupy 32e sites. The 16d sites are shown to be fully occupied by titanium atoms (blue) but 1/6 of these sites are actually randomly occupied by lithium leading to $Li_{1+x}[Li_{1/3}Ti_{5/3}]O_4$ ($0 \leq x \leq 1$).

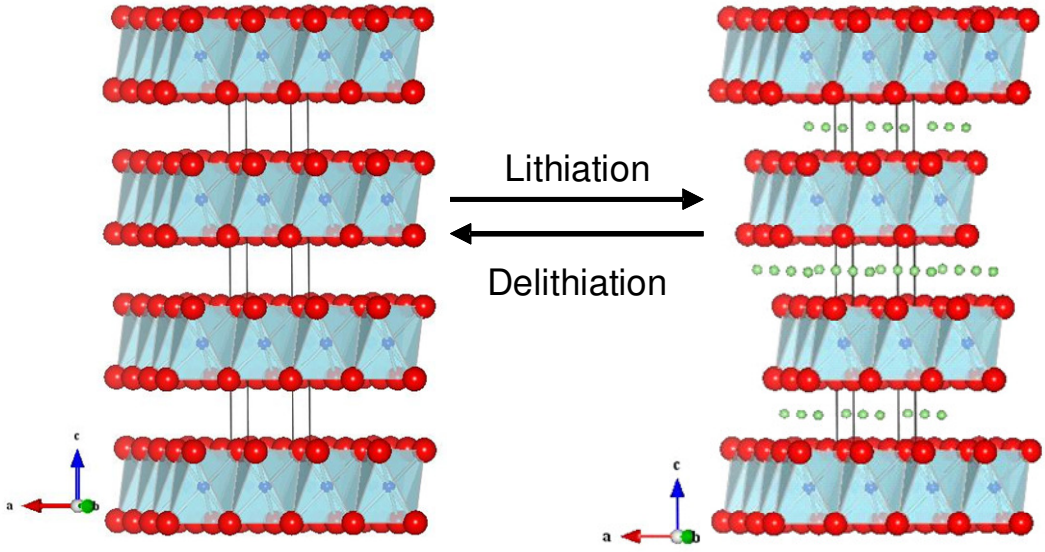

Figure 2.3 The structure of $LiCoO_2$ in a fully lithiated and fully delithiated state. Cobalt atoms are blue, oxygen atoms are red and lithium is shown in green.

Positive electrode active materials are generally layered metal oxides of the form $Li[M]O_2$ (M = Ni, Mn, Co, etc.) or spinel structured materials of the form LiM_2O_4 (M = Mn, Ni, Co, etc.). Figure 2.3 shows a layered oxide material during cycling where lithium is inserted and removed from between layers of atoms similarly to graphite. The spinel structured materials intercalate and de-intercalate lithium through tunnels as shown for LTO in Figure 2.2. Positive electrode materials generally have a lower theoretical capacity than negative electrodes. Commonly used positive electrodes include Li_xCoO_2 ($0.5 \leq x \leq 1$, 150 mAh/g [12]), $LiFePO_4$ (170 mAh/g [13]), $LiMn_2O_4$ (148 mAh/g [14]) and $Li[Ni_{1/3}Mn_{1/3}Co_{1/3}]O_2$ (NMC) (163 mAh/g to 4.3 V vs. Li/Li^+ [15]). Other variants of these common materials such as $LiNi_{0.5}Mn_{1.5}O_4$ [15,16] or $Li[Ni_{0.4}Mn_{0.4}Co_{0.2}]O_2$ [17,18] are also used but not as frequently.

2.2 Electrolytes

In addition to the two electrodes, the third component of a Li-ion cell is the electrolyte. The electrolyte contains a lithium salt dissolved in a combination of solvents. The most commonly used lithium salt is lithium hexafluorophosphate ($LiPF_6$) due to is high conductivity (10^{-2} S/cm), high lithium ion transference number (≈0.35) [19] and relatively low corrosion of aluminum at the high potentials associated with the positive electrode [20] when used with standard solvents mixtures. However, $LiPF_6$ can form hydrofluoric acid in the presence of water which can lead to reduced cell life. Other lithium salts have been studied to investigate the possibility of replacing $LiPF_6$ or for use as an additive such as lithium tetrafluoroborate ($LiBF_4$), lithium bis(oxalato)borate (LiBOB) and lithium (bis) trifluoromethanesulfonimide ($(LiN(SO_2CF_3)_2$ called HQ115) [20-22].

The solvents used are carbonates such as ethylene carbonate (EC), diethyl carbonate (DEC), ethyl methyl carbonate (EMC), propylene carbonate (PC) and dimethyl carbonate (DMC) [23,24]. The use of these carbonates allows for high concentrations (greater than 1 M) of dissolved lithium salt to be solvated. Figure 2.4 shows the

molecular structures of these common solvents. Often the solvent used in the electrolyte is a mixture of the above solvents such as EC:DEC (1:2 v:v) or EC:EMC (3:7 v:v).

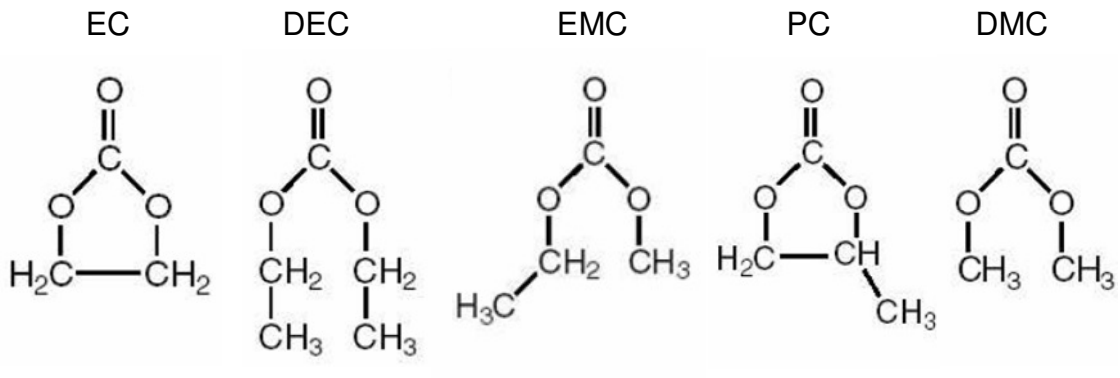

Figure 2.4 The structure of several commonly used carbonates for electrolyte solvents.

In addition to the lithium salt and solvents, very often electrolyte additives are used for any number of possible benefits. Purposes, benefits and examples of electrolyte additives will be discussed in Chapter 5.

2.3 Basic Electrochemical Behavior

Lithium-ion cells made in industry are normally one of two designs: wound or stacked cells. These different constructions can be cased in cylindrical, prismatic or pouch enclosures. Figure 2.5 shows a schematic of a cylindrical wound cell (18650 style, 18 mm diameter and 65 mm length) and its components. While the design of other cells is slightly different, the operation is fundamentally the same. Typically, cells are made with electrode material coated on both sides of their respective current collectors. These electrodes are often compressed to increase density. Alternating layers of the double sided positive and negative electrodes are stacked with a separator in between each layer. The separator must electrically isolate the two electrodes but allow lithium ions to be transported between the electrodes. Generally separators are made of porous polypropylene, polyethylene or a combination of the two materials. The separator acts as an insulator between the electrodes but allows lithium ions to move through the pores.

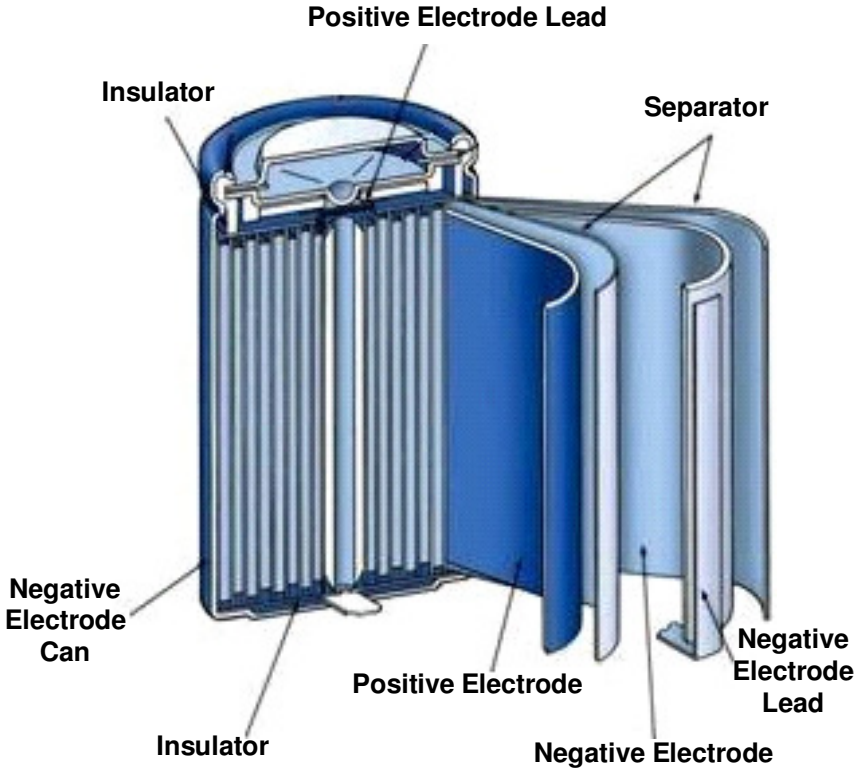

Figure 2.5 The components and design of a cylindrical wound cell.

This stack of electrode material and separator is then made to fit the specified cell design. For wound cells, the stack is wound around a drive pin as is the case with cylindrical cells, until it reaches the desired dimensions. In stacked cells, the stack continues with layers of separator and electrodes until reaching the specified thickness. Electrolyte is then added as the final component of the cell. This method of making cells works well on an industrial scale, but would not be practical for initial studies of materials or electrolytes and additives on a small lab scale. Therefore, smaller coin-type cells are often used for experimental purposes.

Coin-type cells are composed of the same basic components (electrodes on current collectors, separator, electrolyte and casing) as commercial cells. However, coin-type cells use a disk (about 1.25 cm^2) with electrode material coated on only one side of the current collector, a slightly larger area separator and another similarly sized counter electrode. This other electrode can be another lithium insertion material to construct a "full cell" or a lithium disk making a "half cell". A full cell refers to a cell with two

intercalation electrodes and no reference electrode such as a commercial cell, while a half cell has lithium as a common counter/reference electrode to better examine the behavior of the working electrode. Figure 2.6 shows the components of a coin-type cell including a spring and spacer to apply a constant pressure across the electrodes when the cell is sealed. Coin-type cells have the advantages of being cheaper and easier to make with smaller amounts of electrolyte solvents, salts and additives used per cell. Half cells allow the potential of a single electrode to be measured as a function of the amount of lithium in the host material (state of charge) which can be studied to gain understanding of the material or the impact that changing components of the electrolyte has on that material.

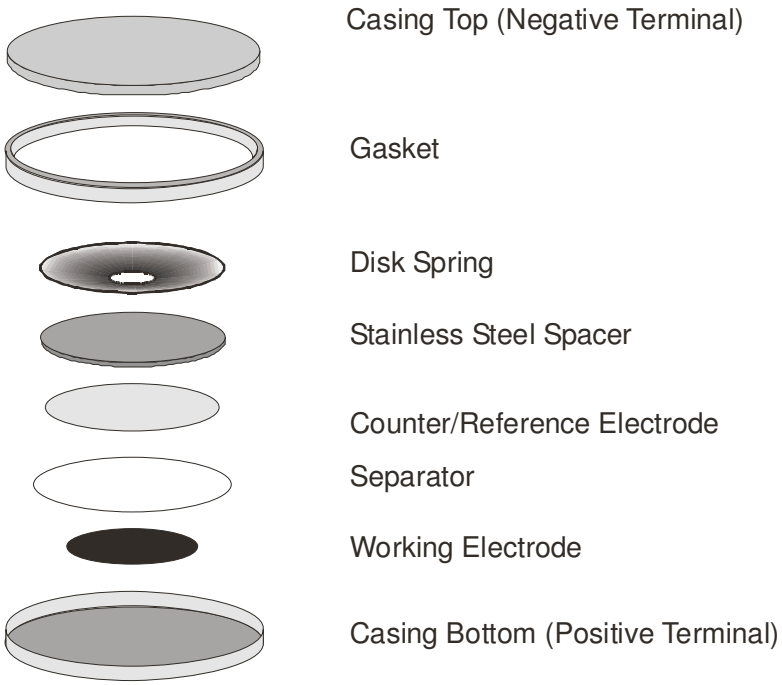

Figure 2.6 The components used in a coin-type cell.

The charge of a half cell is the process during which the lithium is being removed from the host material (so the potential versus Li/Li^+ increases) and the discharge is when lithium is being inserted with the host material (so the potential decreases). As the cell cycles between two voltage limits, the voltage is measured as a function of time. Since the current flowing through the cell is known (and is often constant), the time axis can be converted to capacity as,

$$Q = \int I(t) * dt = I * t \qquad 2.1$$

where I is the constant applied current and t is the measured time of the half cycle (charge or discharge). Figure 2.7 shows NMC, LTO and graphite half cell voltage curves for the first cycle. By convention, the capacity increases during charge and decreases during discharge for positive electrodes while for negative electrodes, the capacity increases during discharge and decreases during charge. This convention allows comparisons to a full cell as the charge of a full cell (increasing capacity) occurs while lithium is being removed from the positive electrode (increasing its potential) and inserted into the negative electrode (decreasing its potential). This leads to an increase in cell voltage during charge as energy is required to move lithium ions from the positive electrode to negative electrode.

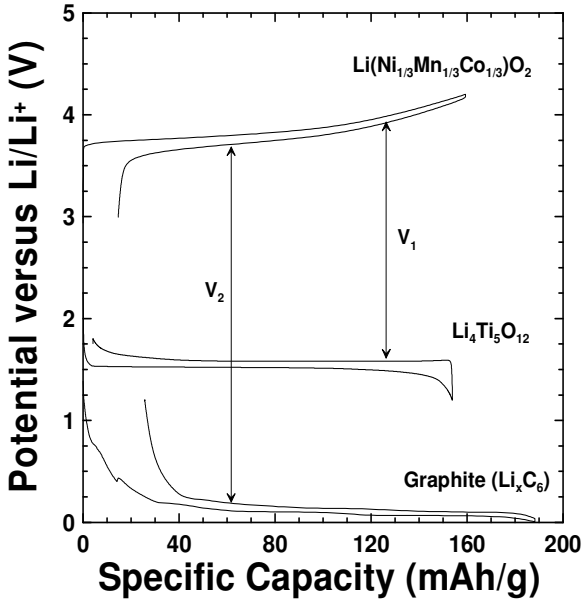

Figure 2.7 The voltage versus specific capacity for different types of electrodes tested in coin-type half cells. The capacity axis for the graphite electrode is divided by two.

The arrows in Figure 2.7 represent the full cell voltages (difference between positive and negative electrode potentials) during the discharge of a NMC/LTO (V_1) or

NMC/graphite (V_2) full cell. Figure 2.7 shows how a higher full cell voltage can be achieved by increasing the operating potential of the positive electrode or lowering the operating potential of the negative electrode. The voltage of a NMC/LTO cell is significantly less than that of a NMC/graphite cell since the operating potential of LTO is higher than that of graphite. Figure 2.7 shows that the full cell voltage depends on the state of charge of the cell as the positive electrode potential varies as a function of lithium content. Since high cell energy is desirable for commercial cells, work is being done to find positive electrode materials with higher average operating potentials to increase cell voltage.

Proper interpretation of a voltage curve is critical to understanding the material or system being studied. When looking at the data for a Li/NMC half cell in Figure 2.7, the capacity of the cell does not return to zero on the x axis when the cell is discharged to 3.0 V. This shift to the right in the voltage curve (referred to as electrode slippage) can continue with cycling and is a consequence of parasitic reactions which decrease the supply of active lithium during cycling [25-27]. This electrode slippage during the first cycle is referred to as irreversible capacity loss. The irreversible capacity loss of a cell comes from the reactions which cause electrode slippage with each cycle as well as other reactions within the cell such as reactions with impurities in the electrolyte. The irreversible capacity is generally much larger than the subsequent electrode slippage per cycle. The data shown in Figure 2.7 was collected from a half cell where the lithium foil counter/reference electrode acts as a large source of lithium relative to the amount of lithium transferred during a charge or discharge. Therefore, this loss of active lithium does not lead to a loss of capacity during cycling, known as capacity fade, as there is always lithium available from the lithium electrode to fully lithiate the material during each discharge.

Figure 2.8a shows the voltage versus capacity for a Li/NMC half cell over 12 cycles. Due to the excess lithium, these parasitic reactions cause a continual slip of the voltage versus capacity curve to the right where the slippage at the top of charge (charge endpoint slippage) and bottom of discharge (discharge endpoint slippage) should be identical so that the discharge (Q_D) and charge (Q_C) capacity are constant during cycling. Figure 2.8a highlights the difference between the irreversible capacity loss compared to

the slippage per cycle. If no parasitic reactions occurred during cycling, there would be no electrode slippage so the charge and discharge capacities would be identical. However, in a positive electrode half cell the discharge capacity is always shorter than the charge capacity by the amount of slippage during that cycle. Therefore, the ratio of the two capacities (where the discharge is immediately after the charge), known as the coulombic efficiency (CE),

$$CE_{Positive} = \frac{Q_D}{Q_C}, \qquad 2.2$$

will always be less than 1.0000 and must be an important quantity to measure. A CE closer to 1.0000 indicates decreased slippage meaning less parasitic reactions are occurring.

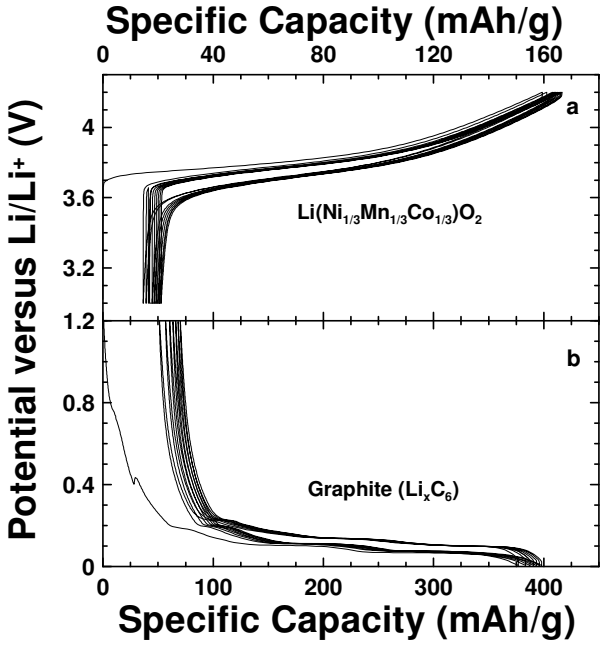

Figure 2.8 Panel a) shows the potential of an NMC electrode in a half cell over 12 cycles between 3.0 and 4.2 V. Panel b) shows the potential of a graphite electrode in a half cell over 8 cycles between 0.005 and 1.2 V

The same analysis can be done with a negative electrode half cell such as a Li/graphite half cell. Figure 2.7 shows the first cycle for a Li/graphite half cell where the

voltage curve does not return to zero on the x-axis when the voltage reaches 1.2 V. This means that not all of the lithium that was transferred to the graphite electrode during a discharge was removed during the following charge because some was converted to inactive lithium as parasitic reactions occur. These parasitic reactions are different from those that occur in a positive electrode half cell since they depend on the potential of the electrodes. Some active lithium is converted to inactive lithium during each cycle as the solid electrolyte interphase (SEI) forms on the negative electrode. This first cycle slippage, again referred to as irreversible capacity, comes from the initial formation of the SEI as well as reactions with impurities in the electrolyte. The SEI forms due to reactions between active lithium at the low potential of the negative electrode and solvent to form LiO_2, LiF, Li_2CO_3, polyolefins and semicarbonates on the surface of the graphite electrode [28]. Therefore when lithium reacts to form these products, it is no longer available to be shuttled between the positive and negative electrode during cycling and has thus become inactive lithium in the cell.

SEI forms on other electrode materials but SEI on graphite electrodes has been extensively studied since graphite is the most common electrode material. Also the SEI on the negative electrode is thicker than that which forms on the positive electrode. The SEI continues to grow with cycling but as the layer on the surface of the electrode gets thicker, the growth rate slows [26]. The parasitic currents associated with the growth and formation of the SEI are larger than any other parasitic reactions occurring in the cell causing it to be the main reason for capacity loss in full cells [29].

In a half cell the lithium removed from the supply of active lithium due to parasitic reactions does not result in capacity fade because the electrode can be fully lithiated during each discharge with lithium from the lithium electrode. Figure 2.8b shows 8 cycles of a Li/graphite half cell showing the continual slippage of the voltage curve with cycling. Once again the much larger irreversible capacity compared to the slippage per cycle in later cycles can be seen in this figure. This slippage continues as the SEI grows which will be shown in Chapter 3. The slippage at the top of charge and bottom of discharge will be identical resulting in the half cell cycles with no capacity fade. The CE of a negative electrode half cell is calculated as the ratio of charge to

previous discharge capacity to correspond to the processes occurring during a full cell discharge and charge,

$$CE_{Negative} = \frac{Q_C}{Q_D} . \quad 2.3$$

Since the charge capacity is less than the previous discharge capacity for a Li/graphite half cell, the CE is also less than 1.0000 meaning that parasitic reactions are occurring during cycling.

Half cells can help better understand the behavior of electrodes while being tested in simpler conditions than full cells. A full cell voltage curve comes from the difference between the positive and negative electrode voltage curves at the given state of charge. The positive and negative electrode masses in a full cell are generally balanced to account for the differences in specific capacity between positive and negative electrode materials. The charge and discharge slippage in a full cell can occur at different rates as different parasitic reactions occur at the two electrodes. However, since the full cell has a limited supply of lithium, based on the amount of lithium in the positive electrode and electrolyte when constructed, this decrease in the supply of active lithium will lead to capacity fade.

Figure 2.9 shows the voltage versus capacity curve, coulombic efficiency and discharge capacity versus cycle number for a full cell over 24 cycles. The charge and discharge slippage are clearly different in this cell which leads to capacity loss with cycling. Since parasitic reactions occur during cycling, the discharge of a full cell will always be shorter than the previous charge, so the CE will again be less than 1.0000,

$$CE_{Full-Cell} = \frac{Q_D}{Q_C} . \quad 2.4$$

Lithium-ion cells do not cycle indefinitely because of parasitic reactions which can deplete the supply of active lithium or electrolyte from a cell. A lithium accounting model keeping track of all lithium used for cycling as well as involved in parasitic reactions can allow for an understanding of what types of reactions result in the measured values of slippage, fade and CE. Information about cell degradation gained through this

type of model will lead to a better understanding of how changes to a cell, such as electrode materials or electrolyte salts, solvents or additives, impact these parasitic reactions and affect the performance and lifetime of the cell.

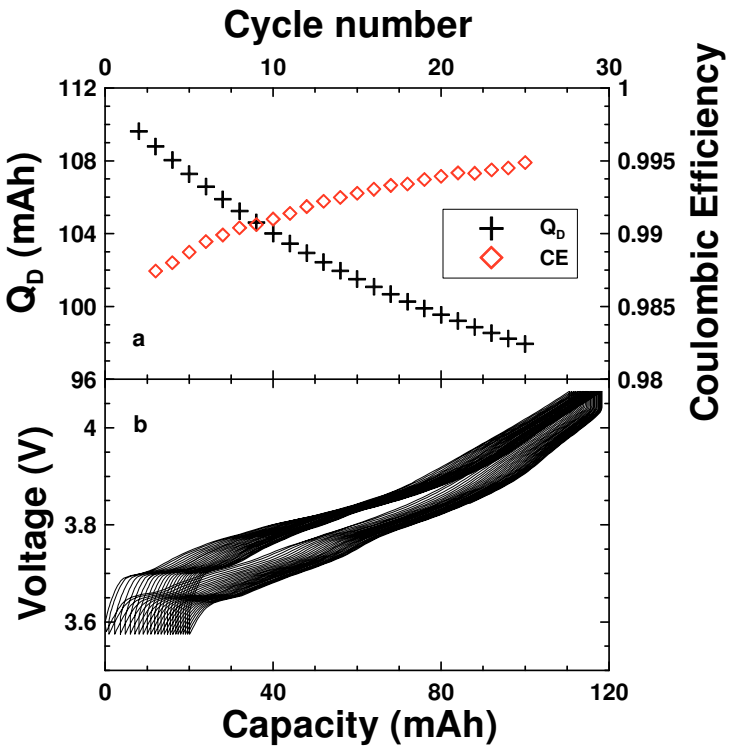

Figure 2.9 Panel a) shows the discharge capacity (left) and coulombic efficiency (right) versus cycle number of a $LiCoO_2$/graphite wound prismatic cell over 24 cycles with constant charge and discharge currents, corresponding to a full charge or discharge in 10 hours (C/10), charge and discharge between 3.575 and 4.075 V. Panel b) shows the voltage versus capacity for the same cell over 24 cycles showing different rates of charge and discharge endpoint slippage.

Chapter 3 Possible Mechanisms Leading to Cell Degradation

Parasitic reactions in Li-ion cells convert small amounts of active lithium to inactive lithium during each cycle. In order to understand how different parasitic reactions can lead to eventual cell failure, possible mechanisms must first be identified. The reactions associated with these mechanisms can then be examined to understand how lithium is removed from the limited supply of active lithium in the cell and how the decrease in active lithium can be detected in electrochemical tests, primarily cell cycling. The main proposed mechanisms that lead to cell degradation by depleting the supply of active lithium, undesirably transferring charge within a cell or damaging the electrolyte are:

- Lithium reacting at the negative electrode leading to the formation, growth or repair of the solid electrolyte interphase (SEI).
- Oxidation of solvent molecules at the high potentials of the positive electrode resulting in depletion of lithium salt or solvent molecules from the electrolyte or a continuous shuttle mechanism moving charges within the cell.
- Dissolution of transition metals from the positive electrode that can migrate and deposit on the negative electrode.
- Damage to the positive electrode limiting future lithiation and delithiation of the electrode.

3.1 The Solid Electrolyte Interphase

While lithium is intercalated and deintercalated from graphite during cycling or storage of a Li-ion cell, some of the active lithium is used to form or modify the SEI. Although the existence of this film is well known, the formation and components of the film are not completely characterized as they depend on the electrode material [30], electrolyte and additives used [31,32], cell temperature [33], etc. The components of

the film contain lithium which is irreversibly lost from the supply of active lithium in the cell. Since the SEI is electronically insulating, electrolyte must be able to diffuse through the surface film to be close enough to the electrode to react with electrons that can tunnel through the insulating layer.

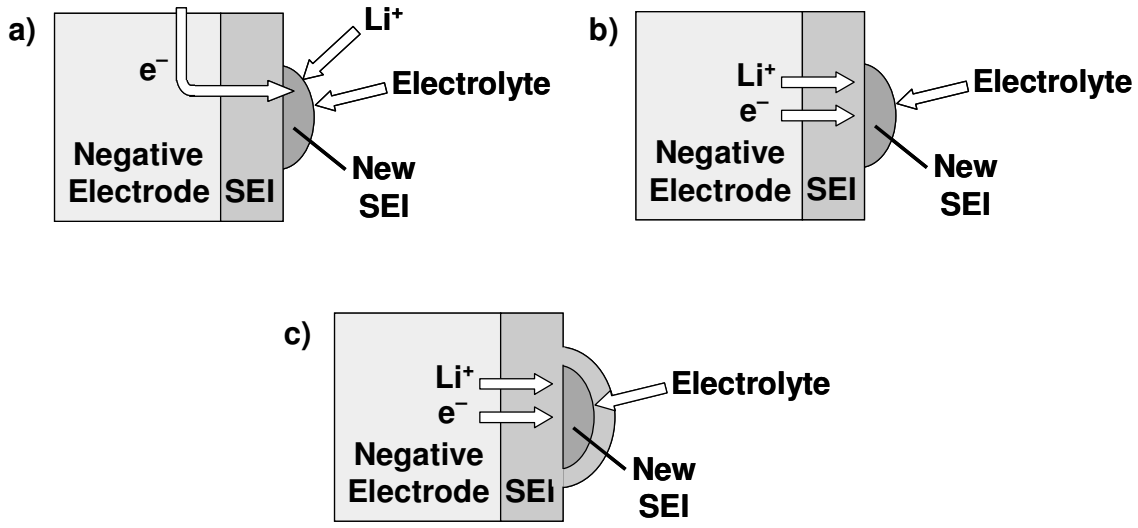

Figure 3.1 Possible SEI growth mechanisms that remove active lithium from the electrolyte (a) or negative electrode (b, c).

Figure 3.1 shows possible growth mechanisms of the SEI resulting in depletion of the supply of active lithium. Figure 3.1a shows the scenario where Li^+ from the electrolyte combines with an electron from the negative electrode to form SEI on the surface of the existing layer. In this scenario, the electron must come through an external circuit as Li^+ is removed from the positive electrode. Figure 3.1b illustrates the possibility of SEI growth where both the Li^+ and e^- come from the negative electrode to react at the surface of the SEI. Figure 3.1c is similar to 3.1b however the SEI can grow not only on top of the existing layer as the electrolyte can diffuse to react closer to the surface of the electrode [34].

In order to discuss the impact of these mechanisms, assume a cell is being cycled with a constant applied charge and discharge current (magnitude equal to I_A) between two specified voltages. The time of a half cycle (t) is measured to give the resulting cell capacity (Q_0),

$$Q_0 = \int I(t) * dt = I_A * t \quad . \tag{3.1}$$

The transfer of electrons and Li^+ to the SEI can be treated as an effective parasitic current, I_{Li}, always flowing in the cell. Therefore, the amount of charge lost to the SEI during each half cycle, q_{Li}, can be calculated using an average parasitic current, I_{Li}^{Ave}, over the time of a half cycle,

$$q_{Li} = \int I_{Li}(t) * dt = I_{Li}^{Ave} * t \quad . \tag{3.2}$$

This effective current flow decreases over time as the growth rate of the SEI slows as the layer thickens [26]. Equations 3.1 and 3.2 can be combined to give,

$$q_{Li} = Q_0 \frac{I_{Li}^{Ave}}{I_A} \quad . \tag{3.3}$$

3.2 Electrolyte Oxidation and Shuttle Mechanisms

Electrolyte oxidation can occur at the high potentials of the positive electrode in a Li-ion cell. As discussed in Chapter 2, higher energy cells can be achieved by increasing the potential of the positive electrode, but this increases the rate of electrolyte oxidation as it is a potential-dependent reaction. The rate of electrolyte oxidation also depends on many other factors such as type of electrode material [35,36], electrolyte composition, types of films formed of surfaces [24], cell temperature [25], etc.

Figure 3.2 shows possible reactions which can occur at the positive electrode that are classified as electrolyte oxidation and shuttle-type mechanisms. These processes can occur during cycling or while the cell is at open circuit. Figure 3.2a shows that if a reduced solvent molecule that has migrated from the negative electrode or an anion from the salt (ie PF_6^-) is oxidized at the positive electrode, some oxidation product could be left on the surface of the positive electrode and a Li^+ is removed from the electrolyte to keep charge neutrality and is inserted into the negative electrode. The insertion of Li^+

into the negative electrode can only occur if there is an external circuit for the electron from the positive electrode to travel to the negative electrode. Figure 3.2b shows how Li^+ can be intercalated into the positive electrode to combine with the electron from the oxidation reaction similar to that occurring in Figure 3.2a. This process does not involve the negative electrode so it can occur under open circuit conditions and leads to a decrease in open circuit potential since the potential of the positive electrode decreases with increasing lithiation. This decrease in cell voltage at open circuit is referred to by some researchers as self-discharge.

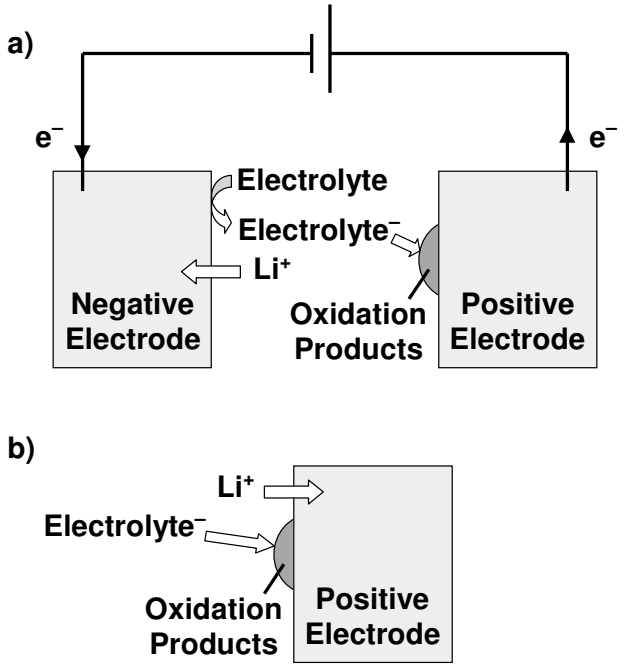

Figure 3.2 Possible electrolyte oxidation reactions that remove active lithium from the electrolyte which is inserted into the negative (a) or positive (b) electrode. In this scenario, the "Electrolyte$^-$" is either a solvent molecule in the reduced form or an anion from the salt.

Both of these processes remove active Li^+ from the electrolyte which when sufficiently depleted will lead to increased impedance in the cell and eventually cell failure. Similarly to SEI growth, this transfer of charge can be written with an associated average current over a half cycle, I_{ox}^a, and charge lost from the cell during the half cycle, q_{ox}^a,

$$q_{ox}^{a} = Q_0 \frac{I_{ox}^{a}}{I_A} \quad . \tag{3.4}$$

Figure 3.3 shows examples of other types of mechanisms known as shuttle-type mechanisms which do not decrease the active supply of lithium in the cell but only transfer charge between electrodes [37]. Figure 3.3a shows how an electrolyte molecule can be oxidized at the positive electrode and the radical cation transported to the negative electrode where it can be reduced back to its original form with electrons flowing through an external circuit. This results in charge transfer without the loss of active lithium which can be highly reversible for certain molecules [38]. Figure 3.3b shows how, under open circuit conditions, a shuttling of electrolyte can remove lithium from the negative electrode which results in Li^+ being intercalated into the positive electrode to keep charge neutrality leading to self-discharge. However, it is likely that the reduction product remains at the negative electrode through a reaction with the electrolyte.

Figure 3.3c shows that an oxidized solvent molecule can migrate to the negative electrode and be reduced leaving a reduction product on the surface. In this case, an electron can travel through the external circuit to participate in the reduction reaction at the negative electrode. Figure 3.3d shows that if reduction products are formed at the negative electrode under open circuit conditions, Li^+ can be removed from the negative electrode and intercalated into the positive electrode based on charge neutrality leading to self-discharge. Figure 3.3e shows a reaction that leaves a polymerized species on the positive electrode. This reaction involves a proton transporting through the electrolyte to the negative electrode where it can be reduced to hydrogen gas. This reaction also moves Li^+ to the positive electrode and can occur at open circuit. The movement of charge through these shuttle type reactions can have an associated average current flowing during charge and discharge, I_{ox}^{b}, and therefore a charge, q_{ox}^{b}, associated with these types of reactions,

$$q_{ox}^{b} = Q_0 \frac{I_{ox}^{b}}{I_A} \quad . \tag{3.5}$$

The impact of oxidation of electrolyte solvent is the depletion of solvent from the electrolyte. If all solvent molecules become oxidized they can no longer solvate the salt which will lead to eventual failure of the cell. This impact is not seen in early cycling but only appears as a larger portion of the solvent molecules become oxidized.

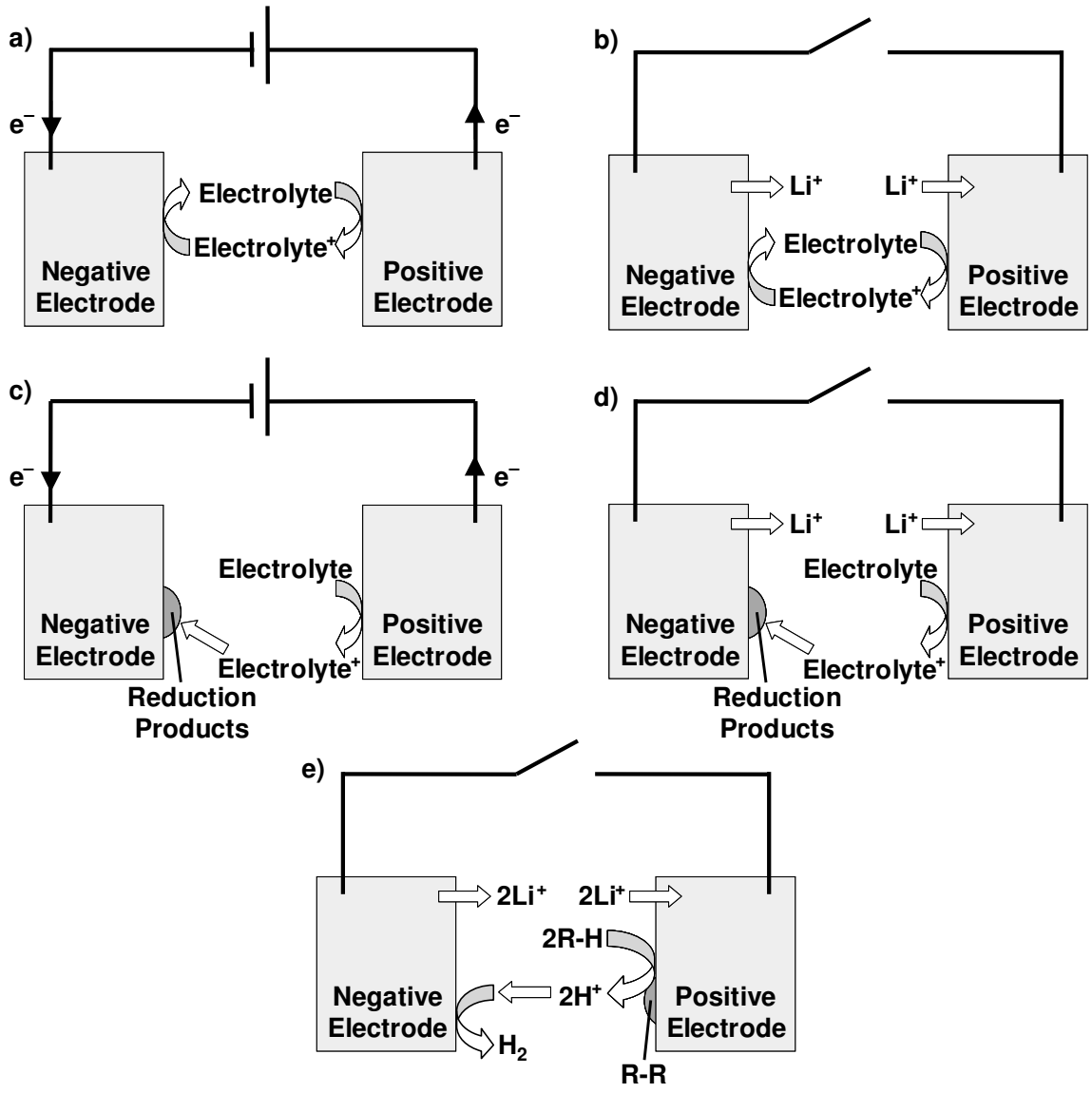

Figure 3.3 Possible shuttle type oxidation reactions that do not remove active lithium from the cell and can run during cycling (a, c) or open circuit (b, d. e) conditions.

3.3 Transition Metal Dissolution

In order to keep charge neutrality in positive electrode materials during delithiation, transition metals are oxidized. As the potential of the positive electrode versus Li/Li^+ increases during delithiation, the transition metal cations in the electrode become highly oxidized and can dissolve into the electrolyte. The resulting structural change in the positive electrode material or damage to the SEI can result in poor cell performance and capacity fade as the delithiation can eventually become limited if all cations reach their highest oxidation state. Transition metal dissolution has been observed with numerous positive electrode materials with the severity depending on the positive electrode potential and oxidation state of the cations [39-42]. Figure 3.4 shows metal ions dissolving from the positive electrode in the presence of an external circuit as well as during open circuit. Figure 3.4a shows the transfer of electrons from the positive to negative electrode through an external circuit to account for charge imbalance with the dissolution of the oxidized metal ions. Figure 3.4b shows the transfer of lithium from the negative to positive electrode under open circuit conditions leading to self-discharge. A certain number of oxidized metal ions, M^{2+}, dissolve during each half cycle and are able to migrate and deposit on the negative electrode. This process does not remove active lithium from the cell but only transfers charge from one electrode to the other. For this reason, the impact of transition metal dissolution can be combined with the I_{ox}^{b} and q_{ox}^{b} terms in Equation 3.5.

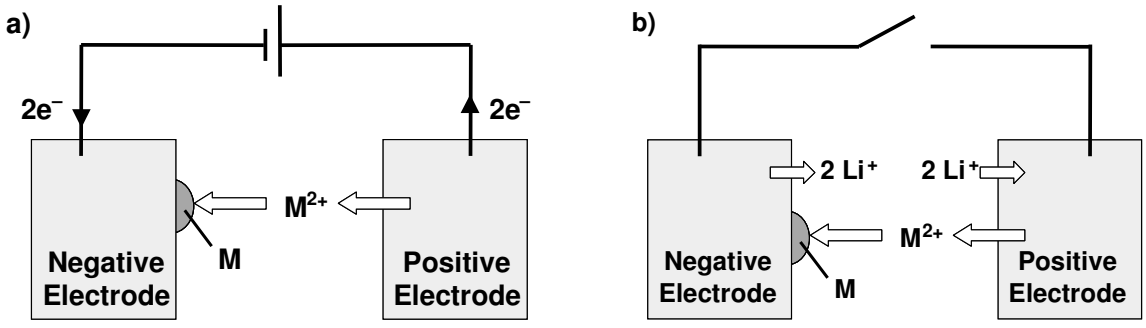

Figure 3.4 Possible transition metal dissolution mechanisms which only transfer charge in a cell during cycling (a) or open circuit (b) conditions.

3.4 Positive Electrode Damage

During cycling, the intercalation and deintercalation of lithium into the electrode can cause volume and phase changes [41,43]. In severe cases, this mechanical strain on the electrode can lead to cracking and pieces of the electrode losing electrical connectivity with the rest of the electrode. This will limit the following cycle capacities as part of the electrode is no longer electrochemically active. Transition metal dissolution can also result in limited lithiation and delithiation if cations remaining in the electrode increase their average oxidation state. Transition metal dissolution is more likely the cause of positive electrode damage as the volume changes associated with lithiation and delithiation for these materials is relatively small. Therefore, some charge, q_p, is lost from the active supply of lithium in the cell during each half cycle due to such damage so an effective average current is flowing to give,

$$q_p = Q_0 \frac{I_p}{I_A}. \tag{3.6}$$

3.5 Summary of desired and parasitic reactions

The diagrams presented in this chapter show possible mechanisms that can occur to consume active lithium or transfer charge. These mechanisms can be written as different combinations of possible oxidation and reduction reactions occurring at both electrodes simultaneously. All possible reactions which can occur at the positive electrode are,

$$Li_x MO_2 \rightarrow Li_{x-\delta} MO_2 + \delta Li^+ + \delta e^-, \tag{3.7}$$

$$X^{Z+} \rightarrow e^- + X^{(Z+1)+}, \tag{3.8}$$

$$Li_x MO_2 \rightarrow \delta M^{2+} + 2\delta e^- + Li_x M_{1-\delta} O_2, \tag{3.9}$$

and

$$\delta Li^+ + e^- + Li_x MO_2 \rightarrow Li_{x+\delta} MO_2 . \quad 3.10$$

In all equations, X refers to a solvent molecule, M refers to a metal atom, Z is an integer value and δ is small. Equations 3.7 – 3.9 are oxidation reactions while Equation 3.10 is a reduction reaction. The possible reactions which can occur at the negative electrode are,

$$Li \rightarrow Li^+ + e^- , \quad 3.11$$

$$Li^+ + e^- \rightarrow Li , \quad 3.12$$

$$X^{Z+} + e^- \rightarrow X^{(Z-1)+} , \quad 3.13$$

and

$$M^{2+} + 2e^- \rightarrow M . \quad 3.14$$

Equation 3.11 is the oxidation reaction which occurs at the negative electrode while Equations 3.12 – 3.14 show possible reduction reactions.

The different scenarios that were depicted in this chapter come from combining a given reaction at the positive and negative electrode. The simplest example is charging a cell which combines the reaction in Equation 3.7 occurring at the positive electrode and the reaction in Equation 3.12 occurring at the negative electrode. A cell discharge comes from combining Equations 3.10 and 3.11. The growth of the SEI through solvent reduction comes from the combination of Equations 3.7 and 3.13 where lithium is deintercalated from the positive electrode but instead of being inserted into the negative electrode, charge is conserved by having a solvent molecule reduce at the negative electrode.

3.6 Accounting of Li^+ in a Li-ion cell during cycling

In order to understand the impact of these different parasitic reactions, the location all lithium atoms and ions present in a hypothetical Li-ion cell must be known at the end of each charge and discharge. First, assume that a cell has been assembled and cycled once so that the initial SEI layer has formed and the cell is in the discharged state

with no active lithium in the negative electrode. Then the location of all lithium that was initially in the cell can be denoted as:

Q_0 – The active lithium in the positive electrode

E – The Li^+ ions present in the electrolyte

S – Inactive lithium lost to the SEI formation and growth

$Q_0 + E + S$ – The total amount of lithium initially in the cell

The variables introduced here are in units of charge (coulombs or more commonly mAh).

Now as the lithium-ion cell is charged, lithium is transferred from the positive to negative electrode. However, all lithium may not be deintercalated from the positive electrode as some might be pinned associated with the q_p term. Not all lithium that is removed from the positive electrode is inserted into the negative electrode as the SEI film uses some charge to grow, q_{Li}. Additionally, some charges from the electrolyte can be intercalated into the electrodes from electrolyte oxidation, q_{ox}^a, during cycling. Table 3.1 shows the capacity during the first 1½ cycles based on the location of all charges in the cell (the impact of q_{ox}^b will be added later) given that the lithium content of the cell must be constant.

	After Single Cycle	First Charge (Q_C^0)	First Discharge (Q_D)	Second Charge (Q_C^1)
Electrolyte	E	$E - q_{ox}^a$	$E - 2q_{ox}^a$	$E - 3q_{ox}^a$
Pos. Electrode	Q_0	q_p	$Q_0 - 2q_{Li} - 2q_{ox}^a$	$3q_p$
Active Li in Neg. Electrode	0	$Q_0 - q_{Li} + q_{ox}^a - q_p$	0	$Q_0 - 3q_{Li} + 3q_{ox}^a - 3q_p$
SEI	S	$S + q_{Li}$	$S + 2q_{Li}$	$S + 3q_{Li}$
Sum	$E + Q_0 + S$	$E + Q_0 + S$	$E + Q_0 + S$	$E + Q_0 + S$
Cycle Capacity		$Q_0 + q_{ox}^a - q_p$	$Q_0 - 2q_{Li} + 2q_{ox}^a - q_p$	$Q_0 - 2q_{Li} + 3q_{ox}^a - 3q_p$

Table 3.1 Lithium accounting in the components of a Li-ion cell over the first 1½ cycles after the initial cycle.

From Table 3.1, the coulombic efficiency of the cell can be calculated,

$$CE = \frac{Q_D}{Q_C} = \frac{Q_0 - 2q_{Li} + 2q_{ox}^a - q_p}{Q_0 + q_{ox}^a - q_p} = 1 - \frac{2q_{Li}}{Q_0} + \frac{q_{ox}^a}{Q_0} \quad . \qquad 3.15$$

This calculation assumes that the amount of lithium trapped in the positive electrode is small relative to the amount of lithium lost to the SEI or removed from the electrolyte during electrolyte oxidation reactions. This assumption is valid as positive electrode materials made in half cells can cycle with no capacity loss over appropriate voltage ranges, indicating no damage to the electrode.

The charge slippage (Δ_C), discharge slippage (Δ_D) and fade per cycle can also be calculated from Table 3.1 along with the relationships with coulombic efficiency,

$$\Delta_C = Q_C^1 - Q_D = q_{ox}^a - 2q_p \quad , \qquad 3.16$$

$$\Delta_D = Q_C^0 - Q_D = 2q_{Li} - q_{ox}^a = Q_0(1 - CE) \quad , \qquad 3.17$$

and

$$Fade = Q_C^0 - Q_C^1 = \Delta_D - \Delta_C = 2q_{Li} - 2q_{ox}^a + 2q_p \quad . \qquad 3.18$$

Combining Equations 3.15 – 3.18 and Equations 3.3 – 3.6 results in measurable quantities expressed in terms of average parasitic currents. In these expressions the effect of the shuttle type mechanism, I_{ox}^b, can be incorporated because although lithium is not being lost with each half cycle, this mechanism increases charge capacity by $Q_0 I_{ox}^b / I_A$ and decreases discharge capacity by $Q_0 I_{ox}^b / I_A$. The resulting expressions are,

$$CE = 1 - \frac{2I_{Li} - I_{ox}^a + 2I_{ox}^b}{I_A} \quad , \qquad 3.19$$

$$\Delta_C = Q_0 \frac{I_{ox}^a - 2I_p + 2I_{ox}^b}{I_A} \quad , \qquad 3.20$$

$$\Delta_D = Q_0 \frac{2I_{Li} - I_{ox}^a + 2I_{ox}^b}{I_A} \quad , \qquad 3.21$$

and

$$Fade = Q_0 \frac{2I_{Li} - 2I_{ox}^{a} + 2I_p}{I_A} \quad . \qquad 3.22$$

Unfortunately, from this set of equations the parasitic currents cannot be directly solved by measuring the discharge slippage, charge slippage, fade and CE as the unknown variables outnumber the independent equations. However, careful measurements and analysis of these quantities can give a qualitative understanding of how the active lithium supply is decreasing during cycling.

3.7 Conclusion

Identifying these types of degradation mechanisms and understanding how they can be detected when testing a cell is an important step in learning about why cells perform differently. By understanding how different parasitic currents impact measurable parameters such as slippage rates and coulombic efficiency, comparisons about the rate of reactions between different cells can be made. However, these parasitic currents (< 1 μA) are very small and therefore the changes to cycling data are difficult to detect without proper equipment. Commercially available battery chargers are unable to make measurements with the accuracy needed to draw definitive conclusions about slippage rates and coulombic efficiency for high performance cells. For this reason, a High Precision Charger (HPC) was constructed at Dalhousie University [44] so all measured capacities are accurate enough to draw conclusions about slippage rates and coulombic efficiencies minimizing error from the testing equipment. The construction of this charger system was the beginning of the work done for this thesis with the goal of being able to measure coulombic efficiency with an accuracy of ±0.01%. The requirements for these types of measurements and the implementation of equipment in an attempt to reach these specifications are discussed in the following chapter.

Chapter 4 High Precision Coulometry

Careful measurements of charge and discharge capacity during cycling allow for accurate calculations of slippage rates, fade and coulombic efficiency. As discussed in the previous chapter, these quantities can give an indication of the mechanisms decreasing the active supply of lithium in the cell. The importance of coulombic efficiency measurements has been recognized in the past. For example, in 1995 Ohzuku et al. [45] stated that matched coulombic efficiencies for a positive and negative material would result in good cycle life in a full cell even if those coulombic efficiencies were not equal to unity. These cells would have excess electrolyte giving a larger supply of active lithium when assembled but as discussed in the previous chapter when enough of the active lithium in the electrolyte has been converted to inactive lithium the internal impedance of the cell will increase which will result in capacity loss.

Yi et al. [46] reported an increase in coulombic efficiency in half cells when using $LiNi_{0.4}Cr_{0.2}Mn_{1.4}O_4$ instead of $LiNi_{0.5}Mn_{1.5}O_4$ despite less capacity loss in the latter material. This confirms that coulombic efficiency and fade are not directly related and the relationship between them is not trivial as shown in Chapter 3. Li et al. [47] reported CE measurements for silicon/graphite/carbon composite electrodes which showed an improvement from 97.5% to 99% when using a mixture of LiBOB and $LiPF_6$ salts in place of either salt used alone.

In the papers discussed above, there is scatter in the coulombic efficiency measurements of at least ±0.5%. The High Precision Charger (HPC) [44] was developed so that coulombic efficiency could be measured accurately enough to detect difference in cell performance between cells of different chemistry that are made to last thousands of cycles. In order to differentiate between cells of this quality (perhaps with different additives), precision in coulombic efficiency measurements of at least ±0.01% is required. If a cell has a measured coulombic efficiency of 0.9999 ± 0.0001, in 1,000 cycles it would be expected that about 90% of the cells initial supply of active lithium and electrolyte would still be usable. The amount of active lithium and electrolyte still usable for the same cell after 10,000 cycles would be only 37%. If a charger could only measure

coulombic efficiency of a cell to be 0.999 ± 0.001, then that cell would be expected have degraded to 37% of its active lithium and electrolyte in only 1,000 cycles. The difference between 1,000 cycles and 10,000 cycles before degradation to 37% is important and thus reducing the error in the HPC to ± 0.01% was the design goal.

4.1 Requirements for High Precision Coulometry

Parameter	Associated Error	Desired Error in Q	For C/10 rate measurements	For C rate measurements
ΔI	**ΔQ = ΔI t**	**< 0.01%**	**ΔI < 0.01%**	**ΔI < 0.01%**
ΔV	**ΔQ = dQ/dV ΔV**	**< 0.01%**	**ΔV < 0.0001 V**	**ΔV < 0.0001 V**
Δt	**ΔQ = I Δt**	**< 0.01%**	**Δt < 3.6 s**	**Δt < 0.36 s**
ΔT	**ΔQ = dV/dT dQ/dV ΔT**	**< 0.01%**	**ΔT < 1 K**	**ΔT < 1 K**

Table 4.1 Factors that impact ability to precisely and accurately measure coulombic efficiency. These factors are current accuracy (ΔI), precision of voltage measurements (ΔV), time between voltage measurements (Δt) and cell temperature (ΔT) all which lead to error in capacity (ΔQ). For these calculations dQ/dV is taken as the full cell capacity in 1 V and dV/dT is assumed to be 100 μV/K.

In order to ensure measurements of capacity with a ±0.01% error, the possible sources of error must first be identified. Table 4.1 shows the that factors that need to be considered to ensure precise measurements are the accuracy of the applied current, the precision of the voltage measurements, the time between voltage measurements and the stability of cell temperature during cycling. In order to understand how error in current (ΔI), voltage (ΔV), time (Δt) and temperature (ΔT) will result in an error of ±0.01% in cell capacity assumptions about dQ/dV and dV/dT must be made. For these calculations, dQ/dV is assumed to be the full cell capacity in 1 V. This is reasonable as positive electrode materials generally have capacity above 3 V (vs. Li/Li^+) and as the potential of the positive electrode increases above 4 V, the rate of reactions such as electrolyte oxidation and transition metal dissolution can also greatly increase. Since graphite intercalates lithium over a 100 mV range, the change in full cell voltage between the charged and discharged state comes mainly from the positive electrode and is slightly greater than 1 V. Another quantity that must be assigned a value for these calculations is

dV/dT. Dahn and Haering [48] conducted experiments to measure dV/dT in Li/Li_xTiS_2 cells to learn about the entropy of the material. Their results showed that 100 μV/K is a reasonable value for dV/dT, so that will be used in these calculations.

Figure 4.1 shows hypothetical voltage versus time data for a cell approaching its lower voltage limit. The time between data points is Δt and each voltage measurement has an associated error of ΔV. Decreasing the time between measurements (smaller Δt) will allow for more voltage readings near the voltage limit allowing for a more accurate time measurement for that half cycle. A smaller error in the measured voltage will give a more accurate calculated capacity because then the measured voltage can be accurately compared to the desired voltage limit.

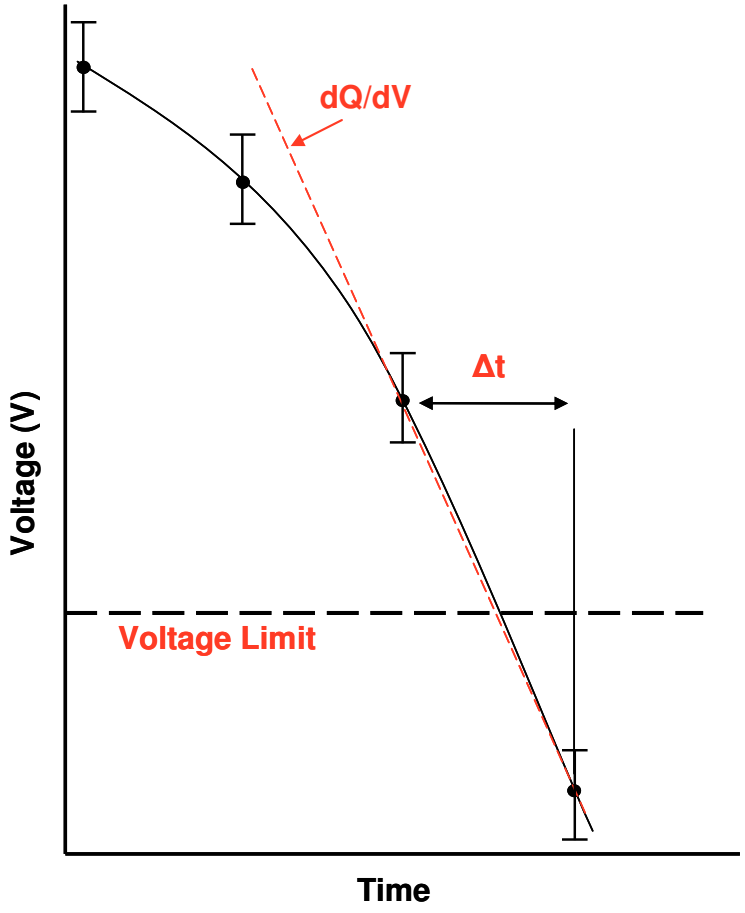

Figure 4.1 Hypothetical voltage versus time data as a cell is approaching the discharge voltage limit showing how the time interval between voltage measurements and error in voltage measurements can lead to errors in capacity.

Table 4.2 shows the quoted errors in different commercially available battery charger systems at the time of construction of the HPC (Sept. 2009). All of these values were obtained from manufacturers' websites or by direct contact with the companies. Based on the requirements given by Table 4.1, Table 4.2 shows that none of these commercially available systems are able to measure coulombic efficiency with an accuracy of ±0.01%. Some data found in literature with the least noise was collected on a Maccor system [6] but an exhaustive search was not conducted. However, based on the specifications of a Maccor 4000 series, the current requirement in Table 4.1 is not met and if a Maccor with a 5 V maximum voltage reading was acquired, the error in the voltage measurements would still be 1 mV which is an order of magnitude larger than required.

Manufacturer	Current resolution	Voltage resolution	Current accuracy	Voltage accuracy	Time between measurements
Maccor 4000 Series	**16 bit**	**16 bit**	**0.02-0.05% of full scale**	**0.02% of full scale**	**0.01 s**
Arbin BT2000	**16 bit**	**16 bit**	**0.02-0.05% of full scale**	**0.05% of full scale**	**0.1 s**
Bitrode MCV	**100 nA**	**100 µV**	**0.1% of full scale**	**0.1% of full scale**	**0.1 s**
Neware BTS-5V1mA	**16 bit**	**16 bit**	**0.05% of full scale**	**0.05% of full scale**	**5 s**
Lisun PCBT-100-32D	**0.1%**	**0.1%**	**< 0.5%**	**< 0.1%**	**1 s**
Land CT2001	**0.1%**	**0.1%**	**N/A**	**N/A**	**N/A**
Xeno WBCS 5000	**16 bit**	**16 bit**	**N/A**	**N/A**	**0.05 s**
Biologic VMP	**0.0003%**	**16 bit**	**0.05%**	**0.1%**	**0.02 s**
Dahousie HPC	**1 in 19,999 (0.005%)**	**10 µV**	**0.05% (over 1 year)**	**0.0025% of full scale**	**<1 s (by software interpolation**

Table 4.2 Specifications for commercially available battery cycling equipment obtained from the manufacturers. A 16 bit resolution corresponds to 1 part in 65,536 or 1 part in $10^{4.8}$. Even though a 16 bit device is used, the accuracy and stability may not be as good as 16 bits.

4.2 The High Precision Charger at Dalhousie University

The HPC at Dalhousie University was first built in a prototype phase in the fall of 2008. In the summer of 2009, the prototype was expanded to a forty channel system and by February 2010 an additional twenty channels were added. Figure 4.2 shows a photograph of the 60 channel HPC. Each channel of the HPC has a Keithly 220 or 6220 as a dedicated precision current source. These instruments are listed to have a current accuracy of ±0.05% over one year. However, it was found that careful and regular calibration (according to the manual) of the instruments allowed for performance better than the listed accuracy. Figure 4.3 shows the absolute value of the voltage across a resistor through which an alternating positive and negative current of the same magnitude was passed before (panel a) and after (panel b) calibration. The arrow in this figure represents 0.01%. Since coulombic efficiency is a ratio of the discharge and charge capacities, it is essential that the magnitude of the discharge and charge current is within the requirements specified in Table 4.1. Although the current accuracy listed in Table 4.2 is larger than 0.01% this accuracy the most important feature of the HPC. Another advantage to using the Keithley 220 and 6220 units is that they have a current range for each decade. Since the quoted 0.01% error is of the full scale for a range, having the range only cover one decade results in a much smaller error compared to systems where a single range can span multiple decades.

Ten of these channels with dedicated current sources make up what is considered to be one system on the HPC. Each of the six systems has one Keithley 2000-20 multimeter which can scan through the ten channels and read cell voltages with an accuracy of 10 μV in the 2 – 5 V range and 1 μV in the 0.2 – 1.99 V range. Therefore the voltage requirements in Table 4.1 are met with the use of these multimeters. Each system also has a control computer with in house Labview software interfaced to the instruments through IEEE connections. The software has the Keithley 2000-20 monitor the voltage on each of the ten channels in the system every five seconds. This time interval between measurements is too long according to Table 4.1 so analysis software (written in house in Visual Basic) extrapolates a line between the final data point collected before reaching the voltage limit and the data point collected just after the voltage limit in order to more

accurately calculate the exact time that the cell reached the specified voltage limit. Figure 4.1 shows this extrapolation as the line of slope dQ/dV. Also to ensure good timing resolution, cells on the HPC are always cycled at low rates (C/10 maximum).

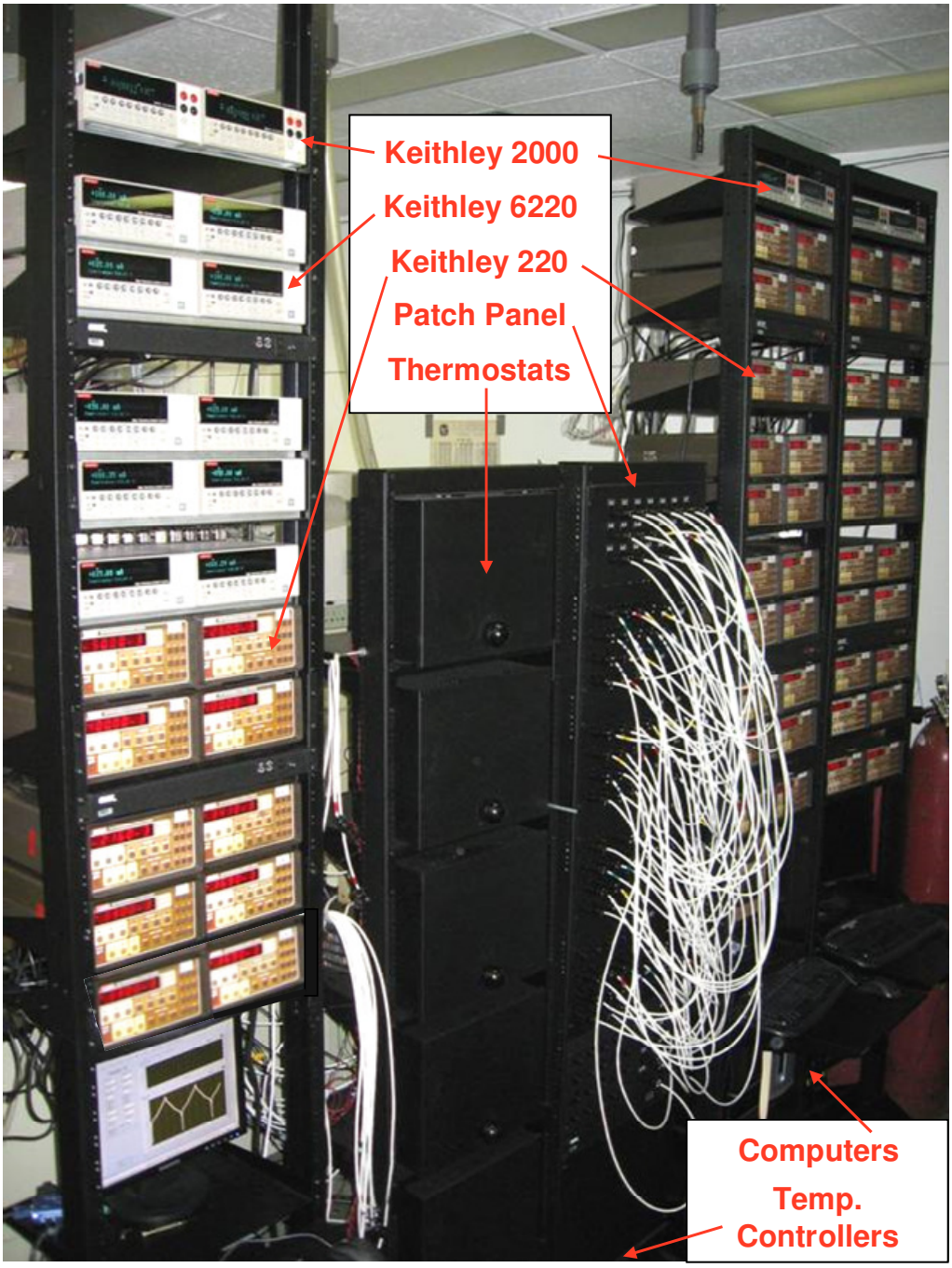

Figure 4.2 A photograph of the 60 channel High Precision Charger at Dalhousie University from March 2010.

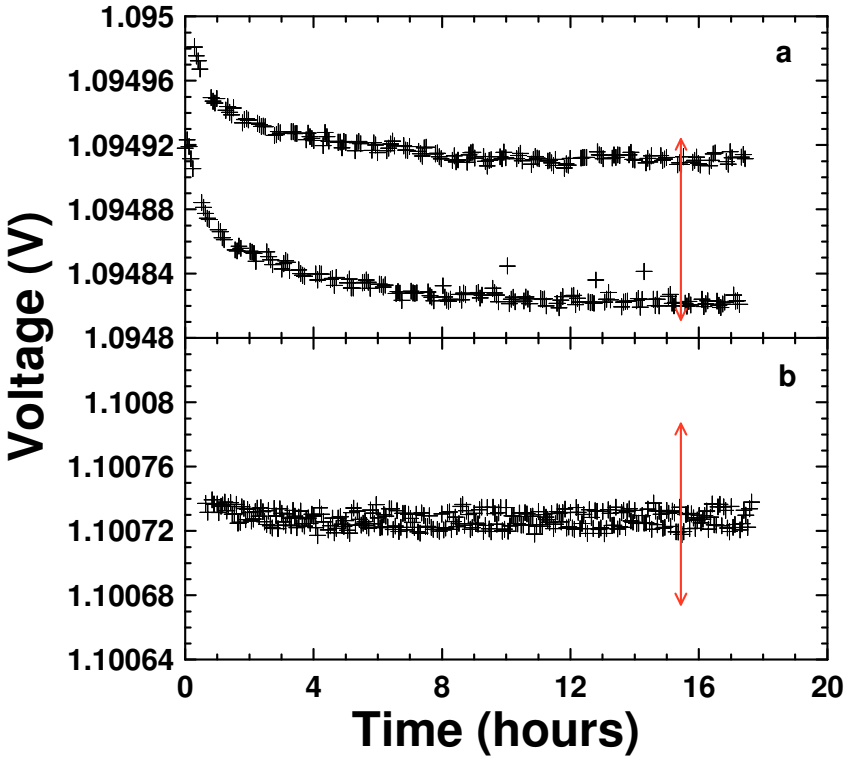

Figure 4.3 Panel a) shows absolute voltage across a resistor with alternating positive and negative currents of equal magnitude before calibration. Panel b) shows the same data for the channel after calibration. The red arrow in each indicates 1 part in 10,000.

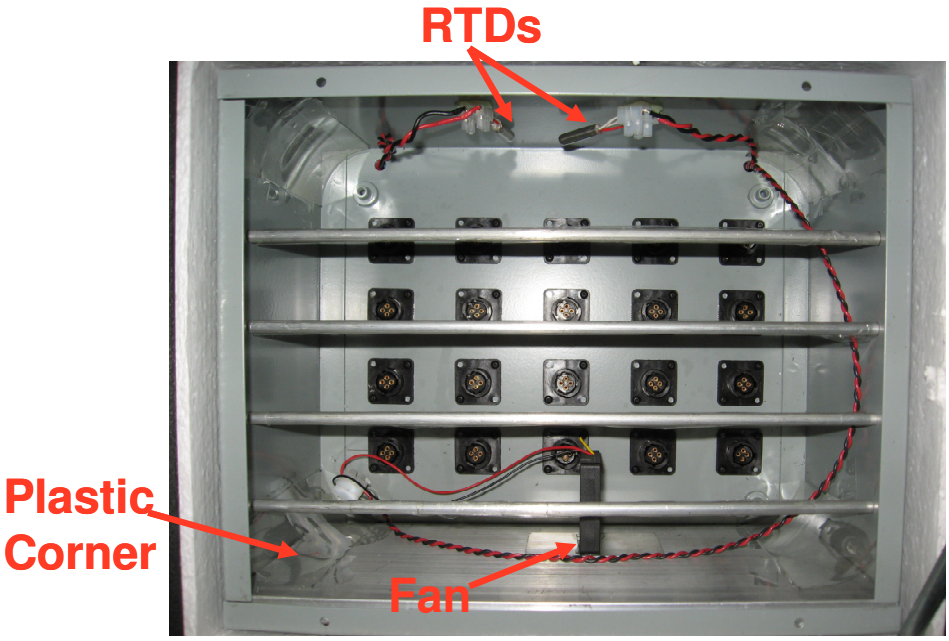

Figure 4.4 A photograph of the interior of a thermostat showing the temperature sensors, fans and "four-wire" connectors for cell holders.

Cells are connected in the thermostats seen in Figure 4.2 and through the "patch panel" so they can be connected to any channel on any of the six systems. This allows for full versatility in terms of operating any channel at any of the temperatures available in the thermostats. The thermostats are generally set to 30.0, 40.0, 50.0 and 60.0ºC (with two boxes at 30.0ºC) but are variable to any temperature between room temperature and 60.0ºC. Figure 4.4 shows a photograph of the inside of one of the thermostats. The connections on the cell, in the thermostat and on the "patch panel" are "four-wire" type connections with two wires carrying current and two wires to monitor voltage. The thermostats are controlled by Omega CNi3233 or 4201A-PC2 temperature controllers connected to 100 Ω RTDs and heating tape wrapped around the steel enclosure.

Each thermostat consists of two steel enclosures. The door is removed off of the inner enclosure and holes are drilled in the back to mount the plugs. This enclosure is then wrapped in the heating tape and surrounded by ¾" insulation. This allows the inner enclosure with insulation to fit snugly inside another steel enclosure that is 2" larger in each dimension. Insulation is then taped to the inside of the outer enclosure's door and weather stripping is placed on the door to ensure a good seal when the door is shut. A magnet is placed between the door of the outer enclosure and the enclosure itself sealing the thermostat from the ambient air. A piece of aluminum (6 x 8 x 1/2") is placed in the bottom of each inner enclosure as a heat sink and a fan is used to circulate air within each thermostat so as not to develop thermal gradients between different cell locations.

Figure 4.5 shows the temperature profile (monitored by the second RTD) as the 60ºC thermostat heats up over the first two hours with differences of less than 1 K between the different locations within the thermostat. Although the temperature does not reach exactly 60.0ºC the consistency in temperature over time and between locations is more important to reduce fluctuations in data.

These initial tests for the current accuracy, timing resolution and temperature stability appeared to meet the requirements for a ±0.01% CE measurement. Therefore the next step was to begin testing cells.

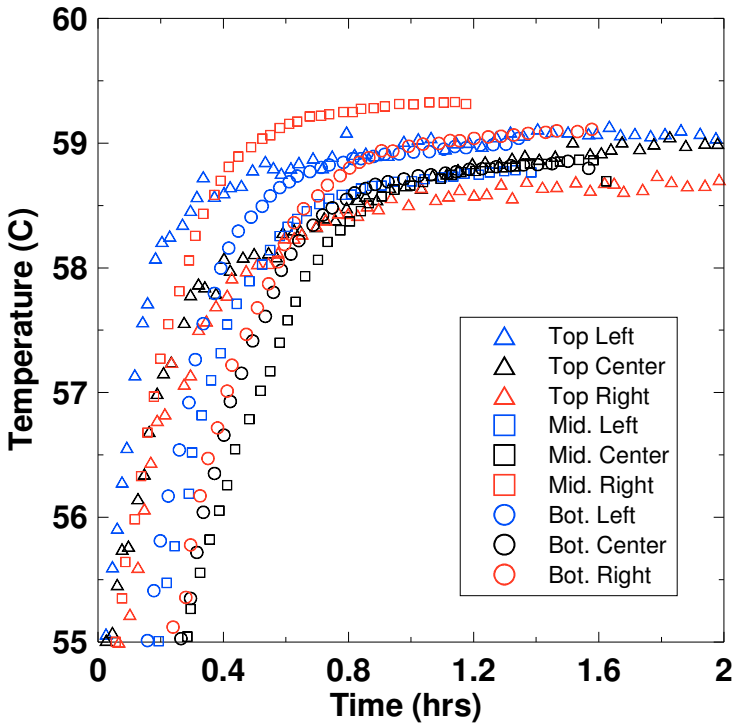

Figure 4.5 Data collected from different locations within the 60.0ºC thermostat as it heats up showing minimal temperature variations after about 1 hour.

4.3 Data Collected on the High Precision Charger

The initial experiment run on the HPC was to cycle 30 commercially manufactured $LiCoO_2$/graphite 18650-style cells in order to see reproducibility between channels on the charger as the cells should be identical. Figure 4.6a shows the measured CE for the cells over ten cycles at a C/24 rate between 3.0 and 4.2 V at 30.0ºC. This data confirms that each of these channels is measuring the same value for cells that should have equal coulombic efficiencies. Data for some of the cells at cycle 2 was lost due to a power outage caused by a hurricane. Figure 4.6b shows the average of the 30 cells (error bars are calculated from the standard deviation) with another of the same $LiCoO_2$/graphite 18650-style cells that was tested at a later date. This confirms that regardless of the channel or time of the test the data is representative of the cell and can be trusted.

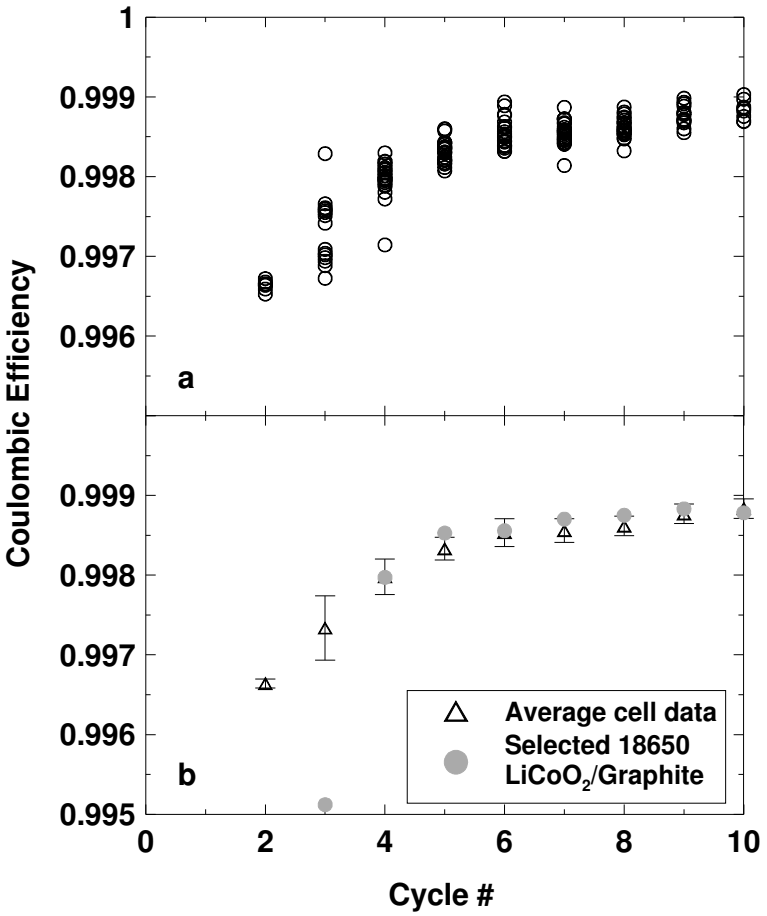

Figure 4.6 Panel a) shows coulombic efficiency versus cycle number for 30 identically made $LiCoO_2$/graphite 18650-style cells. Panel b) shows the average of those cells (with error bars calculated from standard deviation) along with another identically made $LiCoO_2$/graphite 18650-style cell tested at a later date.

Figure 4.7 shows the discharge capacity and coulombic efficiency for Li/graphite and Li/LTO half cells measured on the HPC. These cells were cycled at 40.0ºC at 190 μA for the Li/graphite cell (which corresponds to about C/22) and C/20 for the Li/LTO cell. The voltage limits for the Li/graphite half cell were 0.005 and 1.2 V while the Li/LTO half cell was cycled between 1.3 and 1.8 V. The 190 μA current was chosen as the top of a current range on the Keithley instruments is 200 μA. Therefore, with an error of 0.01% of full scale, the difference between the magnitude of the charge and discharge current is minimized by using a current near the top of the range. Also, this is the current used to calibrate the range so it can be known that the current accuracy is well within the specifications given by Table 4.1.

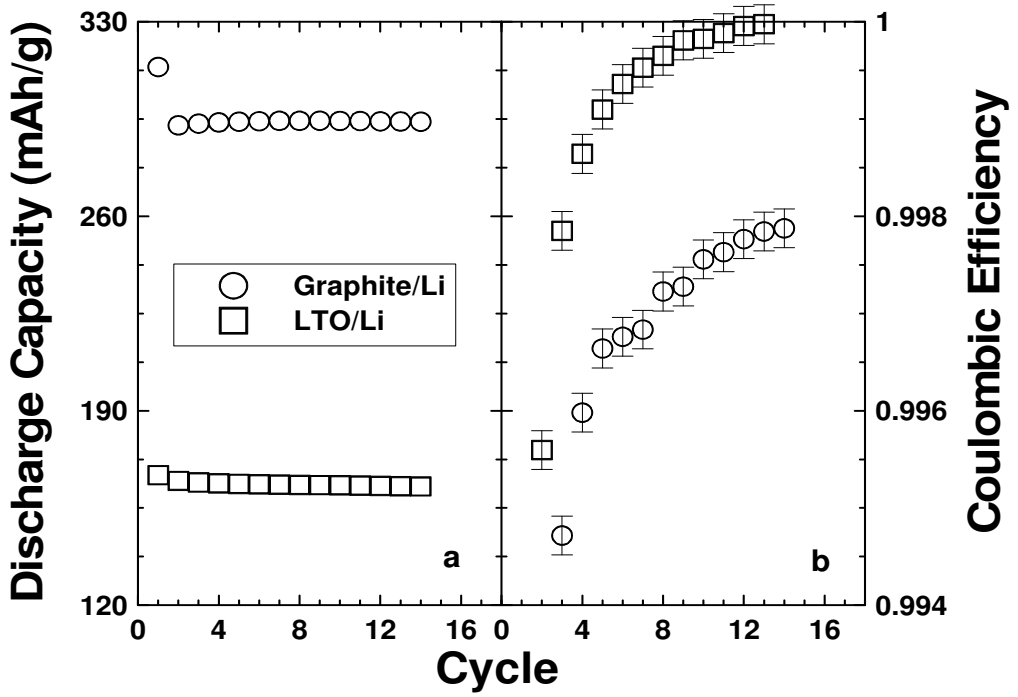

Figure 4.7 Panel a) shows discharge capacity versus cycle number and panel b) shows coulombic efficiency versus cycle number for Li/graphite and Li/LTO half cells.

Both of these half cells cycle with virtually no capacity loss over the approximately 550 hour experiment. The voltage versus capacity curves for these cells have equal and nonzero charge and discharge slippage which results in the coulombic efficiencies being unequal to unity. However, the coulombic efficiencies of these cells give an indication of the active lithium lost to side reactions such as SEI formation. The measured CE of the Li/LTO cell (99.99%) and the Li/graphite cell (99.79%) appear to be asymptotically approaching some constant value. The coulombic efficiency of the Li/LTO cell is much closer to unity than the Li/graphite due to the thinner and more stable SEI layer that forms on the LTO electrode compared to graphite. Also important is the insertion mechanism of lithium into the host material. When lithium is inserted into graphite, the stacking order of graphene planes changes from AB to AA resulting in a volume expansion. The spinel structure of LTO allows lithium to be inserted with zero strain on the LTO structure [11]. Therefore when comparing the coulombic efficiencies of the Li/LTO and Li/graphite cells, one would expect a full cell with an LTO negative electrode to perform better than a full cell with a graphite negative electrode, which will

be shown in Chapter 6. This shows that this technique can easily distinguish between the performances of electrodes with different active material.

Coulombic efficiency measurements can also be used to detect the difference in the amount of parasitic reactions occurring within cells with the same type of material but cycled under different conditions. Figure 4.8 shows Li/NMC half cells cycled at 40.0ºC between 3.0 and 4.2, 4.4 and 4.6 V using a C/20 current. Figure 4.8a shows that the cells cycled to 4.2 and 4.4 V show minimal capacity loss while the cell cycled to 4.6 V is losing capacity with each cycle. This loss of capacity is an indication of damage to the material that does not allow for full lithiation and delithiation with each cycle. As discussed in Chapter 3, electrolyte oxidation can occur at the high potentials of the positive electrode. As the upper cut off voltage of these cells is increased, the amount of electrolyte oxidation and the associated parasitic current should increase which should be detectable in coulombic efficiency measurements. Figure 4.8b shows a decrease in coulombic efficiency as the upper cut of voltage is increased. Again the measured coulombic efficiencies seem to be approaching some value asymptotically, but the CE of cell cycled to 4.6 V is still increasing slightly. However, the coulombic efficiency can be impacted by capacity loss in the half cell. Regardless, after the cycles shown (which took the same amount of time to complete) the measured coulombic efficiencies of 99.44% for the 4.2 V cell, 99.28% for the 4.4 V cell and 99.13% for the 4.6 V cell show the expected increase in parasitic reactions when cycling to higher voltages.

Electrolyte additives can be used in cells for any number of possible benefits to the safety, cycle life or rate capability of a cell. If an electrolyte additive is supposed to increase the cycle life of a cell, using the additive should increase the measured coulombic efficiency of that cell compared to a control cell as it should be decreasing the rate of parasitic reactions in the cell. Comparisons between coulombic efficiencies of tests cells containing an additive and control cells can be made for both full and half cells to study the additive's impact on the full cell or a single electrode. The next two chapters discuss different types of electrolyte additives and the reasons for their use in cells. The methods by which electrolyte additives have been tested in the past will be discussed. It will be shown that how high precision coulometry proves be a valid and potentially better method.

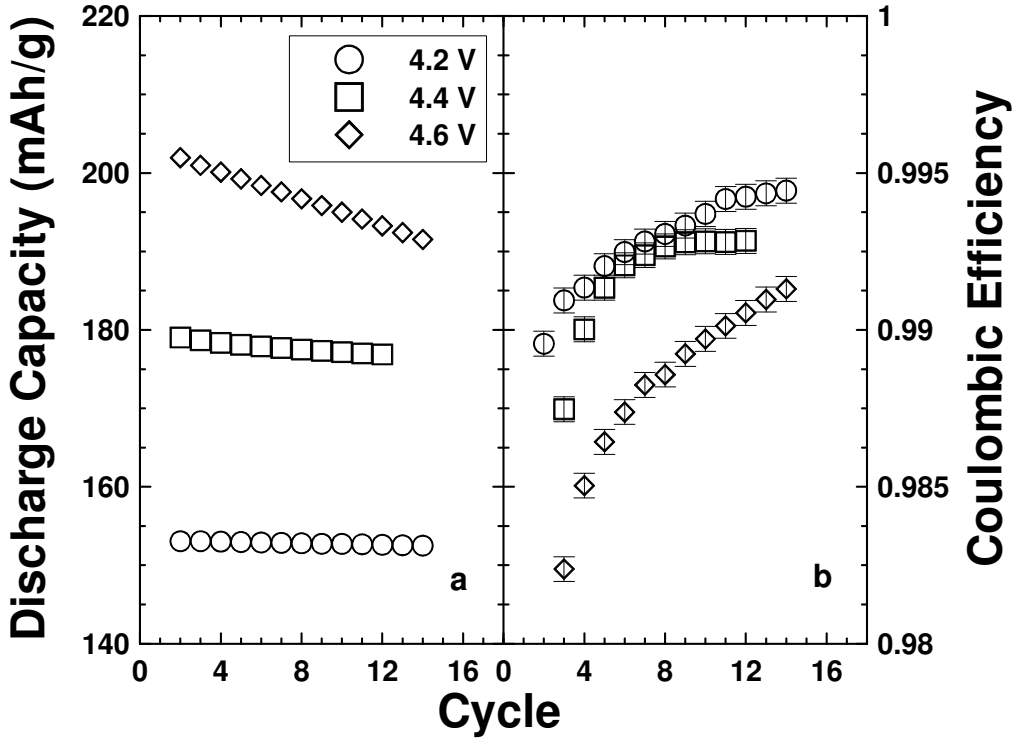

Figure 4.8 Panel a) shows discharge capacity versus cycle number and panel b) shows coulombic efficiency versus cycle number for Li/NMC half cells cycling to different upper cut off voltages.

Chapter 5 The Use of Electrolyte Additives in Lithium-Ion Cells

Electrolyte additives have been studied extensively and are used in commercial lithium-ion cells. Additives have been found that can improve cycling performance in different ways as well as improve the safety of lithium ion cells [49]. Many commercial cells are made with the same basic cell chemistry (for example $LiCoO_2$ as a positive electrode and graphite as the negative electrode) but have differences in performance due to the electrolyte formulation. This formulation includes choice of salt, solvent (generally $LiPF_6$ and some mixture of the solvents discussed in Chapter 2), and additives. The selection of additives can be the distinguishing factor between the performance of different commercial cells. These additives are included in the electrolyte formulation in relatively small quantities (normally on the order of 0.01 – 10 wt%).

Generally additives are initially tested in the lab in full and half cells in order to see the impact on cycling. If an additive is believed to extend the lifetime of a cell by decreasing the rate of degradation mechanisms (such as those discussed in Chapter 3) cells are cycled and the fade and coulombic efficiency of cells with and without the test additive are compared. Other tests such as accelerating rate calorimetry (ARC), differential scanning calorimetry (DSC), electrochemical impedance spectroscopy (EIS) or surface analysis techniques such as x-ray photoelectron spectroscopy (XPS) are conducted in attempts to understand the impact and benefit of an additive. This chapter will discuss several different types of additives as well as their benefits to the cells and how those benefits are quantified.

5.1 Additives to Improve the Safety of Li-ion Cells

A major concern for commercializing lithium-ion cells is safety. The large amount of energy stored within the cells poses a potential risk if a cell is mistreated. Possible problems include cells being exposed to high temperatures in the charged state leading to thermal runaway or being charged past their specified upper voltage limit,

known as overcharge. The thermal stability of different electrode materials in solvents and electrolytes has been studied [50-56]. Generally DSC and ARC testing are used with delithiated positive electrodes or lithiated graphite to correspond to the charged state of a full cell.

MacNeil and Dahn reported thermal studies of reactions between both $Li_{0.5}CoO_2$ [54] and $Li_xMn_2O_4$ ($x \approx 0$) [55] and solvents (EC:DEC 1:2) or electrolyte using ARC. These reports show that in the present of solvent, the $Li_{0.5}CoO_2$ reaches a self-heating rate of 0.02ºC/min at 130ºC while the Mn_2O_4 under the same conditions does not reach a 0.02ºC/min self-heating rate until 200ºC. Also shown in these reports is how varying the concentration of $LiPF_6$ in the electrolyte impacts the thermal stability. It was found that for best thermal stability, $Li_{0.5}CoO_2$ should be used with 1.5 M $LiPF_6$ electrolyte while Mn_2O_4 is safer with lower concentrations of $LiPF_6$ in the electrolyte, such as 0.5 M.

Jiang and Dahn [53] studied different positive electrode materials in solvents and electrolytes containing either $LiPF_6$ or LiBOB. It was found that $LiPF_6$-based electrolyte had better thermal stability (based on the temperature at which a given self-heating rate was reached) for charged $LiCoO_2$ and $Li[Ni_{0.1}Co_{0.8}Mn_{0.1}]O_2$ compared to LiBOB based electrolyte. The third positive electrode tested, $LiFePO_4$, showed very good thermal stability in LiBOB electrolyte with no heat generation until 240ºC in the charged state. This experiment showed how the choice of both material and electrolyte impact the thermal stability of a given system.

Wang et al. [56] reported studies on thermal stability of charged Li_xCoO_2 ($x \approx 0.5$), $Li_x[Ni_{0.8}Co_{0.15}Al_{0.05}]O_2$ ($x \approx 0$) (NCA) and $Li_x[Ni_{1/3}Mn_{1/3}Co_{1/3}]O_2$ ($x \approx 0.5$) with 1 M $LiPF_6$ in EC:DEC 1:2 electrolyte. It was found that charged NCA and Li_xCoO_2 had comparable thermal stability while charged NMC had the lowest self-heating rates under 250ºC. This report also showed the importance of the ratio of active material to electrolyte in these types of thermal tests.

Yamaki et al. [52] used DSC to examine the thermal stability of graphite with 1 M $LiPF_6$ in EC:DMC electrolyte. They found a small exothermic reaction at 140ºC present from the reaction between the intercalated lithium and electrolyte to form the SEI. Then a large exothermic reaction occurs at 280ºC which is attributed to the breakdown of

the SEI which allows further reaction of intercalated lithium with the electrolyte. Jiang and Dahn [51] also examined the impact of varying the solvent and salt used on the thermal stability of graphite. It was found that $Li_{0.81}C_6$ had lower reactivity with EC (a cyclic carbonate) compared to DEC and DMC (linear carbonates). $Li_{0.81}C_6$ showed better thermal stability with the addition of $LiPF_6$ to EC:DEC compared to only the solvent which is attributed to the formation of LiF as a surface film instead of lithium-alkylcarbonates at temperatures below 240ºC. However, it was also shown that $Li_{0.81}C_6$ was less reactive when using LiBOB in place of $LiPF_6$ in the electrolyte.

Given the impact of changing the salt and solvent, others have investigated using additives for both positive and negative electrodes to improve the thermal stability. Two examples of such improvements are using 4-isopropyl phenyl diphenyl phosphate with $LiCoO_2$ positive electrodes [57] and thiophene added to $LiCoO_2$/graphite cells [58]. Since safety at higher operating temperatures is obtainable, additives which improve capacity retention and increase cycle life at high temperatures become necessary as well. Such additives include, but are not limited to: additives which remove water and HF for $LiMn_2O_4$ positive electrodes [59], propane sultone in $LiNi_{0.8}Co_{0.2}O_2$/graphite cells [60] and vinyl ethylene carbonate (VEC) for $LiNi_{0.8}Co_{0.2}O_2$ positive electrodes [61].

Another potential safety risk is the overcharging of lithium-ion cells. As described in Chapter 3, some molecules have a highly reversible shuttling mechanism which can transfer charge within the cell. Such a shuttle can prevent the delithiation of the positive electrode above the oxidation potential of the shuttling molecule from the oxidation reaction. Therefore, criteria for such a molecule is that it has a highly reversible oxidation at a potential is above the upper cut off voltage of the cell in which the molecule will be used. This is not trivial since higher energy cells are being developed to be charged to higher voltages, increasing the potential of the positive electrode in the charged state. In order to find a good shuttling molecule, the oxidation potential must be catered to the charged potential of the positive electrode so that it is relatively close in order to not allow excessive overcharging of the cell.

Several different shuttling molecules have been found and reported in the literature. Such molecules include, but are not limited to, 2,5-ditertbutyl-1,4-dimethoxybenzene [62] and a dimethoxybenzene derivative [63]. The best performance

from a shuttle molecule was reported by Dahn et al. [62]. $LiFePO_4$/LTO cells were constructed with 2,5-ditertbutyl-1,4-dimethoxybenzene and forced into both overcharge and overdischarge conditions. The shuttle molecule is able to keep the cell voltage at 2.35 V in the over charged state as the molecule oxidizes at the positive electrode. During overdischarge, the cell voltage does not decrease below about -0.5 V as the oxidation of the molecule occurs on the LTO negative electrode. $LiFePO_4$/graphite cells containing 0.2 M 2,5-ditertbutyl-1,4-dimethoxybenzene and 0.5 M LiBOB in PC:DEC 1:2 are shown cycling with a 100 % capacity overcharge each cycle. Under these conditions, the shuttle runs well at a cell voltage of about 3.9 V without degradation for over 200 cycles (1000 hours).

It is possible to prevent cells from overcharge by using additives that do not shuttle charge. For example, cyclohexyl benzene [64-66], biphenyl [66-69], diphenyl ether [70] and fluorobenzene [71] have been shown to form a polymer on the surface of the positive electrode above their oxidation potential. The oxidation potential of cyclohexyl benzene is around 4.7 V (vs. Li/Li^+) which is lower than potentials where electrolyte begins to decompose [64]. The oxidation of the molecule results in a polymer forming on the surface of the positive electrode to prevent further delithiation. The use of cyclohexyl benzene is however associated with a slight decrease in capacity and increase in cell impedance. Other work [65] showed how both cyclohexyl benzene and/or tri(β-chloromethyl) phosphate (TCEP) can be used for the same purpose. The oxidation potential of TCEP is about 4.75 V (vs. Li/Li^+) forming a polymer on the positive electrode to prevent overcharge beyond this potential. It was also shown that the oxidation potential of cyclohexyl benzene and TCEP drop to 4.1 and 4.0 V (vs. Li/Li^+), respectively, when the cell is heated to 150ºC to lower the voltage of overcharge protection at high temperature.

Biphenyl also forms a polymer on the surface of the positive electrode at potentials above 4.5 V (vs. Li/Li^+) [66-69]. As the duration of overcharge lengthens, the conductive polymer on the surface grows until the concentration of binphenyl is depleted or the potential of the positive electrode drops below the oxidation potential. If the concentration of binphenyl is high enough and the duration of overcharge long enough, the conductive polymer can grow, penetrate the separator and reach the negative

electrode. This creates a short circuit within the cell so that the cell is discharged from the overcharge condition [67]. Therefore, the use of binphenyl was shown to have good safety features during overcharge with minimal decrease in performance of $LiCoO_2$/graphite cells. Diphenyl ether and fluorobenzene have similar characteristics to cyclohexyl benzene and biphenyl in order to prevent overcharge.

Additives can also be used as flame retardants in the electrolyte. For example, triphenylphosphate (TPP) was shown to be stable to potentials up to 4.9 V (vs. Li/Li^+) and electrolyte containing TPP had enhanced thermal stability compared to control electrolyte [72]. The use of TPP increased the cell impedance in NMC/graphite cells which decreases the available capacity when discharging at high rates. However, the use of 3 wt% TPP with 1 M $LiPF_6$ in EC:DEC was shown to only slightly increase impedance while greatly improving safety. Another additive studied as a flame retardant is allyl tris(2,2,2-trifluoroethyl) carbonate (ATFEC) [73]. Higher concentration of ATFEC, up to 30 vol%, with 1 M $LiPF_6$ in EC:DMC showed better thermal stability. ATFEC was shown to have little adverse impact on the cycling of $LiCoO_2$ and graphite half cells. The use of ATFEC does not lower electrolyte conductivity until concentrations greater than 15 vol% are used. Therefore, the addition of 15 vol% ATFEC to the electrolyte is able to improve the safety while having little adverse affect on cell performance.

5.2 Additives to Improve the Performance of Li-ion Cells

Additives to improve the performance or cycle life of cells can either be used to slow reactions that remove active lithium or electrolyte from the cell, or to prevent the cell hardware from degradation over time. There are many additives used to slow parasitic reactions in the cell which will be discussed in this section. One example of an additive to prevent cell hardware degradation is succinonitrile. It is known that the copper current collected for the negative electrode can corrode over time [74]. Eventually, if the current collector becomes severely corroded, it can lead to an increase in cell impedance and eventually cell failure. The use of succinonitrile slows the

corrosion rate of the copper [75,76] which allows a cell to cycle without degradation of the current collector.

The growth and modification of the SEI on the negative electrode depletes the supply of active lithium within a cell. A great deal of research on additives focuses on forming a more stable passivating layer on the negative electrode (normally graphite) which would result in less active lithium loss during cycling and therefore longer cycle life of the cell. Other additives are used to gear cells towards more specific applications other than long lifetime. For example, the use of Li-ion cells used in electrified vehicles and other high rate discharge applications requires high power. The power of a cell can be limited by internal impedance from surface layers on the electrodes or viscosity, conductivity and Li^+ mobility of the electrolyte. Therefore, additives that can either reduce the impedance associated with the electrode or the electrolyte will benefit cells to be used for high power applications. For cells where a high energy is desired and power requirements are not as demanding, a higher operating voltage or capacity is required. However, as the cell voltage increases, the rate of electrolyte oxidation also increases which can reduce the lifetime of the cell. Therefore, to improve cell performance for high voltage cells, some electrolyte additives are used to suppress electrolyte oxidation which allows cells to cycle well up to 5 V.

Two of the most commonly used electrolyte additives are fluoroethylene carbonate (FEC) and vinylene carbonate (VC). Both additives change the composition and formation of the surface passivating layers on electrode. FEC is commonly used with alloy negative electrodes which normally face lifetime issues due to the volume expansion during lithium insertion. Choi et al. [77] reported increased capacity retention and coulombic efficiency when FEC is added to the electrolyte for a silicon thin film half cell after 80 cycles (800 hours) cycling between 0.005 and 2.0 V.

Vinylene carbonate was first introduced by SAFT in 1995 [78] and since then numerous studies have shown how the use of VC improves the cycling of graphite negative electrodes by forming a more stable SEI [79-81]. Studies about VC in full cells have also examined the possible beneficial reactions at the positive electrode as well decreasing the surface impedance and improving the cycling performance and especially high temperature cycling [79,82,83]. Aurbach et al. [79] reported decreased surface

impedance on $LiNiO_2$ and $LiMn_2O_4$ positive electrodes but attributed the reduction of VC on the graphite negative electrode to be the primary reason for increased performance. The authors claim that the formation of polymeric surface species on the surface of graphite from the reduction of VC lead to less irreversible capacity loss, less salt reduction and improved cycling at elevated temperatures. The surface species that are formed on the positive electrode are reported to occur at potentials above 4.2 V (vs. Li/Li^+) and suppress acid reactions with the electrode material. Ouantani et al. [82] used both theoretical and experimental approaches to conclude that polymer type surface films were forming on both electrodes in a $LiCoO_2$/graphite cell.

Another additive that has been proposed to increase cycle life is trimethoxyboroxine (TMOBX) [84]. The patent for this additive discusses how the presence of boron rings dissolved in non-aqueous electrolytes leads to increased capacity retention. Of these boron-ring based additives, those with the methoxy groups showed the best performance. In order to test these additives, high rate cycling was shown [84] for many cycles of $LiCoO_2$/graphite 18650 cells with different concentrations. After about 400 cycles, 1.0 wt% trimethoxyboroxin with 1 M $LiPF_6$ in EC:PC:DEC showed the best capacity retention (compared to smaller concentrations). A similar test was done to investigate the impact of TMOBX. Capacity retention for $LiMn_2O_4$/graphite 18650 cells with different concentrations of TMOBX was shown over about 350 cycles. The cell containing 0.3 wt% TMOBX added to 1 M $LiPF_6$ in EC:PC:DEC showed better capacity retention than the control cell.

Chen and Amine [85] reported studies on tris(pentafluorophenyl) borane (TPFPB) as an electrolyte additive. This additive both extends cycle life and improves power capabilities. Using AC impedance analysis, it was determined that high concentrations of the additive showed increased internal impedance but concentrations of < 3 wt% decrease cell impedance. Cells containing TPFPB also showed better capacity retention than control cells over 200 cycles (800 hours) of cycling. The mechanism proposed was participation of the additive in formation of passivation layers and causing dissolution of LiF from the layers which improved Li^+ transport through the film.

Liu et al. [86] studied lithium difluoro(oxalato)borate (LiDFOB) as an additive to improve cycle life without hindering power capabilities. Control cells were made with

$LiPF_6$ while other cells contained either $LiPF_6$ and LiDFOB as an additive or LiDFOB as the only salt. While capacity retention was increased for cells containing LiDFOB as an additive and was even better for cells with only LiDFOB, the use of only LiDFOB caused increased impedance. Therefore cells containing 2 wt% LiDFOB showed better capacity retention with minimal increase in impedance leading to the possibility of power cells that have longer lifetimes.

In support of higher energy cells, von Cresce and Xu [87] reported studies of tris(hexafluoro-iso-propyl)phosphate (HFiP) as an additive for a 5 V cell. Half cells containing $LiNi_{0.5}Mn_{1.5}O_4$ as the test electrode were constructed with 1 M $LiPF_6$ in EC:EMC 3:7 with and without HFiP in the electrolyte. Cells were cycled to an upper cut off voltage of 5 V and those containing 1% HFiP showed better capacity retention over 200 cycles compared to the control cell. Also, to support the use of HFiP in a full cell, graphite half cells were made to show good cycling with HFiP. The coulombic efficiencies of the negative electrode half cells are reported showing an improvement in first cycle CE from 89.37% to 95.6% with the addition of HFiP (cells were cycled on a Maccor 4000 series battery tester). Since full cells were not reported these are described as "preliminary yet encouraging results" by the authors [87].

Additives have clearly been shown to have beneficial characteristics in terms of safety and performance when used with the appropriate cell chemistry. In many of the reports discussed in this chapter, high rate cycling was used to test the impact of additives on capacity retention. However, these cycling conditions are unrealistic for many commercial applications of Li-ion batteries. Therefore, conclusions about eventual lifetime of cells should be found through comparison of coulombic efficiencies at slower rates (such as one cycle per day which is more realistic for many applications) using high precision coulometry.

Chapter 6 Evaluation of Additives using High Precision Coulometry

In order to test the importance of high precision coulometry and verify that coulombic efficiency measurements give an indication of long term cycle life, a careful experiment needed to be conducted. In such an experiment, cells with different electrolyte formulations must be cycled for a long time (on the order of a year or longer) in order to see the impact of all parasitic reactions on capacity loss in the cell (including electrolyte oxidation that does not necessarily cause capacity fade in a shorter experiment). The different electrolyte formulations could include additives which are believed to improve cycle life and therefore cells containing the additive should show less capacity loss over the long experiment. To compliment the long term data collected, identically made cells of each electrolyte formulation must be cycled on the HPC so that the coulombic efficiency of each cell can be accurately measured. The coulombic efficiency and long term fade data should correlate so that cells with measured coulombic efficiencies closer to 1.0000 show less fade in the long term experiment. This becomes difficult as each pair of cells (one for HPC and one for long term cycling) must be identically made to ensure the differences detected are based on differences in cell chemistry and not cell construction. This level of reproducibility is not trivial for coin-type cells made in the lab which makes commercially made cells ideal candidates for such an experiment.

The opportunity arose to collaborate with a commercial Li-ion battery manufacturer which already had run long term cycling experiments measuring capacity versus cycle number for several different types of cells. Therefore, if more of the same cells could be manufactured and tested on the HPC, the data could be compared and the experiment would only take the amount of time required for HPC measurements (several hundred hours). The level of reproducibility between the commercial cells that were cycled to measure fade and the commercial cells constructed for testing on the HPC would be high enough to ensure that differences in performance came from changes to the cell chemistry. A design of experiments approach [88] was taken to choose a matrix of cells in order to examine the relationship between coulombic efficiency and long term

capacity fade. The use of the design of experiments allows for the impact of all variables to be statistically analyzed which can lead to more information about the changes in cell performance when using certain additives, electrodes or cycling at different temperatures.

6.1 Experimental

Sixty wound prismatic cells were received from a commercial manufacturer. The sixty cells were comprised of 20 groups of different cell chemistries or electrolyte formulations with three cells for each group. The negative electrodes were either graphite [mesocarbon microbeads (MCMB)] or $Li_4Ti_5O_{12}$ (LTO) while the positive electrodes were one of three types of $LiCoO_2$ with different specific surface areas. Eighteen of the twenty groups contained either $LiCoO_2$ with a specific surface area of 0.4 – 0.7 m^2/g (referred to as positive electrode "0") or $LiCoO_2$ with a specific surface area of 0.1 – 0.25 m^2/g (referred to as positive electrode "1"). The third type of $LiCoO_2$ (referred to as positive electrode "2") with a different specific surface area was used in a different electrolyte formulation than the other eighteen groups. These two groups contained 1 M $LiPF_6$ in PC:EC:DEC (21:35:44) with and without 2.5 wt% biphenyl as the electrolyte and will not be discussed in great detail (the addition of biphenyl slightly improved coulombic efficiency and decreased both the charge and discharge slippage rates). The remaining eighteen groups contained different combinations of trimethoxyboroxine (TMOBX), vinylene carbonate (VC) and lithium (bis) trifluoromethanesulfonimide ($LiN(CF_3SO_2)_2$ called HQ115) in 1 M $LiPF_6$ EC:EMC (3:7) electrolyte. When these additives were present in the electrolyte, their concentrations were 0.30, 2.00 and 4.00 wt%, respectively.

All cells were cycled on the High Precision Charger (HPC). The cells with graphite negative electrodes were cycled between voltage limits of 3.575 and 4.075 V and those with LTO negative electrodes were cycled between 1.8 and 2.8 V. All cells were cycled using constant charge and discharge currents corresponding to a rate of C/10 for ~500 hours and then cycled at a C/20 rate for another ~500 hours. Since three cells were available for each of the twenty groups, duplicate cells were cycled at 40.0 ± 0.1 °C

while the third cell was cycled at 60.0 ± 0.1 °C. This allowed for reproducibility between cells as well as the impact of temperature to be studied. The first cycle for all cells was done at the manufacturer for quality assurance and then the cells were shipped at roughly 90% state of charge. Therefore the formation cycle data will not be seen in the data presented.

In order to keep track of the cells with a large variety of electrode types and electrolyte formulations, a group code was established. The code consists of four digits where the first three are 0 or 1 indicating the absence or presence of TMOBX, VC and HQ115 in the electrolyte, respectively. The fourth digit represents the choice of positive electrode as described above. The cells are always separated by negative electrode type and temperature and thus there is no need to include their parameters in the group code. For example, a high surface area $LiCoO_2$/graphite cell with only TMOBX as an additive would be group code 1000 while a low surface area $LiCoO_2$/LTO cell with VC and HQ115 but no TMOBX in the electrolyte would be group code 0111. This code will be used to discuss cells through the remainder of this chapter.

6.2 Results

6.2a Cycling Results

The sixty cells were designed to have a capacity of roughly 120 mAh. The $LiCoO_2$/graphite cells were constructed so the negative electrode had a greater capacity than the positive electrode when delithiated to the desired fully charged state. The ratio of negative to positive electrode capacity (when charging to the specified voltage limit) was roughly 1.2. The $LiCoO_2$/LTO cells were made with a larger capacity positive electrode so that during each cycle the LTO electrode was fully lithiated. However, there were slight variations in actual measured capacity of the cells based on the active weight of material within the cells. For this reason it was easier to compare both duplicate cells and those of different groups by using normalized capacity which will be used for the discussion of the cell data.

Figure 6.1 shows the cell voltage (V) versus normalized capacity for two different groups of $LiCoO_2$/graphite cells at both 40 and 60 ± 0.1ºC. Only one of the two cells cycled at 40ºC is shown. Panels a) and c) show the control cells in group 0001 while panels b) and d) show cells from the 0100 group. The cells in the 0100 group were selected for comparison to the control cells as the highest measured coulombic efficiency of all the graphite based cells at 40ºC at the end of the C/10 rate testing was for the cells from this group. Each panel shows roughly 25 cycles at C/10 which all took the same amount of time (~500 hours) to measure. As described in Chapter 2, the voltage curve slips to the right (after some initial slippage to the left during early cycles) as the charge is longer than the subsequent discharge due to parasitic reactions such as SEI growth and electrolyte oxidation occurring within the cell.

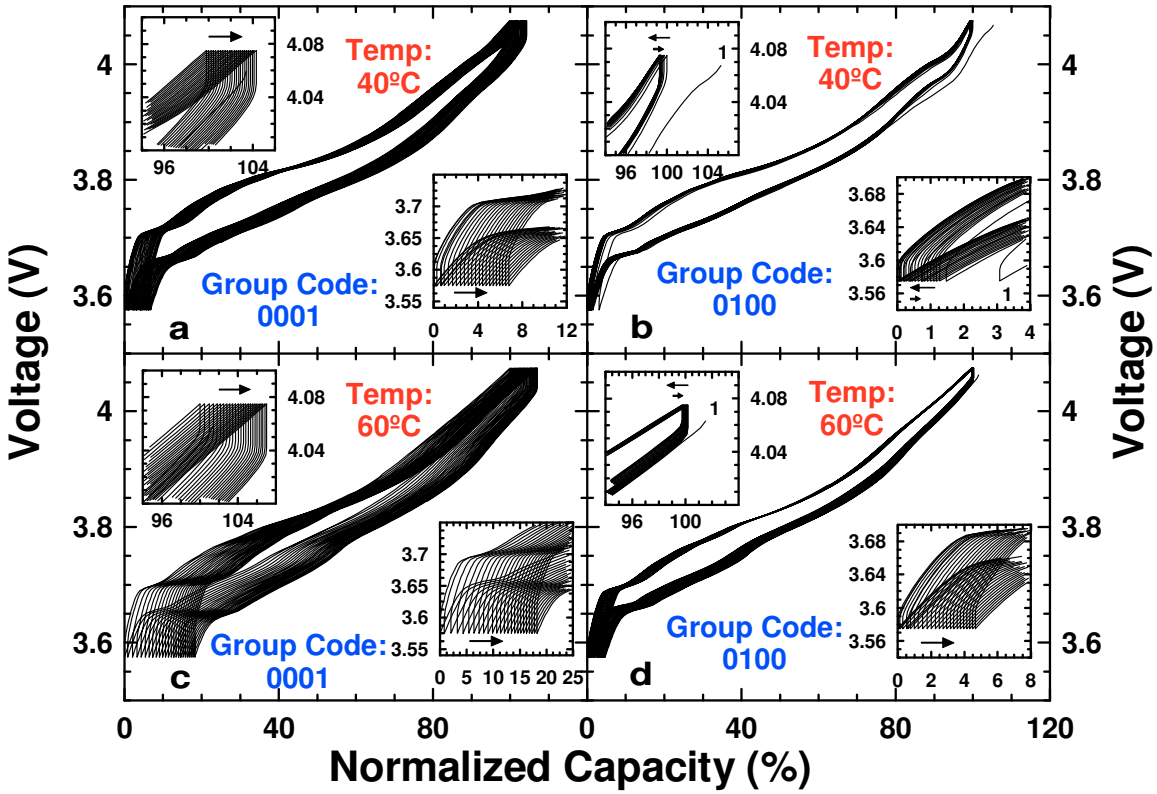

Figure 6.1 Cells with graphite negative electrodes: (Left panels) The potential (V) versus normalized capacity (Q) curves for the control group (0001) at 40°C (panel a) and 60°C (panel c). (Right panels) The V versus Q curves for the group (0100) with the highest measured coulombic efficiency at 40°C (panel b) and 60°C (panel d). The insets in each panel show the top of charge and bottom of discharge endpoints.

The insets in each panel show an expanded view of the charge and discharge endpoints with arrows giving an indication of the direction of slippage. It is clear that the rate of slippage at the top of charge and bottom of discharge increases at elevated temperature and decreases in the presence of the VC containing electrolyte. Therefore, the introduction of VC to the electrolyte must suppress parasitic reactions to result in less slippage of the electrodes. Due to the nature of the design of experiments it was impossible to directly compare a control cell and a cell containing only VC with the same positive electrode material. However, it will be shown during this analysis that the impact of changing the positive electrode on coulombic efficiency is small relative to the impact of adding VC to the electrolyte so this decrease in slippage can be attributed to the use of VC. However, through storage experiments after cycling a difference between the different positive electrodes was found [89]. It was found that cells containing the low surface area $LiCoO_2$ showed less decrease in open circuit voltage (associated with parasitic reactions that insert lithium into the positive electrode). This is likely because parasitic reactions such as electrolyte oxidation must occur on the surface of the electrode so a smaller specific surface area should result in a decreased rate of parasitic reactions on that electrode.

Chapter 3, specifically Equation 3.17, showed how the discharge slippage and coulombic efficiency are related. Since the addition of VC decreased the discharge slippage there should be a measurable increase in coulombic efficiency, shifting it closer to 1.0000. However, the measured fade of the cell is not necessarily decreased by smaller slippage rates as it depends on the difference between the charge and discharge slippages. Figure 6.2 shows both the measured coulombic efficiency (top panels) and normalized cell capacity (bottom panels) versus cycle count for all six cells of the 0001 and 0100 groups. The reproducibility of the cells can be seen as the duplicate cells at 40ºC, shown as crosses and squares, are indistinguishable in both CE and capacity retention over all cycles. The dashed line in the top panels is located at a CE value of 1.0000 which is achievable if no active lithium is lost to SEI growth, no electrolyte oxidation occurs within the cell and there is no damage to the materials. It is clear that the addition of VC to the electrolyte not only causes the measured coulombic efficiency to move closer to

1.0000 but also reduces capacity loss at both 40 and 60ºC. Therefore VC must result in less active lithium loss to the SEI as well as less electrolyte oxidation.

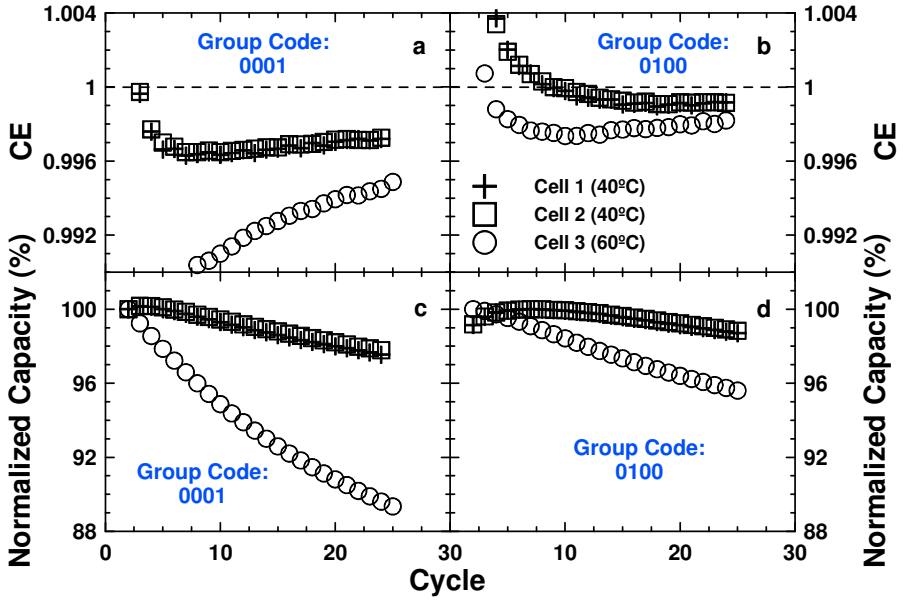

Figure 6.2 Cells with graphite negative electrodes: (Left panels) The coulombic efficiency (panel a) and normalized capacity (panel c) versus cycle number for the control group (0001). (Right panels) The coulombic efficiency (panel b) and normalized capacity (panel d) versus cycle number for the group (0100) with the highest measured coulombic efficiency.

Figure 6.3 shows the normalized charge (top panels) and discharge (bottom panels) endpoint capacities for the same groups of cells. These plots correspond to the endpoints seen in the insets of Figure 6.1. The reproducibility between cells at 40ºC can be seen as the squares and crosses are almost identical again. The lines on each panel come from a linear fit to the final five data points of each data set. Table 6.1 gives the slopes of each of these lines as the slippage rates in percent per cycle. In this table, positive slippage rate values represent a shift to the right in the voltage versus capacity plot. Here the impact of VC is quantified by the decrease in all slippage rates compared to the control cell. Also the impact on fade can be seen as while both the charge and discharge slippages are less in the presence of VC, the difference between these rates is also decreased. For the first several cycles of the cells containing VC show the discharge endpoint capacity decreasing which corresponds to CE > 1.0000 and capacity increase during those cycles.

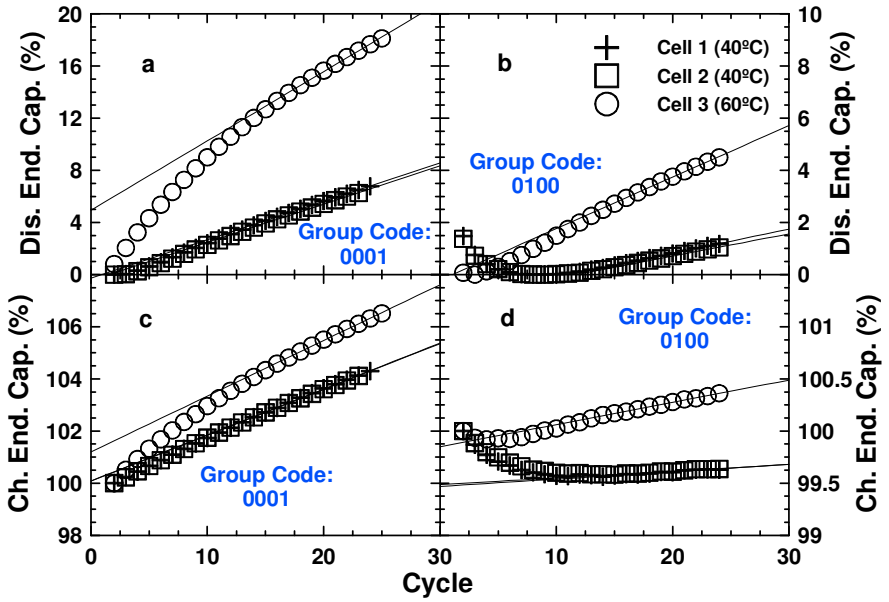

Figure 6.3 Cells with graphite negative electrodes: (Left panels) The bottom of discharge (panel a) and top of charge (panel c) endpoint capacities versus cycle number for the control group (0001). (Right panels) The bottom of discharge (panel b) and top of charge (panel d) endpoint capacities versus cycle number for the group (0100) with the highest measured coulombic efficiency. These are referred to as normalized discharge and charge capacity extent curves.

Group Code	Cell #	Temperature (ºC)	Ch. Slippage (%/cycle)	Dis. Slippage (%/cycle)
0001	**1**	**40**	**0.176**	**0.294**
0001	**2**	**40**	**0.176**	**0.294**
0001	**3**	**60**	**0.214**	**0.532**
0100	**1**	**40**	**0.007**	**0.093**
0100	**2**	**40**	**0.006**	**0.086**
0100	**3**	**60**	**0.021**	**0.198**

Table 6.1 The slopes of the fitted lines in the panels of Figure 6.3.

The impact of different mechanisms on charge and discharge slippage must be carefully considered. Figure 6.4 shows the impact of the different mechanisms proposed in Chapter 3 on charge (red) and discharge (blue) endpoint capacity. Figure 6.4a-d shows the impact of only I_{Li}, I_{ox}^{a}, I_{ox}^{b} or I_p, respectively based on Equations 3.20 and 3.21. Figure 6.4e shows the endpoint capacity assuming no parasitic reactions and only an increase of impedance on the negative electrode (in a negative electrode capacity limited cell). An increase in impedance of the negative electrode causes both the charge and

discharge voltage limits to be reached prematurely. This results in a negative charge slippage and positive discharge slippage. Figure 6.4f shows the endpoint capacity assuming no parasitic reactions and only an increase in impedance of the positive electrode. This increased impedance at the positive causes the charge voltage limit to be reached prematurely but does not impact the discharge endpoint as it is reached when the graphite is delithiated and the electrode potential begins to increase rapidly. Therefore, the slight shift left in charge endpoint capacity in the early cycles could be due to increased impedance at the positive electrode. The shift to the left of the discharge endpoint capacity could be from the excess negative electrode capacity. Since the cells were stored at a high state of charge before cycling, lithium could diffuse to this excess region during the storage. Then when beginning to cycle the cells, the lithium is able to diffuse back to the used region of graphite and it takes longer to fully delithiated the graphite which would cause the discharge endpoint capacity to shift left.

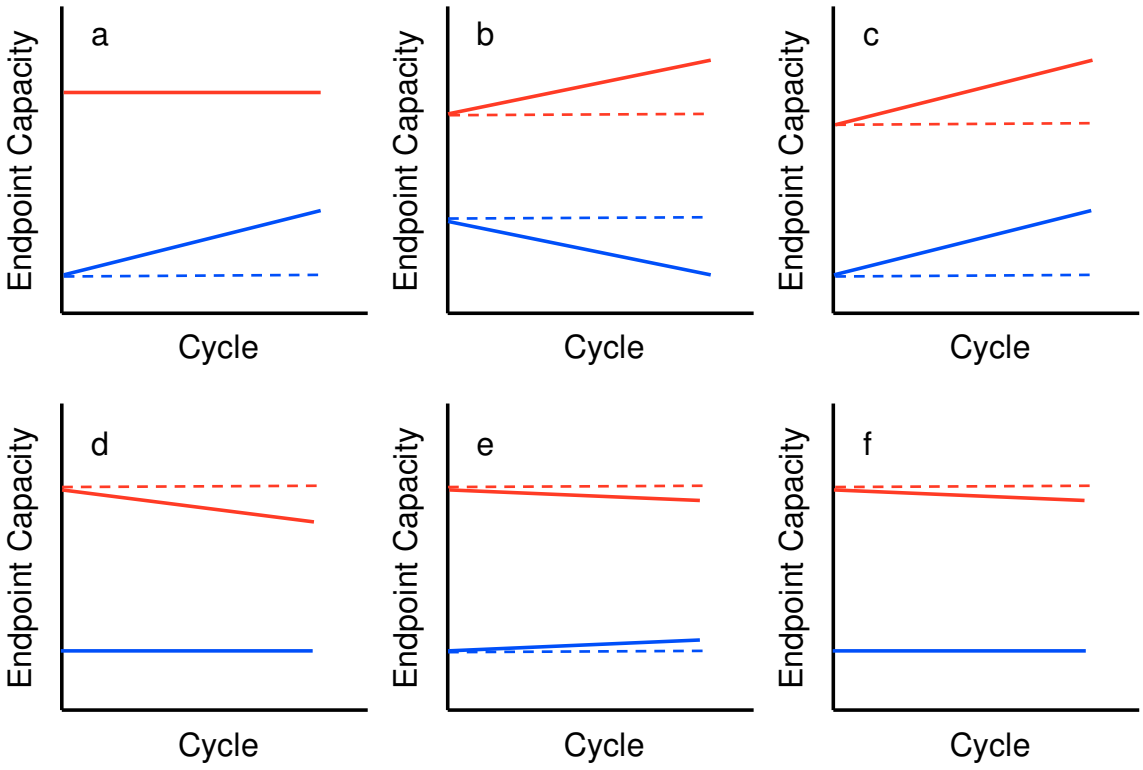

Figure 6.4 Schematics showing the charge (red) and discharge (blue) endpoint capacity over cycling showing the impact of I_{Li} (a), I_{ox}^{a} (b), I_{ox}^{b} (c), I_{p} (d), increased impedance at the negative electrode (e) or increased impedance at the positive electrode (f).

The data collected for the graphite based cells agrees well with the literature in that the addition of VC to the electrolyte appears to form a more stable SEI. This change to the SEI and decrease in rate of active lithium loss at the negative electrode is seen in the reduced discharge slippage rate and shift in the CE closer to 1.0000. However, it is also interesting to see the impact of VC on the positive electrode. The addition of VC clearly decreases the slippage rate at the top of charge as well. This slippage rate is associated with electrolyte oxidation and positive electrode damage (Equation 3.20). Transition metal dissolution is not prominent in $LiCoO_2$ to the delithiated state reached in these cells (< 4.2 V vs. Li/Li^+) [39,90] and it is unlikely that for these commercially made electrodes there are cracking issues leading to pieces becoming electrically isolated. Therefore the positive electrode damage term discussed in Chapter 3 is likely to be negligible compared to the electrolyte oxidation which must be the principle cause of charge slippage. The smaller charge slippage rate in the presence of VC means there is a decrease the rate of electrolyte oxidation which was not discussed extensively in the literature reviewed in Chapter 5 but is an important feature of the additive in full cells.

Figure 6.5 shows the voltage versus capacity curves for two groups of LTO based cells at both 40 and 60ºC. The left panels show control cells (0000) while the right panels show cells containing TMOBX and VC (1100) which had the highest measured CE at 40ºC after the 500 hours of testing at C/10. Again this figure shows roughly 25 cycles for each cell and only one of the 40ºC cells is shown since the reproducibility between cells is quite good. Similarly to the graphite based cells, the LTO based cells show increased slippage rates at elevated temperature and decreased slippage rates at both temperatures in the presence of these additives. When comparing Figures 6.1 and 6.5, it is clear that the slippage rates are significantly smaller for the cells with LTO negative electrodes.

Interpretation of the slippage rates for the cells with LTO negative electrodes cannot come directly from the lithium accounting model presented in Chapter 3 since the capacity is determined by the negative electrode. For these cells the charge endpoint is reached when the lithium titanate is fully lithiated and the potential decreases rapidly which results in the steeper upward slope at the top of charge. The steep downward slope at the bottom of discharge comes from the full lithiation of $LiCoO_2$ which causes the

potential of the positive electrode to decrease rapidly. Therefore the discharge slippage is related to the positive electrode and the charge slippage is indicative of the slippage of the negative electrode. This is the opposite of the model presented in Chapter 3 where the charge endpoint was primarily determined by the state of charge of the positive and the discharge endpoint was a result of the rapidly increasing potential of graphite when fully delithiated.

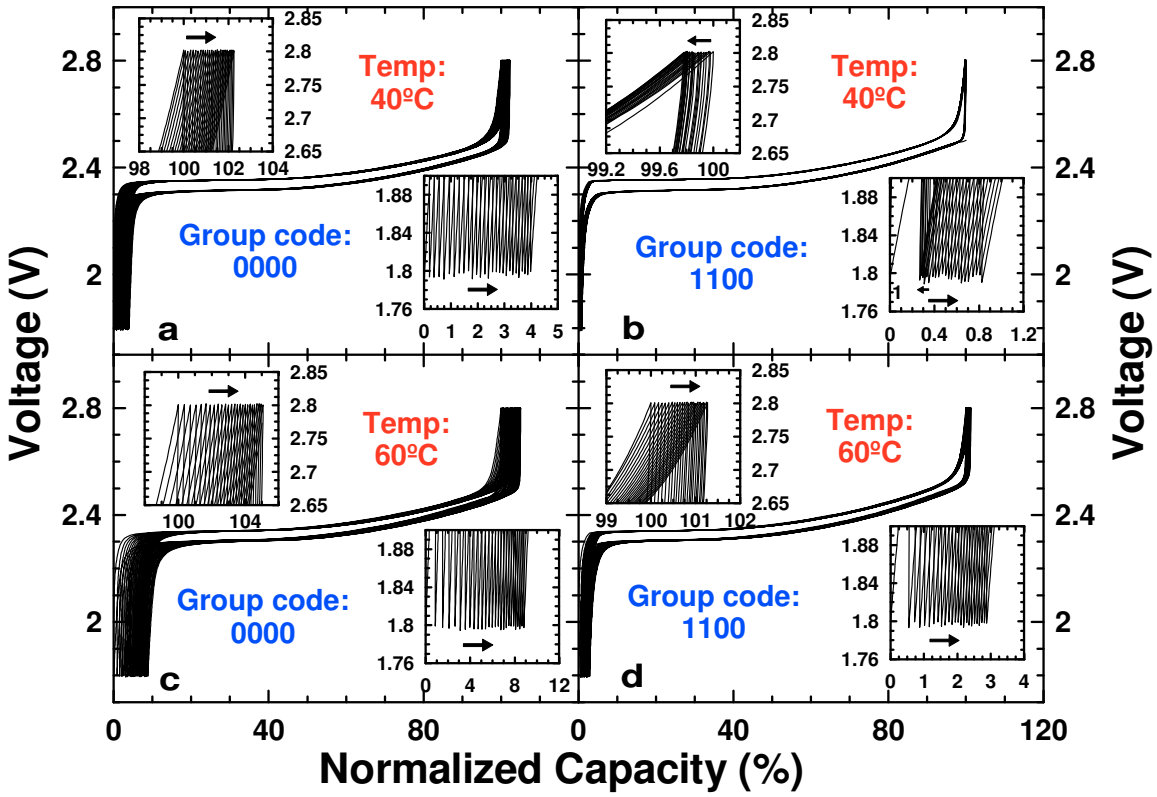

Figure 6.5 Cells with LTO negative electrodes: (Left panels) The potential (V) versus normalized capacity (Q) curves for the control group (0000) at 40°C (panel a) and 60°C (panel c). (Right panels) The V versus Q curves for the group (1100) with the highest measured coulombic efficiency at 40°C (panel b) and 60°C (panel d). The insets in each panel show the top of charge and bottom of discharge endpoints.

Figure 6.6 shows the coulombic efficiency (panel a) and capacity (panel b) versus cycle number for the 0001 and 1101 LTO based cells. It is clear that the addition of TMOBX and VC to the electrolyte benefits the cell as all cells exhibit better capacity retention and more importantly have measured coulombic efficiencies closer to 1.0000.

The final measured coulombic efficiency value for a cell at 40ºC increases from 0.9992 ± 0.0002 to 0.9998 ± 0.0002 (a single cell was selected as the duplicate cells fell within the quoted error) while at 60ºC the use of TMOBX and VC results in an increase from 0.9981 ± 0.0002 to 0.9993 ± 0.0002 in coulombic efficiency. This improvement in coulombic efficiency indicates a decrease in the rate of parasitic reactions occurring within the cell which should increase the lifetime. Figure 6.7 shows the endpoint capacities for both groups of cells with the slope of the fitted lines given in Table 6.2. These values again show reproducibility in the cells as well as the increased performance in terms of both coulombic efficiency and capacity retention. The slight shift to the left of the discharge and charge endpoint in the LTO based cells is not fully understood.

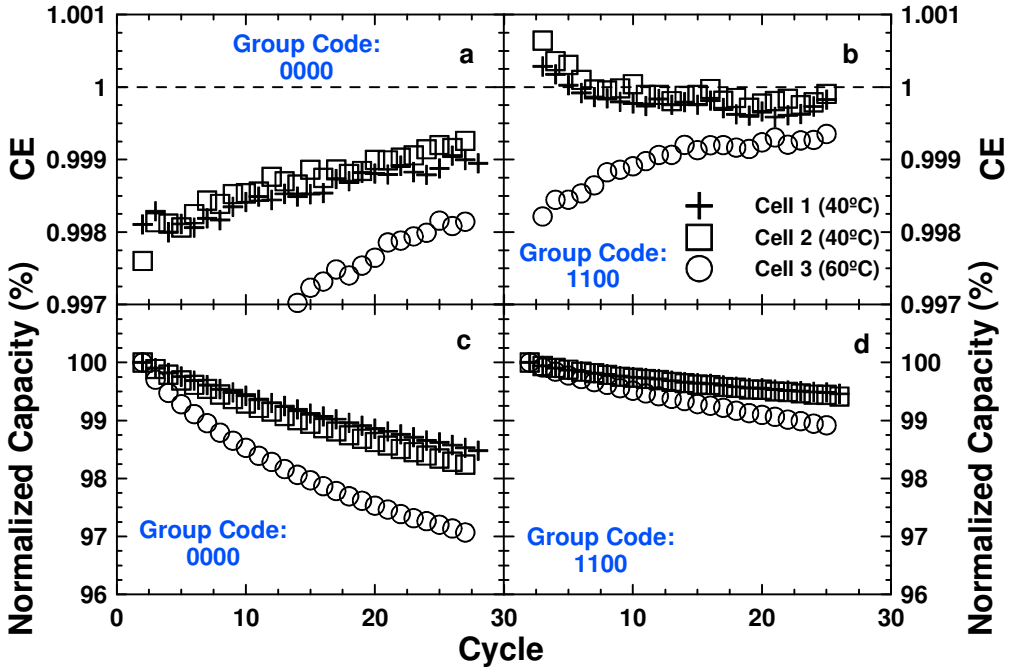

Figure 6.6 Cells with LTO negative electrodes: (Left panels) The coulombic efficiency (panel a) and normalized capacity (panel c) versus cycle number for the control group (0000). (Right panels) The coulombic efficiency (panel b) and normalized capacity (panel d) versus cycle number for the group (1100) with the highest measured coulombic efficiency.

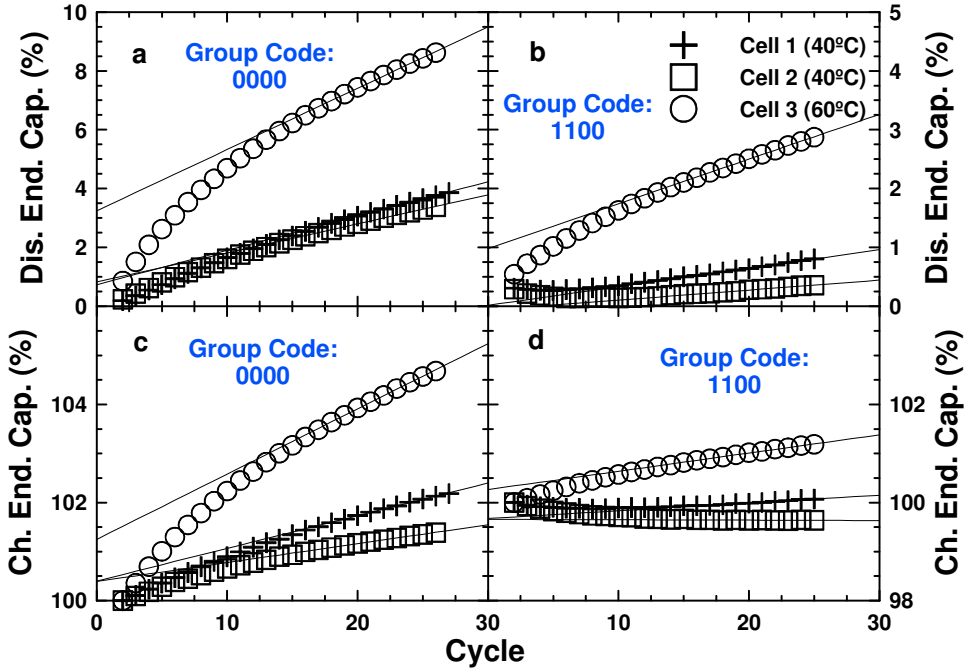

Figure 6.7 Cells with LTO negative electrodes: (Left panels) The bottom of discharge (panel a) and top of charge (panel c) endpoints versus cycle number for the control group (0000). (Right panels) The bottom of discharge (panel b) and top of charge (panel d) endpoints versus cycle number for the group (1100) with the highest measured coulombic efficiency. These are referred to as normalized discharge and charge capacity extent curves.

Group Code	Cell #	Temperature (ºC)	Ch. Slippage (%/cycle)	Dis. Slippage (%/cycle)
0000	1	40	0.067	0.117
0000	2	40	0.039	0.099
0000	3	60	0.133	0.208
1100	1	40	0.016	0.031
1100	2	40	-0.001	0.017
1100	3	60	0.037	0.076

Table 6.2 The slopes of the fitted lines in the panels of Figure 6.7.

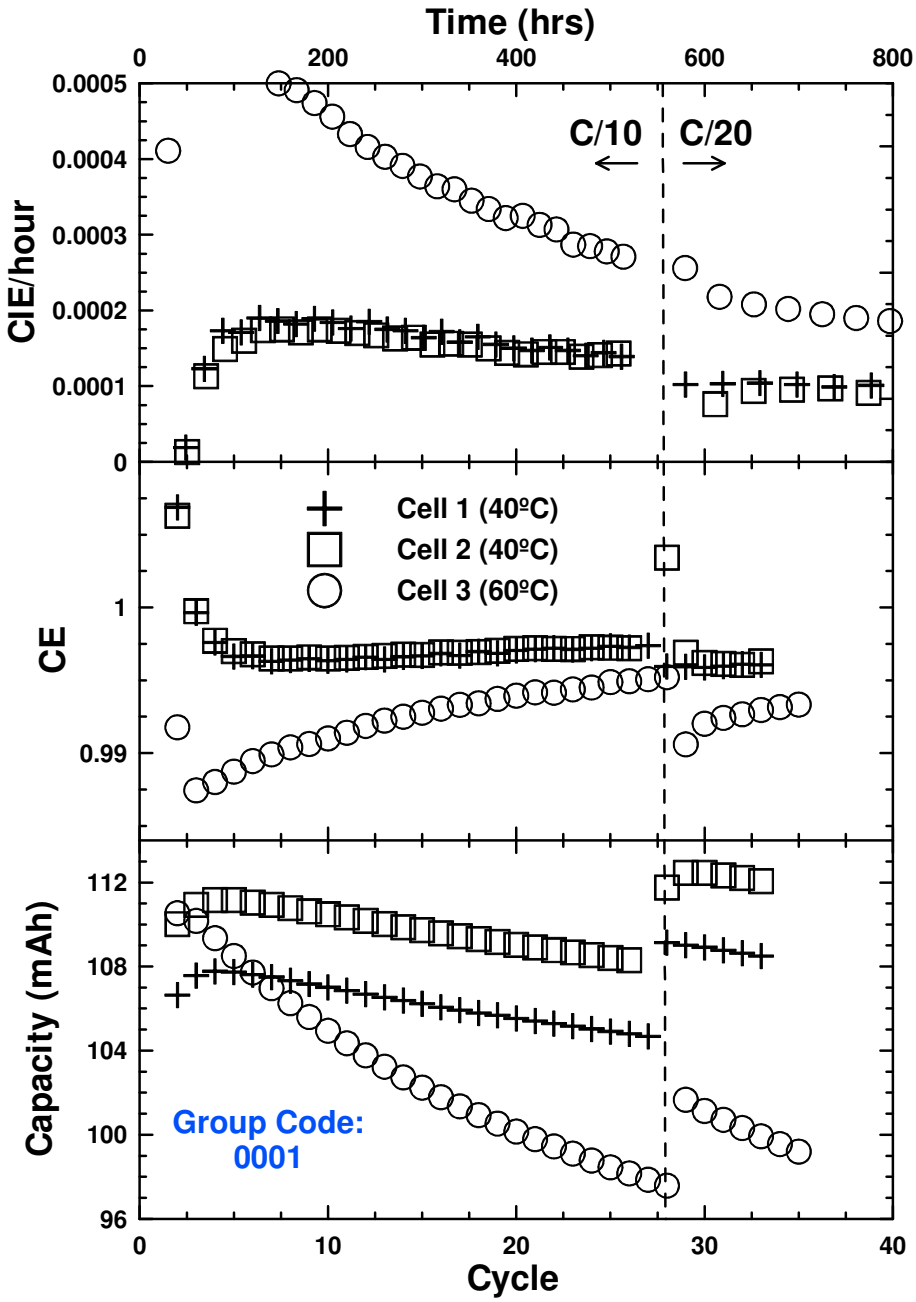

Figure 6.8 CIE/hour versus time (panel a), coulombic efficiency versus cycle number (panel b), and normalized capacity versus cycle number (panel c) for the graphite negative electrode group 0001 with both the C/10 and C/20 data. The vertical dashed line indicates where the rate was changed.

Figure 6.8 shows about 800 hours of cycling data collected for the control $LiCoO_2$/graphite (0001) cells at both C/10 and C/20 rates. Smith et al. [25] showed how in commercial lithium ion cells there are time dependant parasitic reactions that cause the departure from 1.0000 in coulombic efficiency when cycling at slow rates (< C/10).

Therefore, since these reactions are always occurring within the cell, when the rate is slowed so that a cycle takes twice the time to complete, the difference of measured coulombic efficiency from 1.0000 (known as coulombic inefficiency (CIE)) should double. In order to factor out this time dependence, it is useful to consider the coulombic inefficiency divided by the time per cycle (CIE/hour) plotted versus total experiment time. It was shown [25] that when cycling commercial cells at three different rates and several temperatures the CIE/hour versus time plots were identical for all cells cycled at a given temperature. This was shown to be the case for all of the cells tested which were $LiCoO_2$/graphite, $LiFePO_4$/graphite and $LiMn_2O_4$/graphite cylindrically wound cells.

Figure 6.8 shows all expected behavior when changing the cycling rate for these control cells at both temperatures. When the current is reduced by a factor of two, the difference between the measured coulombic efficiency and unity roughly doubles. Therefore when accounting for the difference in time per cycle by plotting CIE/hour versus time, the data follows a smooth curve across the rate change. It appears as though some data points are missing near the rate change as partial cycles occurred immediately before and after changing rates resulting in a small gap in data collected for full cycles.

Figures 6.9 and 6.10 show summary plots of all graphite negative electrode cells at the end of the ~500 hours of C/10 cycling. Panels b), c) and d) are in ascending order for the specified y-axis while panel a) is plotted on the same x-axis as panel d) (ranked by coulombic efficiency). The 40°C data is an average of the two cells cycled at that temperature for each group. All fitted values were calculated based on the final five data points collected for each cell. Several important things can be concluded from Figures 6.9 and 6.10. The first is the obvious acceleration of parasitic reactions and decline in performance when the cell temperature is increased from 40 to 60°C. The two figures are plotted on the same scale so the larger bars directly represent more charge and discharge slippage, fade and departure of coulombic efficiency from 1.0000. The relation between coulombic efficiency and discharge slippage given in Chapter 3 is evident as the ranking of groups for panels b) and c) are almost exactly the same. Also interesting is that the ordering of each panel with its respective axis does not change greatly when increasing the temperature of the cell. This means that the increase in rate of parasitic reactions within the cell is similar for a given temperature change.

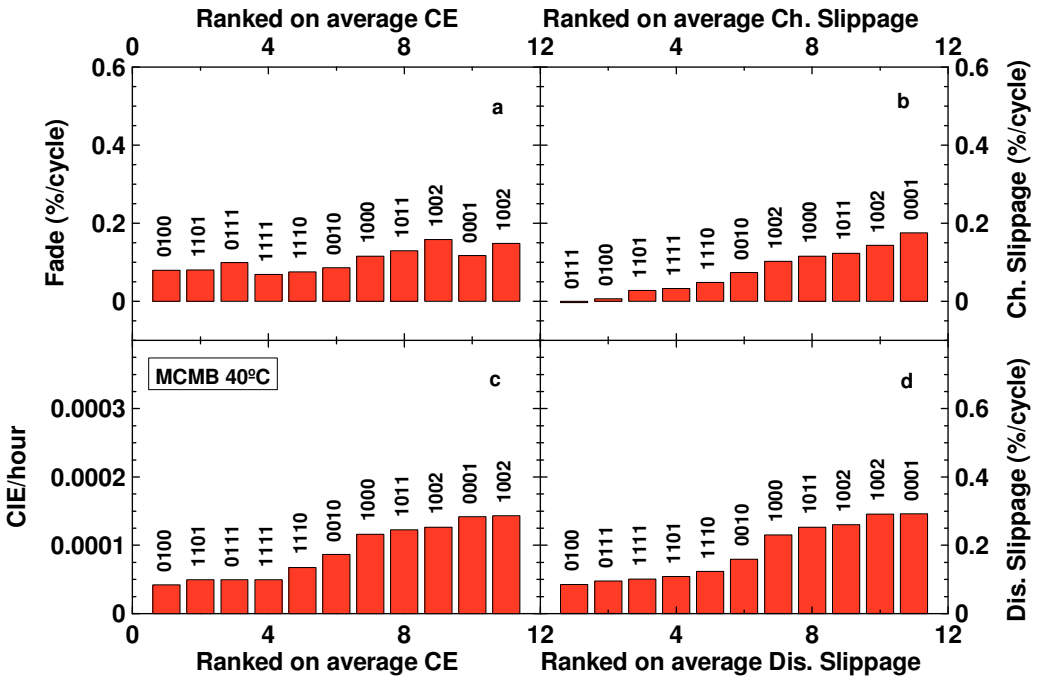

Figure 6.9 A summary of C/10 data for the graphite-based cells cycling at 40°C with fade per cycle (panel a), electrode slippage at the top of charge (panel b), electrode slippage at the bottom of discharge (panel c), and CIE/hour (panel d). The data was measured for the last 5 C/10 cycles (cycles 21-25).

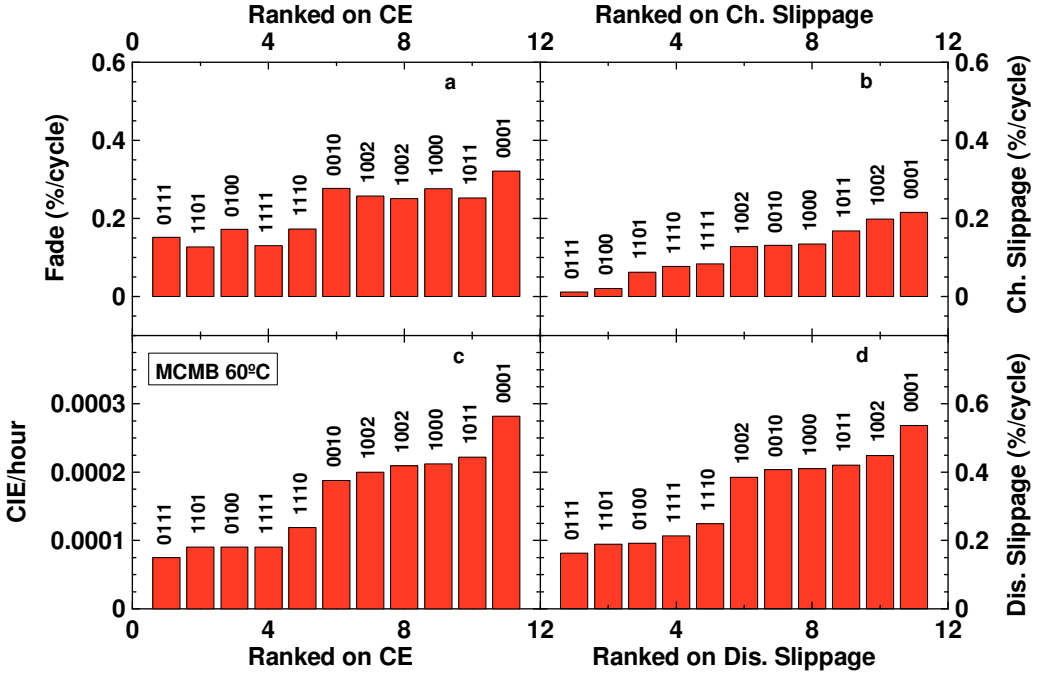

Figure 6.10 A summary of C/10 data for the graphite-based cells cycling at 60°C with fade per cycle (panel a), electrode slippage at the top of charge (panel b), electrode slippage at the bottom of discharge (panel c), and CIE/hour (panel d). The data was measured for the last 5 C/10 cycles (cycles 21-25).

The next most important result from these figures is the impact of the addition of vinylene carbonate to the electrolyte (given by the second digit of the group code). All cells containing VC show lower measured CIE/hour and lower discharge slippage rates which agrees with the lithium accounting model presented earlier. Also interesting is that the charge slippage rate for all VC cells are lower than those cells without VC. This decrease in charge slippage indicates that the addition of VC results in a more stable SEI as literature has previously suggested [79,81] but also decreases the rate of electrolyte oxidation. This decrease in both slippage rates also results in a general decrease in fade. However, it is clear that this short term (~500 hours) fade data is not directly correlated with coulombic efficiency. This is likely because reactions such as electrolyte oxidation do not necessarily influence short term capacity retention however, their impact will appear later in the lifetime of the cell. This means that if coulombic efficiency is an indicator of lifetime, then reports that present decreased fade for cells over roughly this time span do not necessarily indicate the cell will cycle for a longer lifetime.

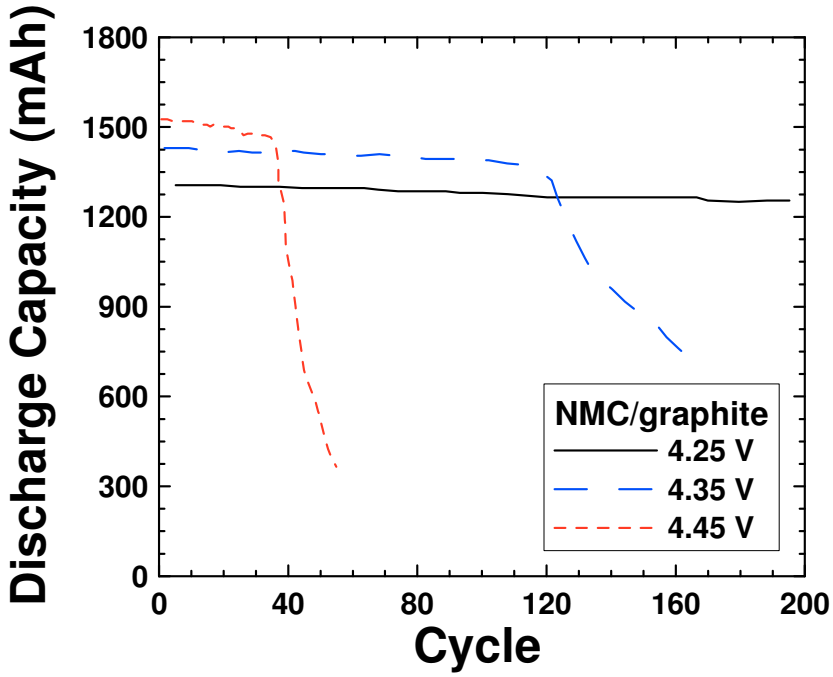

Figure 6.11 Discharge capacity versus cycle number for three NMC/graphite 18650-style cells cycled to different upper voltage limits. This shows the impact of electrolyte oxidation on longer term experiments or when the oxidation rate is high.

As an aside, Figure 6.11 shows capacity versus cycle number for full 18650-style cells [91]. These cells were constructed with a variant of NMC (not equal metal contents in the transition metal layer) as the positive electrode, graphite as the negative electrode and 1 M $LiPF_6$ in EC:EMC (3:7) electrolyte. The three cells were all cycled with a 1 A charge current and 1.4 A discharge current with a brief potential hold at the top of each charge. The cells were cycled between 2.8 V and 4.25, 4.35 or 4.45 V to examine the impact of upper cut off voltage on cell performance. The early cycle fade for the cell cycled to 4.45 V is clearly the highest, but over the first 80-100 cycles, the fade for the cells cycled to 4.25 and 4.35 V is similar. However, at roughly cycle 120, the cell cycled to 4.35 V begins to fade rapidly while the cell cycled to 4.25 V continues to cycle well for over 400 cycles (not all shown). This is evidence of parasitic reactions that do not impact short term capacity fade but are degrading the electrolyte by oxidizing solvent molecules. This type of reaction is detectable with high precision coulometry but not necessarily detectable by simply measuring capacity fade versus cycle number unless cycling for a very long time.

It is difficult from looking at Figures 6.9 and 6.10 to understand the impact of TMOBX, HQ115 and the different positive electrodes on each of the four measured quantities presented as a consequence of the layout of the design of experiments. However, the impact of these factors was detectable through the statistical analysis to be discussed in the next subsection.

Figures 6.12 and 6.13 are made similarly to Figures 6.9 and 6.10 but with the data collected on the $LiCoO_2$/LTO cells. All four of these plots are on the same scale for the y-axis of each quantity in order to visually compare more easily. Similarly to the graphite based cells, all measured values increase at elevated temperature indicating a decrease in performance. However, all values for the LTO based cells are small relative to the graphite based cells indicating a large change in performance based on the choice of negative electrode. The data collected from the LTO based cells also shows that short term fade and coulombic efficiency are not correlated while discharge slippage is directly related to coulombic efficiency. Again the impact of VC is clear as all cells containing VC having smaller CIE/hour, discharge slippage and charge slippage rates as well as generally showing less short term fade.

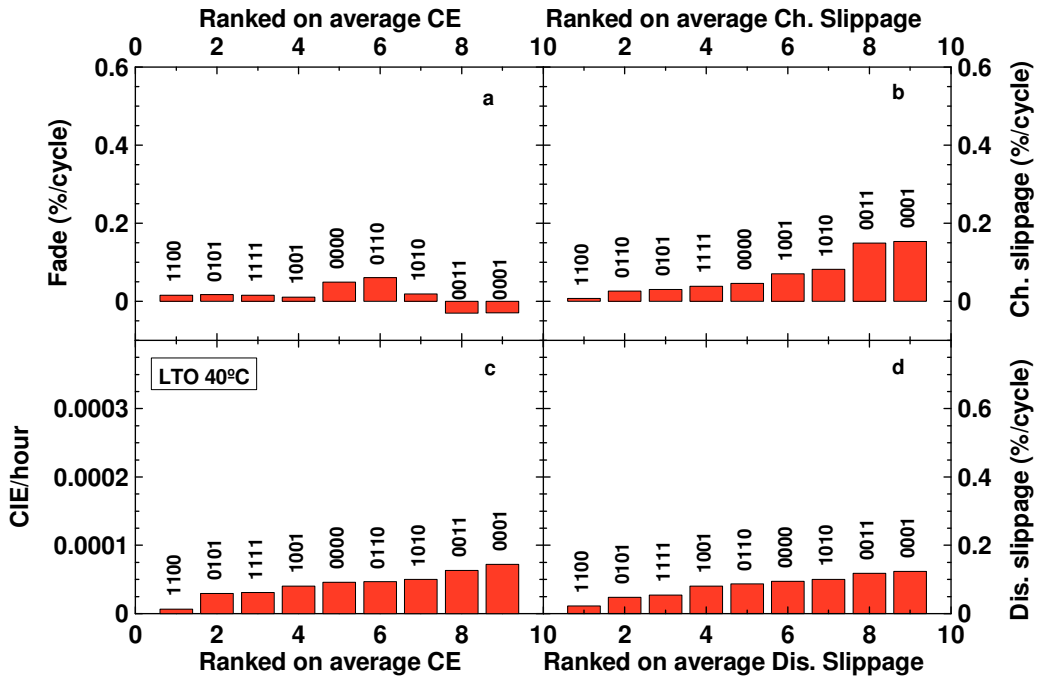

Figure 6.12 A summary of C/10 data for the LTO-based cells cycling at 40°C with fade per cycle (panel a), electrode slippage at the top of charge (panel b), electrode slippage at the bottom of discharge (panel c), and CIE/hour (panel d). The data was measured for the last 5 C/10 cycles (cycles 21-25).

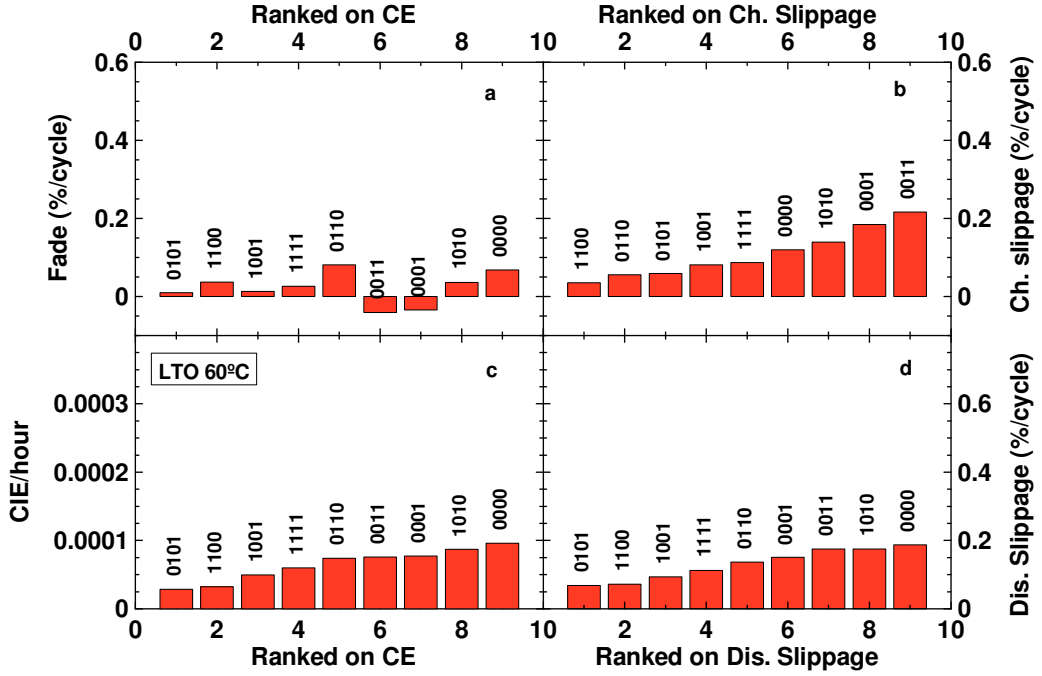

Figure 6.13 A summary of C/10 data for the LTO-based cells cycling at 60°C with fade per cycle (panel a), electrode slippage at the top of charge (panel b), electrode slippage at the bottom of discharge (panel c), and CIE/hour (panel d). The data was measured for the last 5 C/10 cycles (cycles 21-25).

Interestingly there are two groups of cells which show capacity increase in the short term fade measurements. This is a clear argument for why short term capacity fade can not be considered an indication of longer term cycle life. Despite the increase in capacity over these cycles, it can not be expected to continue as there must be loss of active lithium in the cell as the slippages of charge and discharge are not equal to zero. Since these cells are limited in capacity by the LTO electrode, the charge slippage rate is related to parasitic reactions at the negative electrode. This slippage is greater than the discharge slippage rate which for these negative limited cells is related to parasitic reactions at the positive electrode such as electrolyte oxidation leading to the capacity increasing. However, this still means that parasitic reactions are occurring in the cell and eventually the cell will begin to lose capacity. It is also possible that a slight decrease in the internal impedance of the cell during cycling is leading to this increase in capacity. If this capacity increase is impedance related, conclusions about slippage rates are not robust. As was the case for the graphite based cells, the impact of the other additives and choice of positive electrode do not appear as obvious as the impact of temperature and VC but some conclusions can be drawn using a statistical analysis approach which will be discussed in the next subsection.

Figure 6.14 is based on data collected at 40°C during cycling on the HPC as well as the long term cycling data provided by the manufacturer. The y-axis is percent capacity loss over 750 cycles at a rate of C/4 with a brief potential hold at the top of charge and bottom of discharge (done by the manufacturer). Therefore this data was collected over more than ten months of cycling which can be considered longer term cycling. The x-axis is the measured coulombic inefficiency from the HPC after the ~500 hours of C/10 cycling. The plot contains data for the groups which were included in the design of experiment and long term cycling data was available from the manufacturer. An important consideration for this plot is that any trend between long term capacity retention and CIE must go through the origin of the plot since a cell with a measured CE of 1.0000 should have undesired parasitic reactions and therefore exhibit no capacity loss over long term testing. The black symbols on the graph are data for two groups (indicated by their group codes) of each negative electrode choice all with the lower surface are $LiCoO_2$ as the positive electrode. Therefore between the origin and the two

data points for each negative electrode there is a clear linear trend between coulombic efficiency and long term performance or lifetime. This supports that careful coulombic efficiency measurements of cells are a better indicator of long term cycle life than measuring capacity retention during shorter experiments (100s of hours).

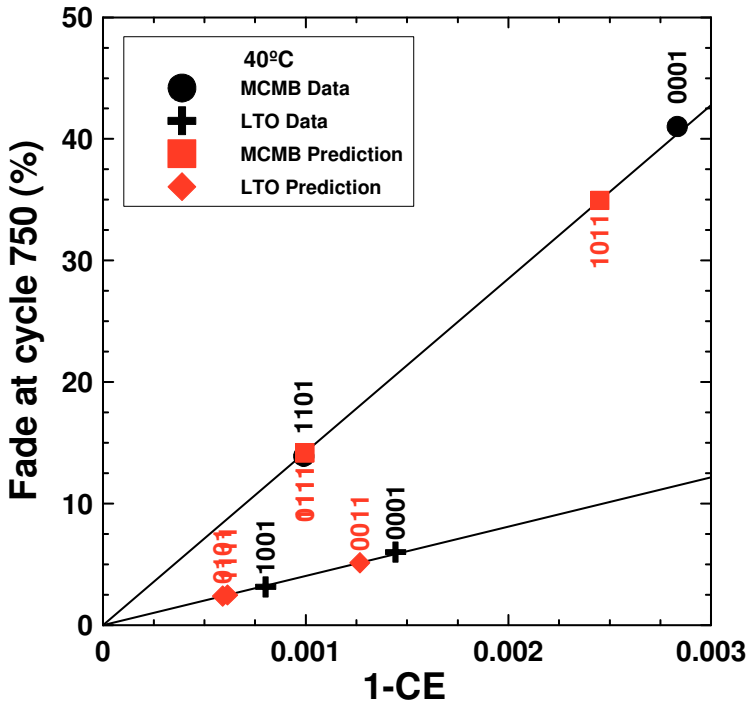

Figure 6.14 Long term capacity loss data versus measured CIE/hour at 500 hours of testing. Black data points are measurements and red data points are predictions. Group codes and negative electrode choices are indicated on the plot.

Also evident from the graph is the impact of electrode choice on long term cycle life. The slopes of the two fitted lines are not equal because the parasitic reactions occurring at the graphite and LTO negative electrodes are different. This causes a measured CIE of 0.003 to indicate a loss of about 43% of capacity for graphite based cells but only about a 12% loss of capacity for LTO based cells over the long term experiment. Also the difference between a measured coulombic efficiency of 0.9970 and 0.9990 corresponds to an increase in capacity retention of about 28% for graphite based cells but only 9% for LTO based cells. Based on the good correlation between the measured capacity loss from the manufacturers testing and the CIE results from the HPC,

the red symbols show predictions of capacity loss over the same length test for other electrolyte combinations tested on the HPC. For a given cell chemistry the capacity loss is proportional to the CIE value so the long term capacity loss for these cells was calculated based on the linear fit and their corresponding measured CIE. This shows that the LTO based cell of group 0101, which was the cell with the highest measured CE at 40°C with the low surface area $LiCoO_2$, would be expected to experience only 3% capacity loss over a similar length test to the one conducted by the manufacturer. It is believed that if more long term cycling data was provided by the manufacturer about the other cell groups in the design of experiment all data would fall on their respective lines.

6.2b Statistical Results

The use of design of experiments allowed for information to be gained about different additive combinations which were not actually tested in a cell and more clearly identify the impact of each variable in the experiment. Two approaches were taken to the analysis of the design of experiments: JMP's statistical software package SAS Business Analytics and Business Intelligence Software's JMP (version 8) and the solver function in Microsoft Excel. All parameters involved in the design of experiments assume a linear response with no middle point available as this would have added 50% more cells to the test matrix. The design of experiments allows for a predictive model based on the variables to be used in an attempt to understand the role of each additive as well as possible cross terms between pairs of variables. In this case, the goal was to maximize long term cycle life so based on the results seen in Figure 6.14 a predictor equation for coulombic efficiency was established. JMP sorts all variables and their cross terms in order of statistical significance. Only considering those which were deemed significant, the variables in order are: cell temperature (higher temperature had a negative impact), the choice of negative electrode (changing to LTO had positive impact), the addition of VC (adding VC had positive impact), the cross term between temperature and VC (increasing the positive impact of VC when temperature is increased), the cross term between VC and negative electrode choice (decreasing the positive impact of VC when using a LTO negative electrode), the cross term between temperature and negative

electrode choice (decreasing the negative impact of temperature when using a LTO negative electrode), and the cross term between HQ115 and negative electrode choice (decreasing the positive impact of LTO with the addition of HQ115).

Figure 6.15 shows the value of the coefficients of these factors when all variables are normalized to take a maximum value of 1 so the magnitude of the coefficients can be directly compared. Although found to be statistically insignificant, the next three parameters in the order of impact were addition of HQ115 (adding HQ115 had a negative impact), choice of positive electrode (using high surface area $LiCoO_2$ had a positive impact, which disagrees with storage experiments [89]), and addition of TMOBX (adding TMOBX had a positive impact). The fit of this model to all collected data resulted in an R^2 value of 0.866974.

The coefficients given in Figure 6.15 can be used to predict the coulombic efficiency for combinations of electrodes and electrolyte additives which were not tested on the HPC. The values for each additive term can vary from 0 (absence of additive) to 1 (full concentration tested) with a linear relationship between the value and concentration added. The negative electrode term can be assigned values of 1 or -1 for the choice of LTO or graphite, respectively. The positive electrode does not appear as a statistically significant term and therefore does not need to be considered. The value for temperature can be set to anything between 0 and 1 indicating 40 and 60°C, respectively, also with a linear response between the two test temperatures. The constant term found for the fit to coulombic efficiency data by JMP was 0.998371. For example, to calculate the CE of a cell with a MCMB negative electrode, no additives and cycling at 40°C, the values for additives and temperature would be 0 and the negative electrode would be −1. This results in CE = 0.998271 – 1*(0.000958) = 0.997413. This value agrees well with the measured value for these cells of 0.9972 and 0.9973. This same approach can be extended to other cells that were tested showing good agreement so it can also be applied to cells with different combinations of these additives and electrodes which were not tested.

This analysis resulted in the highest achievable coulombic efficiency when a cell contained a LTO negative electrode, VC, no HQ115, either positive electrode, with or without TMOBX, cycled at 40°C, which agreed well with the measured values. The

choice of positive electrode and use of TMOBX may have a slight impact no lifetime and CE measurements but was not detectable by this size matrix of cells. If the cell contained a graphite negative electrode, the analysis found the highest coulombic efficiency when the cell was cycled at 40°C with VC, HQ115, and the use of either positive electrode with or without TMOBX. The predicted coulombic efficiency for the best graphite-based cell is still 0.034% less than the highest predicted coulombic efficiency for a cell with a LTO negative electrode. This means that longer lifetimes are expected for LTO based cells compared to cells with graphite negative electrodes. This is true not only from a higher achievable CE, but also that Figure 6.14 showed that LTO based cells with the same measured CE as graphite based cells would show less capacity fade over long term cycling.

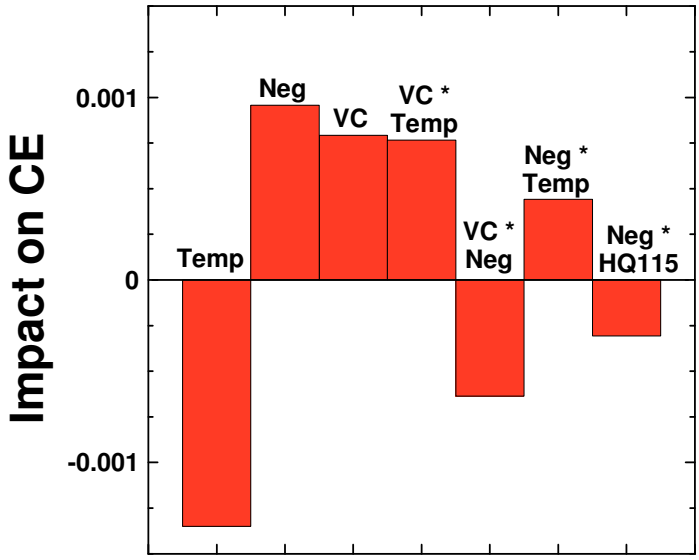

Figure 6.15 Values of the coefficients of terms from the design of experiments ranked in the order of significance showing their impact on coulombic efficiency. All terms except the negative electrode choice (Neg) may be assigned values of 0–1 where 0 indicates no additive of that type (or 40°C) and 1 indicates full concentration of additive (or 60°C). The coefficient, Neg, takes a value of −1 for the choice of MCMB and 1 for the choice of LTO.

A simplified model was also made using the solver function of Microsoft Excel to maximize predicted coulombic efficiency for different combinations of additives. The largest difference from the JMP analysis is that the simplified model divides cells into four groups based on the two temperatures and negative electrodes. The model then has a

constant term, a linear response term for each additive, cross terms for all pairs of additives and a triplet term for the use of all additives together. The equation used was

$$CE = a + b*T + c*V + d*H + e*T*V + f*T*H + g*V*H + h*T*V*H \quad 6.1$$

with the variables T, V and H correspond to TMOBX, VC and HQ115, respectively, which are allowed to vary from 0 to 1. The coefficients a-h are fitting parameters used to minimize the sum of the square of the differences between measured and predicted data. Since changing the positive electrode was shown to be insignificant using the JMP analysis, the ability to choose the positive electrode was eliminated from this simplified model. The impact of additives and their cross terms that were found to be insignificant by JMP were still included in this model and the solver function should find better fits when the coefficients corresponding to the insignificant terms are very small.

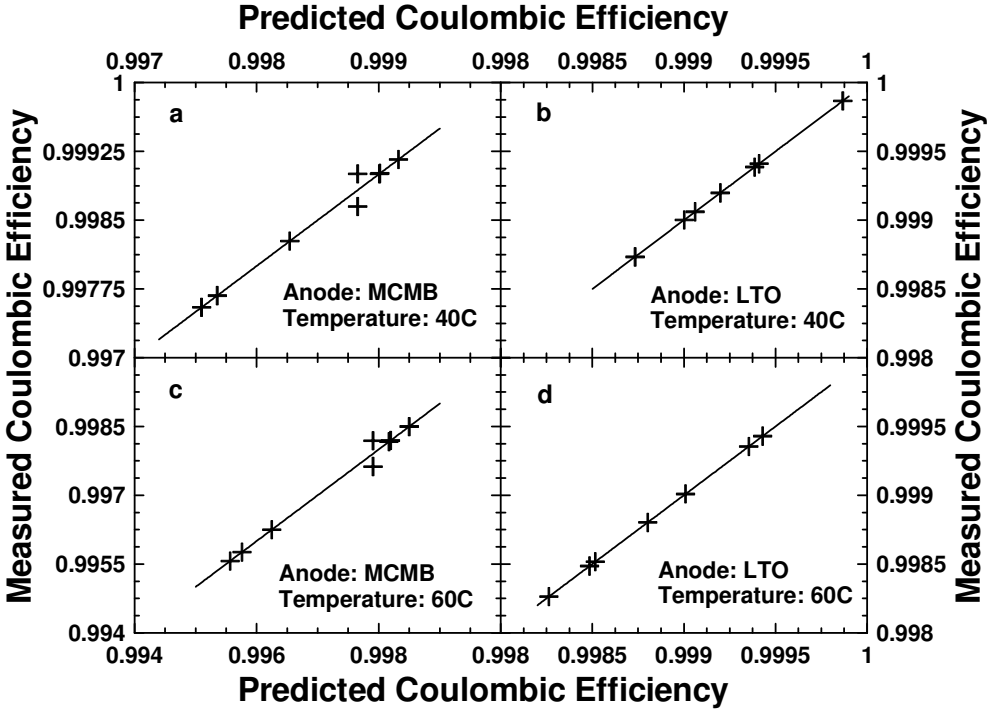

Figure 6.16 Measured coulombic efficiency (at the end of the C/10 cycles – about 500 hours after the beginning of test) versus predicted coulombic efficiency from the design of experiments equation for graphite-based cells at 40°C (panel a), graphite-based cells at 60°C (panel c), LTO-based cells at 40°C (panel b), and LTO-based cells at 60°C (panel d).

Fitting Coeff.	MCMB 40ºC	MCMB 60ºC	LTO 40ºC	LTO 60ºC
A	**0.99717**	**0.99487**	**0.99890**	**0.99827**
B	**0.00051**	**0.00089**	**0.00038**	**0.00074**
C	**0.00199**	**0.00332**	**0.00059**	**0.00116**
D	**0.00110**	**0.00138**	**-0.00009**	**0.00022**
E	**-0.00066**	**-0.00091**	**0.00008**	**-0.00082**
F	**-0.00123**	**-0.00157**	**-0.00011**	**-0.00096**
G	**-0.00126**	**-0.00107**	**-0.00026**	**-0.00113**
H	**0.00121**	**0.00101**	**-0.00002**	**0.00132**

Table 6.3 Coefficients found by fitting the coulombic efficiency equations (Equation 6.1) to the measured coulombic efficiency of each group of matching anode and temperature.

Figure 6.16 and Table 6.3 show the results of modeling the coulombic efficiency with Equation 6.1. Figure 6.16 shows almost perfect fits with the only discrepancy being for two graphite based groups which had the same electrolyte formulation but different positive electrodes and slightly different measured CEs. This difference is undetectable in this model as the impact of changing the positive electrode was not considered. Table 6.3 shows the values of the fitting parameters for each of the four conditions. These coefficients indicate the impact of the associated variable on CE. Positive coefficients lead to an increase in CE as the variable changes from 0 to 1 while negative coefficients lead to a decrease in CE. Since the variables can only range from 0 to 1, the impact of each variable on CE can be seen from a direct comparison between the magnitudes of the coefficients. This model predicts the highest achievable CE to be the highest measured CE under each of the four conditions since when the different positive electrodes are not considered, all of the eight possible electrolyte formulations were tested for each negative electrode. This is a useful model for seeing the impact of additives at different temperatures and in the presence of other additives for a given cell chemistry.

Both of the models presented work well if the linear response is a reasonable approximation for the use of additives (which may not be the case). Unfortunately, even if a linear response is a good approach to model the use of additives, conclusions cannot be made about the impact of additive concentrations beyond that used in the experiment. Regardless, this type of statistical analysis can lead to conclusions about cells which were not physically constructed and tested which can help speed up large scale testing of

different electrodes and additives. The method also helps to identify the impact of additives that is not obvious as well as the possibility of cross terms having impacts. While these models may not be flawless, they both serve a purpose and have a place in large scale experiments for lithium ion battery lifetime evaluation.

Chapter 7 Conclusions and Future Work

7.1 Conclusions

Lithium-ion batteries are used for a variety of applications from portable electronics to electrified vehicles. In the future it is likely that Li-ion batteries will be used for grid energy storage. The demands on the lifetime of cells continue to grow for these applications. In the past additives have been used to extend the cycle life of cells. The impact of these additives was quantified by measuring fade for hundreds of cycles in only several hundred hour experiments. However, it is not clear that this was a robust method to evaluate lifetime under realistic cycling conditions as under realistic conditions the experiment could take over a decade. This thesis has shown that the use of high precision coulometry is a more useful approach to evaluating the lifetime of Li-ion cells. Results showed that measured coulombic efficiency and long term fade correlated perfectly for two different types of cell chemistries containing electrolyte additives. This proves that to test the lifetime of cells accurate measurements of coulombic efficiency are required. Experiment also showed that CE is not directly related to short term fade suggesting that measuring fade over a short period (several hundred hours) is not an effective way of predicting long term capacity retention. Figure 6.11 shows the impact of reactions such as electrolyte oxidation which are not evident during early cycling but play a role in the cycle life of a cell. This means that experiments measuring short term fade in the past and suggesting that less fade would indicate longer cycle life are not necessarily true.

The use of high precision coulometry not only yields reliable coulombic efficiency values but also allows for the slippage rate of the charge and discharge endpoints to be measured accurately. The motion of these endpoints is associated with different parasitic reactions occurring in the cell as discussed in Chapter 3. These parasitic reactions lead to cell degradation and eventually cell failure. Therefore changes in slippage rates for cells with different additives lead to an understanding of the impact of the additive (ie suppressing electrolyte oxidation or forming a more stable SEI on the

negative electrode). This technique does not allow for information about the mechanism of the reactions from the additives but the result of these reactions can be detected.

High precision coulometry experiments showed how the use of LTO in place of graphite as a negative electrode can greatly enhance cycle life. Also shown was how the use of additives undoubtedly can extend the lifetime of a cell. Vinylene carbonate was found to increase coulombic efficiency with both choices of negative electrodes and thus extend cell lifetime. The use of VC was found to decrease the discharge slippage rate which agrees with literature suggesting that the different surface groups formed on the negative electrode from the reduction of VC form a more stable SEI which consumes less active lithium from the cell with each cycle [79,81]. Surprisingly, the addition of VC to the electrolyte also greatly decreased the charge slippage rate. This suggests that VC is limiting reactions such as transition metal dissolution and electrolyte oxidation at the positive electrode. The cells tested contained $LiCoO_2$ as the positive electrode which was charged to about 4.15 V (vs. Li/Li^+) in the fully charged state. To this potential, there is little cobalt dissolution from the material [39,90] which indicates that VC must be suppressing the electrolyte oxidation occurring in the cell.

The impact of other additives may not be as clear that of VC, but statistical analysis can be used to help identify differences in performance. Design of experiments can be used which allows for predictor equations for different quantities (such as CE, charge or discharge slippage, fade, etc.) to be established based on a given matrix of cells. This predictor equation can then be applied to cells which were not actually tested and could contain different combinations of the additives used such as in the experiment presented in Chapter 6. From the good correlation established between the predictor equations using both statistical software and Microsoft Excel's solver function it is clear that there is a place for this type of analysis when attempting to test many additives or cell types in a shorter period of time.

7.2 Future Work

The work done for this thesis lays the foundation for future high precision coulometry work. It is clear that electrolyte additives can be used to extend the cycle life of cells which can be seen using this technique in several hundred hour long experiments. Experiments on the impact of changes in the cell design do not have to be limited to different materials and additives but should also include an investigation of a variety of salts and solvents for the electrolyte with different cell chemistries. With the ability to compare cell performance between a control group and that with a given test condition (different salt, solvent, additive combination, etc.) in relatively short experiments, the possibility of tests is innumerable.

Cycling cells and seeing the impact of additives (or other changes to the cell design) on cell performance does not allow for the mechanisms to be identified. Work can be done to better understand the actual mechanisms occurring when VC is added to the electrolyte which appears both decrease the rate of electrolyte oxidation at the positive and form a more stable SEI on the negative electrode. If the actual mechanisms behind the beneficial reactions are understood, work can be done to develop new additives which may have similar mechanisms and therefore result in improvements in cell performance.

As the coulombic efficiencies of well made commercial lithium-ion cells approach values closer to 1.000000, more accurate chargers are needed to detect small performance differences between cells. While the HPC was demonstrated to be able to measure coulombic efficiency with an accuracy of 0.01%, chargers with at least an order of magnitude better accuracy are required. The highest measured coulombic efficiency values in the data presented in this work were 0.9999 which is at the limit of the accuracy of the HPC. Commercially available chargers should be made with the ability to measure coulombic efficiency to the level of the HPC or better so that high precision coulometry becomes a cost competitive test. As this thesis has shown that coulombic efficiency is directly related to long term cycle life, this would allow relative cycle life testing to be done on standard battery cyclers in a shorter period of time.

Cycling is not the only important type of experiment to learn about the behavior and degredation mechanisms of lithium ion cells. As shown in Chapter 3, the parasitic currents occurring within a cell cannot be determined from cycling data alone so other types of testing might result in the ability to solve directly for these parasitic currents. Such experiments include high precision storage where a cell can be cycled and then left under open circuit conditions at a given temperature before being cycled again as well as carefully conducted chronoamperometry where cells are held at constant voltage and the current flow through the cell is measured.

The combination of cycling and open circuit storage allows for the investigation of the internal self discharge reactions presented in Chapter 3 [89]. An example of the procedure for such an experiment begins with charging and discharging a cell twice while accurately measuring the capacities (with similar equipment used for the HPC) and then charging the cell to the upper voltage limit. At this point the cell would be left at open circuit with a mechanical relay closing for only a second on a specified interval (for example every six hours) to read the voltage and then returning to the open condition so the cell cannot slowly discharge through an external circuit. After a given period of storage time (perhaps several hundred hours), the cell is cycled again beginning with a discharge. Then one full charge discharge cycle occurs before being charged to the upper voltage limit again for another storage interval if desired.

In a half cell, the voltage change while at open circuit comes directly from the potential of the working electrode since the potential of the lithium foil is constant. In a full cell the voltage drop can come from potential changes of either electrode. However, near the fully charged state of graphite based full cells, the potential of graphite is relatively constant and therefore the voltage change in the cell comes primarily from the potential changes of the positive electrode. The potential of the positive electrode can only decrease if lithium is inserted into the material. Therefore the decrease in open circuit voltage is related to those types of mechanisms shown in Chapter 3 which insert lithium into positive electrode such as electrolyte oxidation or transition metal dissolution.

The voltage drop is not the only quantity that can indicate the types of reactions occurring in the cell during this type of storage experiment. Since the discharge capacities before (D_0), immediately after (D_1) and one charge after storage (D_2) were

accurately measured, they too can be compared. The discharge before storage is the largest of the three as there has been the least amount of time for parasitic reactions to occur. The discharge immediately after storage is the smallest as the cell has self discharged during storage. The next discharge after storage is larger than D_1, since the cell was fully charged before discharging so there is little impact from self discharge reactions. However, D_2 is not as large as D_0, since there has been irreversible loss of active lithium in the cell due to reactions such as SEI growth over time. These capacities and voltage drops can be correlated with data from high precision cycling over the full range and correlate even better when cycling a cell only in the range between the upper cut off voltage and about 100 mV below this upper limit. This work is currently being done in the group showing these correlations and how storage experiments can play an important role in understanding cell degradation [89].

Another experiment that can add to the understanding of internal reactions within a cell is keeping a cell at a constant voltage and measuring the current flow, or chronoamperometry. These types of tests are best conducted in half cells to examine the reactions on a single electrode at a given potential. Testing of full cells becomes more complicated as the measured current can come from reactions at either electrode. High precision instrumentation is required to ensure accurate current measurements from the cell as this can be impacted by the stability of the voltage as well as the cell temperature. Also the experimental hardware must be carefully chosen so that all measured currents come from only the electrode material [92]. In half cells these currents are a direct measure of the parasitic current flowing at the given potential. This type of experiment can be conducted on negative electrode materials to directly measure the current from SEI growth or positive electrode materials to measure the current due to electrolyte oxidation and transition metal dissolution. These types of experiments are also currently being conducted in this lab.

As the demands on cycle life for lithium ion cells increase, methods of testing life time must become more advanced. Combinations of accurate cycling, storage, and potential hold experiments help to identify the parasitic reactions occurring in a cell that will eventually limit its cycle life. The use of additives should continue to be extensively studied as it has been shown through cycling experiments that different additives can

impact the lifetime of cells. Combinations of carefully conducted experiments examining parasitic reactions allow for thorough screening of new additives and electrode materials for cells that require long cycle life.

Bibliography

[1] J. Li and J. R. Dahn, *J. Electrochem. Soc.* **154**, A156 (2007).

[2] M. N. Obrovac and L. Christensen, *Electrochem. Solid-State Lett.* **7**, A93 (2004).

[3] M. Winter and J. O. Besenhard, *Electrochimica Acta* **45**, 31 (1999).

[4] N. Tamura, R. Ohshita, M. Fujimoto, S. Fujitani, M. Kamino, and I. Yonezu, *J. Power Sources* **107**, 48-55 (2002).

[5] Y. Hamon, T. Brousse, F. Jousse, P. Topart, P. Buvat, and D. M. Schleich, *J. Power Sources* **97-98**, 185 (2001).

[6] M. N. Obrovac and L. J. Krause, *J. Electrochem. Soc.* **154**, A103 (2007).

[7] A. D. W. Todd, P. P. Ferguson, M. D. Fleischauer, and J. R. Dahn, *Int. J. Energy Res.* **34**, 535 (2010).

[8] J. R. Dahn, T. Zheng, Y. Liu, and J. S. Xue, *Science* **270**, 590 (1995).

[9] Guerard, D and Herold, A., *Carbon* **13**, 337 (1975).

[10] K. M. Colbow, J. R. Dahn, and R. R. Haering, *J. Power Sources* **26**, 397 (1989).

[11] T. Ohzuku, A. Ueda, and N. Yamamoto, *J. Electrochem. Soc.* **142**, 1431 (1995).

[12] R. Koksbang, J. Barker, H. Shi, and M. Y. Saïdi, *Solid State Ionics* **84**, 1 (1996).

[13] A. Yamada, S. C. Chung, and K. Hinokuma, *J. Electrochem. Soc.* **148**, A224 (2001).

[14] R. J. Gummow, A. de Kock, and M. M. Thackeray, *Solid State Ionics* **69**, 59 (1994).

[15] F. Zhou, X. Zhao, A. van Bommel, X. Xia, and J. R. Dahn, *J. Electrochem. Soc.* **158**, A187 (2011).

[16] Q. Zhong, A. Bonakdarpour, M. Zhang, Y. Gao, and J. R. Dahn, *J. Electrochem. Soc.* **144**, 205 (1997).

[17] S. K. Martha, H. Sclar, Z. Szmuk Framowitz, D. Kovacheva, N. Saliyski, Y. Gofer, P. Sharon, E. Golik, B. Markovsky, and D. Aurbach, *J. Power Sources* **189**, 248 (2009).

[18] J. K. Ngala, N. A. Chernova, M. Ma, M. Mamak, P. Y. Zavalij, and M. S. Whittingham, *J. Mater. Chem.* **14**, 214 (2004).

[19] T. Reddy, *Linden's Handbook of Batteries, 4th Edition*, 4th ed. (McGraw-Hill Professional, 2010).

[20] S. S. Zhang and T. R. Jow, *J. Power Sources* **109**, 458 (2002).

[21] A. B. McEwen, H. L. Ngo, K. LeCompte, and J. L. Goldman, *J. Electrochem. Soc.* **146**, 1687 (1999).

[22] J. L. Nowinski, P. Lightfoot, and P. G. Bruce, *J. Mater. Chem.* **4**, 1579 (1994).

[23] A. B. McEwen, S. F. McDevitt, and V. R. Koch, *J. Electrochem. Soc.* **144**, L84 (1997).

[24] K. Xu, *Chemical Reviews* **104**, 4303 (2004).

[25] A. J. Smith, J. C. Burns, and J. R. Dahn, *Electrochem. Solid-State Lett.* **13**, A177 (2010).

[26] A. J. Smith, J. C. Burns, X. Zhao, D. Xiong, and J. R. Dahn, *J. Electrochem. Soc.* **158**, A447 (2011).

[27] A. J. Smith, J. C. Burns, and J. R. Dahn, *Electrochem. Solid-State Lett.* **14**, A39 (2011).

[28] E. Peled, D. Golodnitsky, and G. Ardel, *J. Electrochem. Soc.* **144**, L208 (1997).

[29] M. Broussely, P. Biensan, F. Bonhomme, P. Blanchard, S. Herreyre, K. Nechev, and R. J. Staniewicz, *J. Power Sources* **146**, 90 (2005).

[30] R. Fong, U. von Sacken, and J. R. Dahn, *J. Electrochem. Soc.* **137**, 2009 (1990).

[31] D. Aurbach, Y. Ein-Eli, O. C. (Youngman), Y. Carmeli, M. Babai, and H. Yamin, *J. Electrochem. Soc.* **141**, 603 (1994).

[32] R. B. Wright, J. P. Christophersen, C. G. Motloch, J. R. Belt, C. D. Ho, V. S. Battaglia, J. A. Barnes, T. Q. Duong, and R. A. Sutula, *J. Power Sources* **119-121**, 865 (2003).

[33] K. Araki and N. Sato, *J. Power Sources* **124**, 124 (2003).

[34] H. J. Ploehn, P. Ramadass, and R. E. White, *J. Electrochem. Soc.* **151**, A456 (2004).

[35] D. Aurbach, Y. Gofer, and J. Langzam, *J. Electrochem. Soc.* **136**, 3198 (1989).

[36] G. Pistoia, A. Antonini, R. Rosati, and D. Zane, *Electrochimica Acta* **41**, 2683 (1996).

[37] J. Christensen and J. Newman, *J. Electrochem. Soc.* **152**, A818 (2005).

[38] J. Chen, C. Buhrmester, and J. R. Dahn, *Electrochem. Solid-State Lett.* **8**, A59 (2005).

[39] G. G. Amatucci, J. M. Tarascon, and L. C. Klein, *Solid State Ionics* **83**, 167 (1996).

[40] K. Amine, J. Liu, and I. Belharouak, *Electrochem. Commun.* **7**, 669 (2005).

[41] J. Vetter, P. Novák, M. R. Wagner, C. Veit, K.-C. Möller, J. O. Besenhard, M. Winter, M. Wohlfahrt-Mehrens, C. Vogler, and A. Hammouche, *J. Power Sources* **147**, 269 (2005).

[42] G. Amatucci, A. Du Pasquier, A. Blyr, T. Zheng, and J.-M. Tarascon, *Electrochimica Acta* **45**, 255 (1999).

[43] A. D. Pasquier, A. Blyr, P. Courjal, D. Larcher, G. Amatucci, B. Gerand, and J.-M. Tarascon, *J. Electrochem. Soc.* **146**, 428 (1999).

[44] A. J. Smith, J. C. Burns, S. Trussler, and J. R. Dahn, *J. Electrochem. Soc.* **157**, A196 (2010).

[45] T. Ohzuku, A. Ueda, N. Yamamoto, and Y. Iwakoshi, *J. Power Sources* **54**, 99 (1995).

[46] T.-F. Yi, C.-Y. Li, Y.-R. Zhu, J. Shu, and R.-S. Zhu, *J Solid State Electrochem* **13**, 913 (2008).

[47] M. Q. Li, M. Z. Qu, X. Y. He, and Z. L. Yu, *J. Electrochem. Soc.* **156**, A294 (2009).

[48] J. R. Dahn and R. R. Haering, *Can. J. Phys.* **61**, 1093 (1983).

[49] S. S. Zhang, *J. Power Sources* **162**, 1379 (2006).

[50] D. D. MacNeil, D. Larcher, and J. R. Dahn, *J. Electrochem. Soc.* **146**, 3596 (1999).

[51] J. Jiang and J. R. Dahn, *Electrochimica Acta* **49**, 4599 (2004).

[52] J.-ichi Yamaki, H. Takatsuji, T. Kawamura, and M. Egashira, *Solid State Ionics* **148**, 241 (2002).

[53] J. Jiang and J. R. Dahn, *Electrochem. Commun.* **6**, 39 (2004).

[54] D. D. MacNeil and J. R. Dahn, *J. Electrochem. Soc.* **148**, A1205 (2001).

[55] D. D. MacNeil and J. R. Dahn, *J. Electrochem. Soc.* **148**, A1211 (2001).

[56] Y. Wang, J. Jiang, and J. R. Dahn, *Electrochem. Commun.* **9**, 2534 (2007).

[57] Q. Wang, J. Sun, and C. Chen, *J. Power Sources* **162**, 1363 (2006).

[58] K.-S. Lee, Y.-K. Sun, J. Noh, K. S. Song, and D.-W. Kim, *Electrochem. Commun.* **11**, 1900 (2009).

[59] H. Yamane, T. Inoue, M. Fujita, and M. Sano, *J. Power Sources* **99**, 60 (2001).

[60] M. Xu, W. Li, and B. L. Lucht, *J. Power Sources* **193**, 804 (2009).

[61] J. Li, W. Yao, Y. S. Meng, and Y. Yang, *The Journal of Physical Chemistry C* **112**, 12550 (2008).

[62] J. R. Dahn, J. Jiang, L. M. Moshurchak, M. D. Fleischauer, C. Buhrmester, and L. J. Krause, *J. Electrochem. Soc.* **152**, A1283 (2005).

[63] J. K. Feng, X. P. Ai, Y. L. Cao, and H. X. Yang, *Electrochem. Commun.* **9**, 25 (2007).

[64] M. Q. Xu, L. D. Xing, W. S. Li, X. X. Zuo, D. Shu, and G. L. Li, *J. Power Sources* **184**, 427 (2008).

[65] Y.-B. He, Q. Liu, Z.-Y. Tang, Y.-H. Chen, and Q.-S. Song, *Electrochimica Acta* **52**, 3534 (2007).

[66] K. Abe, Y. Ushigoe, H. Yoshitake, and M. Yoshio, *J. Power Sources* **153**, 328 (2006).

[67] L. Xiao, X. Ai, Y. Cao, and H. Yang, *Electrochimica Acta* **49**, 4189 (2004).

[68] K. Shima, K. Shizuka, M. Ue, H. Ota, T. Hatozaki, and J.-I. Yamaki, *J. Power Sources* **161**, 1264 (2006).

[69] H. Mao, U.S. Patent 5,879,834 (1999).

[70] J.-soon Shin, J.-sung Kim, E.-sun Hong, J.-wook Lee, Y.-gyu Kim, and J.-seob Kim, U.S. Patent 6,645,674 (2003).

[71] K. Abe, K. Miyoshi, and T. Kuwata, U.S. Patent 7,629,085 (2009).

[72] E.-G. Shim, T.-H. Nam, J.-G. Kim, H.-S. Kim, and S.-I. Moon, *J. Power Sources* **172**, 919 (2007).

[73] S. Chen, Z. Wang, H. Zhao, H. Qiao, H. Luan, and L. Chen, *J. Power Sources* **187**, 229 (2009).

[74] J. W. Braithwaite, *J. Electrochem. Soc.* **146**, 448 (1999).

[75] Y. S. Kim, S. H. Ahn, and M. Y. Son, (2006).

[76] B. H. Loo, Y. G. Lee, and D. O. Frazier, *The Journal of Physical Chemistry* **89**, 4672 (1985).

[77] N.-S. Choi, K. H. Yew, K. Y. Lee, M. Sung, H. Kim, and S.-S. Kim, *J. Power Sources* **161**, 1254 (2006).

[78] B. Simon and J.-P. Boeuve, U.S. Patent 5,626,981 (1997).

[79] D. Aurbach, K. Gamolsky, B. Markovsky, Y. Gofer, M. Schmidt, and U. Heider, *Electrochimica Acta* **47**, 1423 (2002).

[80] L. El Ouatani, R. Dedryvere, C. Siret, P. Biensan, and D. Gonbeau, *J. Electrochem. Soc.* **156**, A468 (2009).

[81] H. Ota, Y. Sakata, A. Inoue, and S. Yamaguchi, *J. Electrochem. Soc.* **151**, A1659 (2004).

[82] L. El Ouatani, R. Dedryvere, C. Siret, P. Biensan, S. Reynaud, P. Iratcabal, and D. Gonbeau, *J. Electrochem. Soc.* **156**, A103 (2009).

[83] I. B. Stojkovic, N. D. Cvjeticanin, and S. V. Mentus, *Electrochem. Commun.* **12**, 371 (2010).

[84] H. Mao, U. V. Sacken, and J. N. Reimers, U.S. Patent 5,891,592 (1999).

[85] Z. Chen and K. Amine, *J. Electrochem. Soc.* **153**, A1221 (2006).

[86] J. Liu, Z. Chen, S. Busking, and K. Amine, *Electrochem. Commun.* **9**, 475 (2007).

[87] A. von Cresce and K. Xu, *J. Electrochem. Soc.* **158**, A337 (2011).

[88] J. Antony, *Design of Experiments for Engineers and Scientists*, 1st ed. (Butterworth-Heinemann, 2003).

[89] N. N. Sinha, A. J. Smith, J. C. Burns, G. Jain, K. W. Eberman, E. Scott, J. P. Gardner, and J. R. Dahn, *Submitted to J. Electrochem. Soc.* (2011).

[90] W. Choi and A. Manthiram, *J. Electrochem. Soc.* **153**, A1760 (2006).

[91] J. Singh and J. Choi, *Unpublished Data* (2011).

[92] N. N. Sinha, J. C. Burns, R. J. Sanderson, and J. R. Dahn, *Submitted to J. Electrochem. Soc.* (2011).